EVAPORATION DEPTH CONTROLS THE RELATIONSHIP BETWEEN SOIL WATER MOBILITY AND SOIL WATER ISOTOPIC COMPOSITION

by

John Byars Shuler

A thesis

submitted in partial fulfillment

of the requirements for the degree of

Master of Science in Hydrologic Sciences

Boise State University

August 2018

BOISE STATE UNIVERSITY GRADUATE COLLEGE

DEFENSE COMMITTEE AND FINAL READING APPROVALS

of the thesis submitted by

John Byars Shuler

Thesis Title: Evaporation Depth Controls the Relationship Between Soil Water Mobility and Soil Water Isotopic Composition

Date of Final Oral Examination: 4 May 2018

The following individuals read and discussed the thesis submitted by student John Byars Shuler, and they evaluated his presentation and response to questions during the final oral examination. They found that the student passed the final oral examination.

James P. McNamara, Ph.D.	Chair, Supervisory Committee
Shawn Benner, Ph.D.	Member, Supervisory Committee
Matthew J. Kohn, Ph.D.	Member, Supervisory Committee

The final reading approval of the thesis was granted by James P. McNamara, Ph.D., Chair of the Supervisory Committee. The thesis was approved by the Graduate College.

ACKNOWLEDGEMENTS

I would like to thank my Supervisory Committee chair, Dr. Jim McNamara, for his guidance during the completion of this thesis and his patience while I learned how to be a student again. I would also like to thank the members of my Supervisory Committee, Dr. Shawn Benner and Dr. Matt Kohn, for their invaluable input throughout the process. Without my committee's expertise, this thesis would not have been possible. I owe additional gratitude to Dr. Kohn for access to his Stable Isotope Laboratory, where I spent many late hours processing samples.

Research Scientists Samantha Evans and Pam Aishlin provided endless assistance and advice in both the lab and field and I cannot thank them enough. The list of individuals who gave their time to assist with field and lab work is too long to list here, but their selflessness and companionship was vital to the project and my sanity. The love and encouragement of my friends, family, and wife, Kathleen Pritchard, have been a steadying influence during my graduate school career and throughout my life.

Last, I would like to acknowledge the National Science Foundation and Boise State University for their financial assistance during my time at Boise State.

ABSTRACT

Recent studies of plant water uptake assume that soil water isotopic composition can be used to infer soil water mobility. However, the strength of the relationship between mobility and isotopic composition remains poorly constrained. In addition, many ecohydrologic investigations are restricted by low sampling frequencies and insufficient soil moisture and matric potential data to support assumptions of soil water mobility. We sampled bulk soil water every 14 to 21 days in hillslope and riparian profiles during the 2016 and 2017 growing seasons in a semi-arid watershed outside Boise, ID. We collected twig samples of four tree and shrub species concurrently. Plant and soil water samples extracted by cryogenic vacuum distillation were analyzed for $\delta^{2}H$ and $\delta^{18}O$ composition. We installed volumetric water content and soil matric potential sensors at five and four depths in the hillslope profile, respectively. Shallow bulk soil water became progressively enriched in both isotopes as mobility declined over the two growing seasons, particularly at the hillslope site. Strong correlations existed between isotopic composition and mobility in shallow layers but isotopic composition alone failed to predict soil water mobility. No relationship existed in deeper soil water, suggesting water loss only through transpiration and drainage. We propose that evaporation depth is a strong control on the relationship between soil water mobility and isotopic composition. Plant water isotope evolution suggests that Douglas Fir relies on deeper water sources than sagebrush or

chokecherry. These results underscore the utility of measurement of soil water mobility proxies in future ecohydrologic studies.

TABLE OF CONTENTS

LIST OF TABLES

LIST OF FIGURES

LIST OF ABBREVIATIONS AND SYMBOLS

C1E	Confluence 1 East stream gaging location on Dry Creek
C1S	Confluence 1 groundwater spring
CI	Confidence interval
Con 1	Primary field site in Dry Creek Experimental Watershed
DCEW	Dry Creek Experimental Watershed
ET	Evapotranspiration
GMWL	Global Meteoric Water Line
LMWL	Local Meteoric Water Line
VSMOW	Vienna Standard Mean Ocean Water
VWC	Volumetric water content
σ	Standard deviation

INTRODUCTION

Stable isotopes of water have aided hydrologic investigations at a variety of scales. Naturally occurring isotopes have been used in tandem or independently to explore a variety of vadose zone processes including groundwater recharge [review by Koeniger et al., 2016], infiltration and mixing [Gat and Tzur, 1967; Gazis and Feng, 2004; Stumpp and Masloszewski, 2010; Zhao et al., 2013], plant water uptake [Brunel et al., 1991; Dawson, 1996; Gaines et al., 2016; Koeniger et al., 2010], and evaporation [Allison et al., 1983; Barnes and Allison, 1988]. Some of these processes alter soil water chemistry. For instance, evaporation enriches soil water in ^{2}H and ^{18}O, two commonly used isotopic tracers.

In addition to this evaporative enrichment, soil water mobility appears to decrease in drying soils. Mobility is most commonly defined by the volumetric water content and matric potential thresholds of field capacity that differentiate mobile from immobile water. Recent studies suggest that isotopically enriched soil water exists primarily as immobile water and this assumption has influenced interpretations of plant water isotopes. However, the strength of the relationship between VWC, matric potential and soil water isotopes remains poorly constrained. In this study, we investigate the relationship between soil water mobility and soil water isotopic composition.

A breadth of hydrological, biological, and geological processes occurs in unsaturated soil layers, often referred to as the vadose zone. The hydrological fluxes that

occur in these layers are referred to collectively as the plant-soil-atmosphere continuum. Thus, the vadose zone plays a critical role in partitioning precipitation into evaporation from soils, transpiration from plants and groundwater recharge. The processes by which precipitation is routed into these fluxes have important implications for solute transport [Nimmo, 2005], streamflow and groundwater dynamics, and plant productivity [Good et al., 2015]. Consequently, watershed model performance is partially dependent upon accurate representation of water infiltration and redistribution in the vadose zone.

Infiltration is most often discussed in the context of two conceptual frameworks, translatory flow and the mobile/immobile model. Hewlett and Hibbert [1967] asserted that water previously existing in a profile is displaced by infiltrating precipitation, a process also referred to as translatory or piston flow. However, there is considerable evidence that the translatory flow model does not fully explain all infiltration processes.

In contrast to the translatory flow model, the mobile-immobile model states that some fraction of soil water is tightly bound to the soil matrix and does not actively drain [Van Genuchten and Wierenga, 1976]. In the mobile-immobile model, the soil matrix consists of larger pores through which mobile water drains and smaller pores where water is held at tensions that are not overcome by the force of gravity. Immobile water is found in these pores as well as thin films around soil aggregates [Landon et al., 1999]. Several studies found evidence of mobile and immobile domains in lab [De Smedt and Wierenga, 1984; Gaudet et al., 1977] and field studies [Gierke et al., 2016; Oerter and Bowen, 2017]. Horton and Hawkins [1964] found that a tracer pulse of infiltrating water only displaced 87% of antecedent water, suggesting that the remaining portion is relatively immobile. Good et al. [2015] analyzed a global dataset and reported considerable spatial

separation between mobile and immobile waters, estimating that only 38 % of surface runoff is derived from plant-accessible reservoirs.

Better understanding of soil water mobility is critical for constraining plant water uptake dynamics that can dominate water movement out of a watershed. Researchers explored plant uptake at least as far back as the early 18th century, with Hales' [1727] studies of plant physiology. Jasechko et al., [2013] reported that plants account for 80 – 90% of total global evapotranspiration. If plants extract immobile soil waters that maintain different isotopic compositions from mobile water, such a finding would complicate hydrologic models that represent soil water as a single reservoir.

Recent studies suggest that plants and streams may indeed return different water pools to the hydrosphere. This idea was first referred to as the 'two water worlds hypothesis' by McDonnell [2014] then renamed the 'ecohydrological compartmentalization hypothesis' by Evaristo et al. [2015]. McCutcheon et al. [2017] referred to the two hypotheses collectively as the 'ecohydrological separation hypothesis,' which is the term we utilize in this study. Evidence for ecohydrologic separation has been observed in a variety of climates including seasonally dry forest in western Oregon [Brooks et al., 2010], tropical montane forest in Mexico [Goldsmith et al., 2011] rainy temperate forest in south-central Chile [Herve-Fernandez et al., 2016], summer monsoon-dominated forest in southeastern New Mexico [Gierke et al., 2016], and Puerto Rican forest with low precipitation seasonality [Evaristo et al., 2016]. Evaristo et al. [2015] found evidence for ecohydrologic separation on a global scale, as 80 % of sites from a wide variety of biomes showed differences in plant and stream water composition.

Evaluation of the ecohydrologic separation hypothesis is commonly determined through analysis of stable isotope composition of water samples, most frequently both ^{2}H and ^{18}O ratios. In the context of the ecohydrologic separation studies mentioned previously, seasonal $\delta^{2}H$ and $\delta^{18}O$ variations in precipitation plot linearly to produce a local meteoric water line [LMWL, Rozanski et al., 1992]. Stream and ground water plot on or very close to the LMWL, with seasonal variation along the line. Soil water that has experienced evaporation plots along a soil evaporation line with a lesser slope than the LMWL. Ecohydrologic separation is considered present when vegetation plots right of the LMWL and close to the soil evaporation line, rather than on the LMWL as would be expected if plants drew upon the same water pool that eventually contributes to streamflow.

Despite growing evidence for the existence of ecohydrologic separation, several issues remain unresolved. Many field campaigns suffered from low temporal frequency of isotope sampling, particularly some of the earliest work on the subject [Brooks et al., 2010; Geris et al., 2015; Goldsmith et al., 2011]. In their review, Sprenger et al., [2016] noted that most field campaigns only sampled a few times per season and at a limited number of soil depths. Sprenger et al. [2017] demonstrated the utility of increased temporal and spatial sampling frequency in the Scottish Highlands to capture relatively weak evaporation signals in soil water.

A major implication of several ecohydrologic separation studies is that immobile soil water and soil water contributing to streamflow can be identified by the presence or absence of an evaporative signal in isotopic composition [Evaristo et al., 2016; Gierke et al., 2016; Sprenger et al., 2016]. However, few studies employ in situ soil moisture data

[Oerter and Bowen, 2017] and even fewer use data from tensiometers or matric potential sensors [Song et al., 2009; Sprenger et al., 2016] to corroborate this assumption. McCutcheon et al. [2017] demonstrated that some ecohydrologic separation research presupposes that soil water fates (plant uptake vs. drainage) can be used to identify soil water mobility, though these relationships remain poorly studied. The authors show that waters of the same mobility can differ in isotopic composition and that waters of similar isotopic composition can have differing mobility. Hence, the relationship between mobility and isotopic composition remains unclear, despite the prevailing interpretation of isotopic data.

There is a considerable need to evaluate ecohydrologic separation in semi-arid ecosystems. Despite the apparent ubiquity of ecohydrologic separation globally, 20% of the locations in Evaristo et al. [2015] showed no evidence of ecohydrologic separation. Likewise, Geris et al. [2015] reported limited evidence for ecohydrologic separation in a rainy, low energy environment in the Scottish boreal forest. Semi-arid and arid ecosystems comprise 30% of the world's land area [Peel et al., 2007], though ES-specific investigations in this environment are relatively few. Brooks et al. [2010] found evidence for ecohydrologic separation in isotopic data in western Oregon, which experiences a similar precipitation regime to our study location in southwestern Idaho. In northern California, Oshun et al. [2016] found that isotopic composition of water in saprolite layers was related to VWC and therefore matric potential, though the use of suction lysimeters limited access to water held at tensions close to plant extraction limit. McCutcheon et al. [2017] observed evidence for ecohydrologic separation across elevation and plant community gradients in Dry Creek Experimental Watershed, Idaho,

which is also the location of our field site. However, no direct connection between mobility and isotope composition was observed by the authors. McCutcheon et al. [2017] utilized VWC data present at several index sites in the watershed, but not at specific sampling sites.

The goal of this study is to define the relationship between soil water isotopic composition and soil water mobility. To improve temporal sampling frequency, we sampled soil, plant and stream water isotopes at least every 2-3 weeks during the dry-down period (April – July/August) of the 2016 and 2017 growing seasons and outside of these periods every 30-60 days. We installed VWC and matric potential sensors to identify soil water retention characteristics of our sample site and to make more informed observations of soil water mobility on isotope sampling dates. Last, we gathered detailed soil texture information in consideration of recent studies that investigate the interplay between soil texture and soil water isotopic composition [Newberry et al., 2017b; Orlowski et al., 2016; Oshun et al., 2016].

Specific objectives of this study are to:

1) Assess seasonal evolution of soil water isotopic composition in a hillslope and riparian profile.
2) Determine the relationship between soil water mobility and isotopic composition.
3) Use plant water isotopes to support observations of soil water mobility and make inferences about plant water source.

SCIENTIFIC BACKGROUND

General Soil Water Dynamics

Soil moisture is a critical control on processes in the plant-soil-atmosphere interface, influencing the fluxes of evapotranspiration and groundwater recharge. Soil moisture is frequently expressed as a unitless value representing the volume of water per unit volume soil (m^3/m^3, VWC). Closely related to VWC is water potential, which is a measure of potential energy at a given point in the subsurface. Water potential governs the ability of water to move from one area to another. Matric potential is the most important component of water potential in unsaturated soils and is frequently used to establish endpoints for water drainage and plant uptake to determine soil parameters. In unsaturated soils, soil water is held under tension or negative water potential.

Two VWC thresholds influence water fluxes in the vadose zone. The VWC at which drainage due to gravity ceases is termed field capacity [Veihmeyer and Hendrickson, 1931]. Plant wilting point was defined as the VWC at which wilting occurs in plants by Briggs and Shantz [1912]. The accuracy of these terms has been questioned as far back as Miller and McMurdie [1953] and their utility is still being assessed [Assouline and Or, 2014]. Some research has sought to determine water potential values for these parameters, since characteristic wetting and drying curves for some soils can show marked hysteresis wherein soil moisture values sometimes correspond to different water potentials [Dingman, 2015].

Precise determinations of field capacity are problematic since it is difficult to determine precisely when drainage due to gravity ends. Water potential values from -33 to -5 kPa have been suggested in the literature as the field capacity threshold, as reported by Chandler et al. [2017]. Most germane to this study, Romano and Santini [2002] established -10 kPa as the water potential corresponding to field capacity in coarse-grained soils. This value was supported by results from Chandler et al. [2017]. Constraining wilting point is difficult due to variation across plant species and soil texture. Wilting point is also complicated by the fact that incremental changes in VWC can result in relatively large changes in matric potential at the dry end of the characteristic curves. Most studies use -1500 kPa to define wilting point, [Arslan et al., 2014; Monanty et al., 2015] but there is variation about this number. Seyfried et al. [2009] used plant extraction limit in place of wilting point, since transpiration in some species stops between -3000 and -5000 kPa with no apparent wilting [Chandler et al., 2017; Seyfried et al., 2009]. We use plant extraction limit here for this reason.

Soil moisture release or characteristic curves result when VWC and matric potential for a given soil sample are measured concurrently and plotted against each other. This relationship is most often determined in a laboratory using multi-step outflow or falling-head permeability tests. However, Gribb et al. [2009] used co-located VWC and WP sensors to derive in situ characteristic curves for soils in DCEW. An alternative approach is to use grain size analysis of soil samples coupled with empirically-derived pedotransfer functions to predict the van Genuchten parameters for unsaturated flow [Gribb et al., 2009]. The resulting characteristic curves are frequently used to assess plant available water, which is defined as VWC at field capacity minus VWC at plant

extraction limit. In addition, characteristic curves can provide information about soil water mobility by constraining field capacity and plant extraction limit thresholds.

Defining Mobile and Immobile Soil Water

Varying definitions of mobile and immobile water exist in past studies and make inter-study comparisons difficult. The mobile-immobile model as originally proposed by Van Genutchen and Wieranga [1976] defines immobile water as that which does not actively drain and remains bound to the soil matrix. Landon et al. [1999] defined mobile water in temporal terms as 'water entering the soil during the most recent precipitation or irrigation event' and immobile as 'water present in soil prior to most recent precipitation or irrigation event.' Similarly, Gazis and Feng [2004] assumed that the immobile water portion is that which is not displaced after an infiltration event. These definitions may be physically accurate, but do not consider any VWC or tension thresholds to improve replicability. Zhao et al. [2013] employed a similar definition as Landon et al. [1999], but also proposed 'a more specific definition of mobile pre-event water as the water extractable with a suction lysimeter,' though this definition is problematic for reasons discussed below. McCutcheon [2015] defined the mobile-immobile threshold as water above or below field capacity which is the definition employed here.

Sampling Mobile and Immobile Water

Mobility of the sampled soil water component impacts observed isotopic content as noted by Landon et al., [1999] and Gierke et al., [2016]. The mobile portion of soil water is most frequently sampled via suction lysimeter [Beier and Hansen, 1992; Geris et al., 2017; McDonnell et al., 1991; Zhao et al., 2013]. Gierke et al., [2016] used wick samplers for the mobile portion and bulk samples to make inferences about the immobile

portion but did not employ any specific VWC thresholds for field capacity. Suction lysimeter extraction ranges frequently vary. Many suction lysimeters cannot sample water held below ~ -60 kPa, below field capacity but well above plant extraction limit. If the commonly accepted mobile-immobile threshold of -33 to -5 kPa is assumed, then studies using lysimeters set below this value extract water from both the mobile and immobile portion, assuming mobile water exists at the time of sampling. Berry et al. [2017] address this inconsistency by noting that variations in the lower limit of lysimeter extraction can lead to erroneous interpretations of ecohydrologic separation.

Sampling immobile soil water is often more problematic than sampling of mobile water. Because suction lysimeters cannot sample water held much below -60 kPa, many studies rely on destructive sampling of bulk soil water. An auger or other device is used to manually extract a plug of soil from a given depth from which water is then extracted through one of several laboratory methods discussed later. In situ assessments of field capacity and plant extraction limit thresholds are rarely used to help determine the relative mobility of a bulk soil sample. Gierke et al., [2016] used bulk samples to make inferences about immobile water but no VWC or water potential thresholds were established. In addition, bulk soil sampled above field capacity contains a mixture of both mobile and immobile portions, usually in unknown proportions [Herve-Fernandez et al., 2016]. Oshun et al. [2016] found consistent isotopic differences in mobile versus bulk soil samples in a hilly Mediterranean environment. These differences occurred along the MWL, suggesting the existence of an unsampled, highly immobile and unfractionated compartment of water. Song et al. [2009] was one of the few studies to combine stable isotope analyses with soil water potential data to more accurately assess mobility of

sampled waters. However, the basic tenets of the ecohydrologic separation hypothesis assert that isotopic signature can be used to determine infer mobility. If this is the case, then accurate observation of mobility would be unnecessary.

Water Isotope Analysis

Stable isotope distribution in the subsurface is controlled in part by stable isotope composition of precipitation. An empirical linear relationship exists between δ^2H and $\delta^{18}O$ composition in meteoric water. Rozanski et al., [1992] established a model for the relationship of these stable water isotopes globally, termed the Global Meteoric Water Line (GMWL) and defined as:

$$\delta^2H = 8.2 * \delta^{18}O + 11.27$$

Local meteorological conditions affect the relationship established by the GMWL. Therefore, a Local Meteoric Water Line (LMWL) is more commonly used in watershed isotopic analyses and often differs slightly from the GMWL in slope and intercept.

Evaporation of water can take place under equilibrium (relative humidity ≈ 100%) or non-equilibrium conditions (relative humidity < 100%). Lighter isotopologues containing ^1H and ^{16}O are preferentially evaporated, while those containing ^2H and ^{18}O are preferentially condensed. Under equilibrium conditions, a water sample experiencing evaporation would move up the GMWL, but not deviate from it. Conversely, under non-equilibrium conditions, heavier isotopologues evaporate at lower rates than lighter isotopologues relative to equilibrium conditions [Gat, 1996]. This mechanism results in

an increased accumulation of ^{18}O relative to ^{2}H in the residual water [Craig et al., 1963]. Water experiencing non-equilibrium fractionation plots to the right of the GMWL.

Soil Water Isotope Dynamics

Stable isotopes of water are increasingly used to study hydrological processes at a variety of scales but controls on isotopic composition of soil pore water remain poorly understood [McDonnell, 2014; Sprenger et al., 2016;]. These isotopes are considered conservative tracers given that the tracer is the water molecule itself. Zimmerman et al. [1967b] was among first to use stable isotopes of soil water to explore soil moisture dynamics. In their review, Sprenger et al. [2016] demonstrated that isotopic analyses are useful at the catchment, hillslope and profile scale. Uniform volumetric and isotopic input at the plot scale is assumed in most cases, though spatio-temporal variation almost certainly exists [Sprenger et al., 2016]. Generally, spatial heterogeneity in soil water isotopes is much greater in the vertical direction than horizontal [Brooks et al., 2010; Zhao et al., 2013].

Water entering shallow soil layers may experience evaporation during infiltration. Fitting a trendline to evaporated soil samples can yield a soil evaporation line with a lower slope than the MWL. Several ecohydrologic separation studies have used the soil evaporation line to infer soil source water. However, evaporation of water in a soil profile can take place under equilibrium or non-equilibrium conditions and how these processes relate to mobility remains uncertain. Furthermore, a recent study by Benettin et al. [2018] shows many shallow-angled soil evaporation lines of various source waters can result in the erroneous assumptions of a single soil evaporation line produced from source water of a single isotopic composition. Herve-Fernandez et al. [2016] observed that lysimeter-

extracted water plotted on the LMWL and bulk water did not, suggesting that evaporation from the mobile water compartment occurs under equilibrium conditions' and that non-equilibrium evaporation occurs after 'water has been adsorbed/absorbed in soil particles.' This description is analogous to first-stage and second-stage evaporation, as described by Or et al. [2013] and Dingman [2015].

The depth of evaporative influence on a soil profile is highly dependent on soil type and environmental factors. Sprenger et al. [2016], in a review of global isotope data from Evaristo et al. [2015], inferred that evaporative influence extends to 30 cm below the surface on average. Geris et al. [2015, 2017] found relatively little evidence for non-equilibrium soil water fractionation in a Scottish Highland forest. In the same wet, low-energy environment, Sprenger et al. [2017] detected limited isotopic enrichment in the upper 10 cm of the soil column. Similarly, Zhao et al. [2013] observed evaporative influence on soil water down to 10 cm in subtropical southwestern China. Studies conducted in arid environments and sandy soils report soil water evaporation as deep as ~50 cm [Oerter and Amundson, 2016]. Both Wythers et al. [1999] and Oshun et al. [2016] observed evaporative influence down to 40 cm in sandy soils and saprolitic layers. This evaporative demand increased in layers 10 cm and shallower. Rothfuss et al. [2015] reported fractionation down to only 20 cm in a lab experiment simulating ~280 days of strong evaporative conditions. Interestingly, McCutcheon et al. [2017] reported enriched isotopic composition suggesting evaporative influence down to 70 cm in an earlier study in DCEW on southerly aspects. However, the authors suggest that this effect was due to preferential uptake of lighter isotopes by certain plant species, which will be addressed later in this work.

Infiltration Mechanisms and Soil Water Isotopes

Controls on infiltration in a soil profile include soil texture [Stumpp and Maloszewski, 2010], the existence or absence of preferential flowpaths [Stumpp and Maloszewski, 2010; Beven and Germann, 2013], vegetation [Liu et al., 2015], antecedent moisture conditions [Gazis and Feng, 2004; Dahlke et al., 2012], and duration and magnitude of precipitation event [Gazis and Feng, 2004]. Infiltration is most often described in terms of two distinct end-members: piston or diffuse flow, in which water systematically moves downward in a relatively uniform wetting front [Hewlett and Hibbert, 1967] and preferential flow, in which infiltrating water bypasses upper soil layers via larger soil pores [Beven and Germann, 1982]. Myriad isotope-based studies corroborate the existence of preferential flowpaths [Mueller et al., 2014; Stumpp and Maloszewski, 2010; Gazis and Feng, 2004; Liu et al., 2015; Mathieu and Baric, 1996]. Still others found evidence for both piston and preferential flow in the same soil profile [Ma et al., 2017; review by Beven and Germann, 2013; Song et al., 2009; Mathieu and Baric, 1996]. Zhao et al. [2013] noted both preferential flow and diffuse flow in soils in southwestern China, with piston flow dominating during high antecedent moisture conditions.

Antecedent conditions and the presence of plant roots in a soil profile can alter infiltration mechanisms. In an infiltration experiment, Piayda et al. [2017] found that 20 mm water added to profiles with < 0.1 VWC penetrated only the upper ~25 cm of the soil column, though a very small amount reached below 60 cm, presumably via preferential flowpaths. Gehrels et al. [1998] found evidence for preferential flow in the root zone in both forests and grass/heathlands. Preferential flow reached to greater depths in forest but

diffuse flow dominated below the root zone in grass and heather. Zhao et al. [2013] observed the opposite effect as piston flow dominated in the grass-dominated upper soil layers and preferential flow through macropores drained soil in layers lower than 20 cm.

Recent stable isotope studies show varying degrees of mixing between mobile and immobile soil water compartments, often linked to the prevailing infiltration mechanism. Vargas et al. [2017] found strong evidence for mixing of antecedent and infiltrating soil water portions during a series of experiments with potted avocado plants. VWC was just below field capacity, but the authors made no inferences of infiltration mechanism. Gazis and Feng [2004] observed significant mixing between mobile and immobile water due to piston flow. Conversely, McDonnell et al. [1991] found existence of a poorly mixed subsurface on short time scales in small NZ watershed, despite wet soil conditions that suggest piston flow should predominate. Zhao et al. [2013] showed that isotope ratios changed significantly after infiltration events at a given depth despite little change in VWC, suggesting piston flow moving past a sensor or isotopic spatial heterogeneity. The authors also found that 'isotopic difference between lysimeter-extracted water and bulk soil water was large under low VWC, indicating that the mobile fraction was not well mixed with stationary water.' In column infiltration experiments in sand, Gouet-Kaplan et al. [2012] observed initial piston flow displacement of antecedent water. Piston flow was the predominant mechanism and lasted longer at higher initial θ. A longer and slower mixing mechanism followed, which was attributed to the formation of preferential flow paths. This two-stage mechanism was observed in field experiments including Collins et al., [2000] and Sklash et al. [1986] in Norway and New Zealand, respectively.

Isotope Sampling of Vegetation

Stable isotope studies in vegetation commonly assume that no fractionation of soil water takes place during uptake based on studies including Allison et al., [1984], Zimmerman et al. [1967a] and Zhang et al. [2010]. Studies show that sapwood, heartwood [White et al., 1985] and plant cellulose isotopic composition matched that of source water [Rodan and Ehleringer, 1999]. Likewise, evaporation from suberized stems has long been considered negligible [Geris et al., 2017 via Ehleringer and Dawson, 1992]. Brunel et al. [1991] found no significant isotopic differences in twig samples versus water from the main stem. This effect is likely due to the relative volume of xylem versus bark and phloem.

More recent studies have shown evidence of fractionation within plant tissues [Zhao et al., 2016] or selective uptake of lighter isotopes in plant water. Ellsworth and Williams [2007] found variations of up to 0.2 ‰ in $\delta^{18}O$ between bark and xylem samples and $\delta^{2}H$ variations up to 6 ‰ between the two tissues in *Prosopis velutina*, a woody xerophyte. The authors propose that symplastic uptake pathways contribute to fractionation specifically in xerophytes and halophytes. Results from Vargas et al. [2017] were interpreted to imply preferential uptake of lighter isotopes by avocado plants, leaving soil water with an enriched composition.

Plant water isotope interpretations between studies are complicated by inconsistent plant sampling procedures. Extracted plant water is frequently referred to as ‘xylem water’ even when the water’s origins include other parts of the plant in addition to xylem. Trees cores containing only xylem material are ideal [Brooks et al., 2010], but removal of phloem and other non-xylem tissues is either ignored or not noted in other

studies [Beyer et al., 2016; Herve-Fernandez et al., 2016; Goldsmith et al., 2011; McCutcheon et al., 2015; White et al., 1985]. Twig cuttings are commonly used when coring is impossible due to plant size or species growth habit. Twig cuttings are extracted with the bark removed [Brunel et al., 1991; Oerter and Bowen, 2017; Vargas et al., 2017], intact [McCutcheon et al., 2015] or not specified as removed or intact [Geris et al., 2017; Herve-Fernandez et al., 2016]. Still other studies sample transpired water [Beyer et al., 2016] or leaves [Piayda et al., 2017] and back-calculate xylem water composition.

Isotope extraction methods

Cryogenic vacuum distillation is the most commonly utilized method for extracting water from soil and plant samples in ecohydrologic separation and other studies [Brooks et al., 2010; Herve-Fernandez et al. 2016; Goldsmith et al., 2011; Koeniger et al., 2016; Zhao et al., 2013]. Araguas-Araguas et al., [1995] and West et al., [2006] showed that complete water extraction from a plant or soil sample is not necessary to achieve accurate results. However, extraction time does depend on the material in question, as plant samples require longer extraction times than soils [Jia et al., 2012; West et al., 2006]. Despite concerns about the influence of clay content on isotopic results [Orlowski et al., 2016], Newberry et al. [2017a] successfully recovered water with the same isotopic composition as spiked water in four soils with clay contents from 11.7 to 30.9 %. In the same experiment, hydrogen isotope composition was recovered from *Salix viminalis* cuttings but oxygen composition of recovered water showed a 0.84 ‰ offset from irrigation water. Questions about the accuracy of cryogenic vacuum distillation remain and are addressed further in the Discussion section. Other popular extraction methods include direct equilibration [Gazis and Feng, 2004; Mueller et al.,

2014; Sprenger et al., 2017; Wassenaar et al., 2008] and centrifugation [Gehrels et al., 1998].

METHODS

Approach

To track isotopic evolution, we sampled soil, plant and stream water isotopes from May 2016 to July 2017. We installed VWC and matric potential sensors at two locations to identify soil water retention characteristics of our sample site and to make more informed observations of soil water mobility on isotope sampling dates. Last, we gathered detailed soil texture information that was used to model soil characteristic curves for comparison to field data.

Study Site Description

Dry Creek Experimental Watershed (DCEW, Figure 1) is a 27 km^2 research catchment located approximately 16 km north of Boise, ID. Elevation ranges from 950 m at Dry Creek's outlet near Bogus Basin Road to 2130 m at Bogus Basin ski area. The main branch of Dry Creek flows generally southwest and is subject to seasonal loss of flow at lower elevations. Shingle Creek is the only perennial tributary, though multiple ephemeral streams and springs exist in winter through late spring.

DCEW has a semi-arid climate with moderately cold to cold winters and hot, dry summers [DCEW, 2017]. Average precipitation in DCEW is highly dependent on elevation, with around 400 mm falling at lower elevations and 900 mm at upper elevations [Aishlin and McNamara, 2011]. Smith [2010] noted that the majority of annual

precipitation occurs between November and April. Most winter precipitation falls as snow in upper elevations and a rain/snow mixture or rain in lower elevations of DCEW.

The Atlanta Lobe of the Idaho Batholith underlies DCEW. This Cretaceous-aged unit is approximately 75 to 85 million years old [Johnson et al., 1988]. The predominate rock type in DCEW is medium to coarse-grained fractured biotite granodiorite. Soils in DCEW form from in situ weathering of the underlying bedrock. Smith [2010] reported soil types in DCEW hillslopes as loamy sands and sands, both with high gravel contents. DCEW [2017] states that DCEW soils range from loam to sandy loam.

Vegetation communities in DCEW are dependent on aspect, elevation and proximity to the riparian zone. A sagebrush steppe community of cheatgrass (*Bromus tectorum*) and big sagebrush (*Artemisia tridentate*) dominate most aspects of lower elevations. Ponderosa pine (*Pinus ponderosa*) and Douglas fir (*Pseudotsuga menziesii*) predominate on most aspects in upper elevations with scattered populations of deciduous species such as aspen (*Populus tremuloides*) and chokecherry (*Prunus virginiana*). Middle elevations serve as an ecotone between the lowland sagebrush steppe community and conifer-dominated uplands. Riparian areas host considerably more biomass and diversity than hillslopes [McCutcheon, 2015]. Predominate riparian species include water birch (*Betula occidentalis*), yellow willow (*Salix lutea*) and Pacific willow (*Salix lucida*). Refer to McCutcheon [2015] for more detailed information regarding vegetation distribution in DCEW.

Several watershed-scale studies have quantified the contribution of discharge and ET to the water balance of DCEW. Stratton et al. [2009] applied the Soil Water Assessment Tool and found that ET accounted for 39 and 44% of precipitation in 2006

and 2007, respectively. Aishlin and McNamara [2011] used a chloride mass balance to calculate ET withdrawals as high as 70 % for the 2005-2009 water years. For water years 2002-2011, Parham [2015] used hypsometrically distributed precipitation data to estimate ET at 48% of total precipitation. Geisler [2016] noted that much of DCEW is water-limited during the growing season, and that potential ET is generally higher than actual ET.

General Description of Con 1 Study Site

For this study, we chose the Con 1 site in DCEW (Figure 2) due to its previous use in BSU ecohydrological studies and its unique vegetation communities. Con 1 is located at 1335 m at the transition between sagebrush steppe and mixed conifer-deciduous forest, which allowed us to sample plant species from both communities. We accessed Con 1 via a pullout off Bogus Basin Road near the DCEW Treeline site. From this point, Con 1 is located down a ~1.5 km trail with 250 m of elevation loss.

Stream discharge has been recorded at Con 1 since 2004 [DCEW, 2017]. Geisler [2016] installed sap flux sensors in multiple plant species on both the hillslope and in the riparian zone. A meteorological station with a tipping bucket precipitation gage was also installed by Geisler [2016] and we used these data to identify precipitation timing and magnitude from 5-10-16 to 3-31-2017. A power failure at this station occurred on 3-31-17. After this date, we used hydrometeorological data from the DCEW Treeline site where necessary.

We chose two locations for soil profiles and instrumentation installation. The first soil profile was on a ~25° north-facing hillslope ~30 m upslope from the eastern branch of Dry Creek (C1E) where we could ensure no connectivity between vegetation and the

saturated zone. The second profile was located in the riparian zone ~2 m from the north bank of C1E (riparian site). Slope was < 5° at the riparian pit.

Instrumentation

To assess VWC changes within the soil profile, we dug a 100 cm pit at the hillslope site. Digging was impractical below this point due to impenetrable rock. We inserted Campbell Scientific CS655 soil water content reflectometers into the pit wall at 5, 20, 45, 70 and 100 cm to assess changes in VWC and soil temperature over time. The CS655 sensors were connected to a Campbell Scientific CS6 data logger. At the riparian site, we dug a 25 cm soil pit. The saturated zone began at 20 cm on the installation date. CS655 VWC sensors were placed at 5 and 25 cm in the pit wall. At both sites, we took pains to backfill soil in the original layers maintained before excavation.

The CS655 sensors measured VWC every 60 seconds and the data logger averaged these readings every 15 minutes from May 10, 2016 to September 30th, 2017. The CS6 data logger compiled the averaged readings to produce time series of VWC at each sensor depth. After September 30th, 2016, we programmed sensors to take readings every five minutes and the data logger to average these readings hourly. We decreased the sampling rate due to decreased battery life with the onset of colder weather. Our observations up to this point showed that hourly measurements were sufficient to identify sub-daily trends in soil moisture, which was more than adequate for our research goals. Analytical precision of CS655 sensors is 0.05 % and VWC accuracy is ± 3 % of reading [Campbell Scientific, 2017]. The resulting soil moisture time series were further processed to account for the change in sampling frequency and the influence of daily temperature fluctuations as described below.

We acknowledge that VWC sensors placed at 5 cm likely underestimate soil moisture because the sensing volume extends slightly above the ground surface at this depth **[**Campbell Scientific, 2017]. We chose this depth to constrain infiltration timing and detect low-volume precipitation inputs rather than the most accurate volumetric measurements.

We placed Decagon MPS-6 calibrated matric potential sensors at depths of 5, 20, 45, and 70 cm in the hillslope soil pit. These depths corresponded with our four uppermost VWC sensors. We made small excavations in the pit face and placed the MPS-6 units into these openings to ensure maximum connectivity to the soil matrix. The MPS-6 units measure the moisture content of a ceramic disc with a known moisture-matric potential relationship. These moisture content sensors use changes in dielectric permittivity to determine VWC, similar to the functionality of the CS-655 VWC sensors. The range of the MPS-6 sensors is -9 kPa to -100,000 kPa. Measurement accuracy for the MPS-6 sensors is ± 10 % of the reading between -9 kPa and -100 kPa, and Decagon Devices reports good sensor-to-sensor agreement and accuracy down to -1500 kPa. Below -1500 kPa, validation with other measurement sources is difficult, but Decagon [2017] suggests that accuracy in this range is around 25%. For calibration standards and general information on the MPS-6 units, refer to Decagon [2017].

Soil Sampling for Grain Size Distribution

To investigate soil texture at the hillslope pit, we used a 245 cm^3 soil core sampler to extract three cores at each paired sensor depth on June 6, 2017. We extracted cores 3 meters downslope from the pit to avoid influencing water evaporation dynamics within the hillslope pit. We observed that root density was greatest in the upper 10 cm of the soil

profile. At the riparian site, one bulk soil sample was taken at each sensor depth. The soil core sampler was not used at the riparian site due to excessive root density throughout the profile past the water table. All soil samples were sealed in Ziploc bags and transported back to the BSU Soils Lab.

Bags were left open for one month, then placed in a 105° C oven for two days to ensure complete drying. Samples were weighed then broken up using a mortar and pestle to discourage clumping and to homogenize any root mass. Root mass was negligible in all hillslope samples except those collected at 5 cm.

We tested all soil samples for total organic carbon using the loss on ignition method. Loss on ignition is commonly used in soil studies as an inexpensive and easy way to measure organic carbon in soil samples [Ball, 1964; Goldin, 1997]. We removed a 5 g subsample from each bag and placed it in a muffle furnace at 375° C for 16 hours as described by [Robertson, 2011]. We calculated mass lost over this time to determine soil organic carbon content.

We sieved the entire soil sample (minus 5 g for loss on ignition) using the following sieve stack: 8, 4, 2, 1, .5, .250, and .125 mm. Each subset was weighed and the sub-.125 mm fraction was set aside for hydrometer analysis. We performed a 7-hour hydrometer analysis on each sample following Bouyoucos [1962] to determine silt and clay fractions. Wet sieving with a .062 mm sieve was used to separate very fine sand from silt and clay. The very fine sand fraction was dried overnight in a 105° C oven then weighed. Grain size distributions were calculated and soil textures were classified according to the USDA soil classification system [*USDA*, 1999].

The results from grain size distribution analysis were used to model water release curves using the artificial neural network Rosetta, as described by Schaap et al. [1998, 2001]. Calibration of the Rosetta network was performed using samples from temperate climate zones of the northern hemisphere. Rosetta solves for van Genuchten parameters as below [van Genuchten, 1980]:

$$\theta(h) = \theta_r + (\theta_s - \theta_r) / (1 + \left| \alpha h \right|^n)^{1-1/n}$$

where $\theta(h)$ defines the characteristic curve which relates θ [cm^3/cm^3] as a function of the soil water pressure head h [cm], also referred to as capillary pressure or matric potential [Guber and Pechepsky, 2010]. θ_r and θ_s [cm^3/cm^3] are residual and saturated water contents, while α (1/cm) and n are curve shape parameters. We compared the modeled curves to the field curves generated by the in situ VWC and MP sensors.

Liquid Water Sampling

Precipitation collection was complicated by the limited accessibility of the field site. No precipitation samples were collected in summer 2016. Precipitation sampling began in November 2016 and continued through June 2017 when possible. We used 16.5 cm diameter screened plastic funnels taped to a 500 mL bottle to prevent evaporation. Samples were collected as soon after precipitation ended as possible. If precipitation exceeded the capacity of the collector bottle or if the collector was knocked over, the remaining sample was discarded due to intra-storm variation. Pionke and DeWalle [1992] observed intra-storm variation in stable isotope composition in precipitation in

Pennsylvania. Our precipitation samples reflect net isotopic composition over a single storm cycle and do not address any intra-storm variations.

We sampled stream water at the C1E gaging station immediately adjacent to the riparian site. Twenty mL scintillation bottles were filled completely then capped for transport from the field. A small spring (C1S) enters Dry Creek near Con 1. We sampled water from this spring as above to use as a proxy for groundwater isotopic composition. C1S dried completely from late summer to late fall 2016 and we gathered no samples during this time.

Soil and Plant Sampling for Isotopic Composition

To investigate isotopic evolution within our soil profiles, we gathered soil samples beginning in May 2016. Since sampling in the sensor-soil interface was impossible, we took pains to sample within ~4 meters of the VWC and matric potential installations. We used an open-bit auger (5 cm x 20 cm) and sampled every 5 cm until we encountered impenetrable rock, usually between 70 and 100 cm at the hillslope site. We usually encountered standing water and/or impenetrable roots at 20 or 25 cm at the riparian site. One sample was taken at each depth to manage extraction and analysis time and costs, though we acknowledge some spatial heterogeneity likely exists even at this small scale as observed by Sprenger et al. [2017]. Soil samples from each depth were immediately transferred from the auger to a 19x150 mm test tube to discourage isotopic fractionation. We capped and sealed samples for transport to BSU.

At the hillslope site, we initially took cuttings from a Douglas fir and a single sagebrush plant, SB1. On 5-30-17, it was apparent that SB1 would not provide enough material through the growing season if sampled in duplicate and triplicate, so another

sagebrush, SB2 was sampled after this date. SB1 data were not used in this study. From February to July 2017 at the hillslope site, we sampled a chokecherry specimen to investigate a deciduous species. At the riparian site, cuttings were taken from a Douglas fir and water birch. Plants were sampled roughly every two weeks from May to October 2016, once a month from November 2016 to April 2017, and every two weeks from April 2017 to July 2017.

For all species, we selected mature, suberized branches to minimize any possible isotopic fractionation suspected in new growth [Ehleringer and Dawson, 1992]. Douglas fir cuttings were taken at roughly breast height. Water birch samples were taken from breast height to ~ 6 feet from tree base due to preponderance of sample-size branches in this range. Samples were cut as close to the main stem as possible, then quickly cut into ~ 1 cm pieces with the bark intact. We stored plant samples in 19x150 mm test tubes that were capped and sealed for transport to BSU.

In the field, we stored plant, soil and liquid water samples in a small cooler that contained dry ice or frozen water bottles to prevent evaporation. Upon return from the field, we immediately placed samples in a -20^0 C freezer until extraction. Precipitation, stream water and groundwater samples were stored at 4^0 C to prevent explosion of glass containers. Total time between sample collection and transfer to cold storage was no more than five hours, which minimized any evaporative effects.

Water Extraction: Cryogenic Vacuum Distillation

We extracted water from plant and soil samples using the cryogenic vacuum distillation line at Boise State University. Robin Trayler, a doctoral student, built the system in 2015 based on the extraction line described in Araguas-Araguas et al. [1995].

The system consists of eight U-shaped stainless steel units which each accommodate two 19x150 mm test tubes. Two test tubes fit tightly in each end of the unit, one containing a plant or soil sample, the other empty. Each unit is connected to a stainless steel manifold which is attached to a pump. This apparatus achieves pressures as low as 15 millitor when not in active use.

We used tweezers to remove any plant material from the soil samples. A plug of glass wool was placed in the top of each soil sample test tube to prevent any soil from being drawn into the system during pumping. Glass wool is non-reactive during extraction [Newberry et al., 2017a]. We submerged test tubes containing plant and soil samples in liquid nitrogen for two minutes to immobilize our sample before pumping. The pump system created pressures of 20-30 millitor between the sample test tube and the empty tube. Swagelock valves were closed above each unit to maintain these pressures. We placed the sample test tubes in small furnaces that maintained temperatures of 100^0 C to evaporate water within the samples. We were careful to keep furnace temperatures below 105° C to avoid possible liberation of water from soil mineral structure [Sacchi et al, 2000]. The empty test tube was submerged in liquid nitrogen for the duration of extraction. Water vapor was drawn into the empty test tube from the sample test tube where it froze to the empty test tube wall.

Plant samples were extracted for 60 minutes and soil samples for 45 minutes. These extraction times were chosen based on lab experiments by West et al. [2006], Orlowski et al. [2013] and Jia et al., [2012]. The original sample test tubes were examined after extraction was completed. We noticed a very small number (< 5) contained water that collected around the mouth of the original sample tube. We assume

this was due to loss of pressure inside these units and we discarded these samples. When extraction was completed, we removed the test tubes from liquid nitrogen and allowed them to reach room temperature until all ice had melted in the extracted water. We transferred the extracted water into 12x35 mm vials and stored them at -20^{0}C until analysis.

Plant and Soil Water Isotopic Analysis

All water samples were analyzed for isotopic composition on a ThermoFisher High Temperature Conversion Elemental Analyzer connected to a Delta V+ Isotope Ratio Mass Spectrometer. These units were housed at the BSU Stable Isotope Laboratory. Standard deviation of measurements of a reference gas for $\delta^{18}O$ and $\delta^{2}H$ was 0.08 ‰ and 0.27 ‰, respectively. We used four water standards with known $\delta^{18}O$ and $\delta^{2}H$ values during sample runs to determine instrument accuracy and repeatability of results. These standards were chosen to represent the breadth of isotopic compositions expected in our samples. Standard deviation from the four standards was 0.51, 0.41, 0.54 and 0.38 ‰ for $\delta^{18}O$ and 1.94, 2.28, 1.86, and 1.46 ‰ for $\delta^{2}H$. Isotope values are reported in parts per mil (‰) as calculated below:

$$\delta^{2}H \text{ or } \delta^{18}O = [R_{sample} / R_{VSMOW} - 1] * 1000$$

where $R_{sample} = {}^{2}H/{}^{1}H$ or ${}^{18}O/{}^{16}O$ and R_{VSMOW} is the isotope ratio of the standard, Vienna Standard Mean Ocean Water (VSMOW). VSMOW isotopic ratios are ${}^{2}H/{}^{1}H$ = 155.76 ppm and ${}^{18}O/{}^{16}O$ = 2005.20 ppm.

Isotope Data Analysis

For data visualization in dual isotope plots, we used the LMWL derived for the Treeline location by McCutcheon [2015], based on data collected and weighting factors determined by Tappa [2013] and McCutcheon [2015]:

$$\delta^2 H = 7.70 * \delta^{18} O + 4.95$$

For isotopic composition comparisons, we use line-conditioned excess (lc-excess) as described by Landwehr and Coplen [2006] and defined as:

$$\text{lc-excess} = \delta^2 H - a * \delta^{18} O - b$$

where a and b represent the slope and intercept of the LMWL. This means that lc-excess is the vertical distance from the LMWL of a sample as measured by δ^2 H deviation. Lc-excess of precipitation is 0 ‰ by definition, making it a preferable metric for assessing deviation from the MWL [Sprenger et al., 2017]. Ecohydrologic separation studies commonly employ a combination of dual-isotope plots and lc-excess, as waters can share similar lc-excess values but very different combinations of δ^2H and δ^{18}O.

VWC and matric potential temperature correction

We observed diurnal fluctuations in the VWC (Figure 3) and matric potential data. Daily increases in VWC correlated strongly with soil temperature (Figure 4), which was recorded by the same CS655 sensors. Lu et al. [2015] and Cobos and Campbell [2007] noted that diurnal fluctuations in VWC data can result from the influence of temperature

on permittivity of the soil matrix. Campbell Scientific [2017] notes that CS655 sensors first measure permittivity then use the Topp equation to derive VWC. Since VWC sensors depend upon permittivity to measure VWC, soil temperature-induced changes in permittivity can be recorded incorrectly as changes in VWC. We hypothesized that our VWC data displayed a temperature-induced diurnal signal.

To confirm our visual assessment of VWC changes over 24-hour cycles, we isolated a rainless subset of the soil moisture data from August 17th to September 28th, 2016. This subset was selected due to minimal linear trends in VWC over this period. We generated a periodogram to analyze this data subset at all sensor depths. This analysis revealed a periodicity of 24.008 hours for the 5 and 20 cm sensors (Figure 5). The periodogram showed that daily soil temperature fluctuations at the 45, 70 and 100 cm depths were too small to influence the VWC data.

We temperature-corrected the raw VWC data as described by Cobos and Campbell [2007]. This method was intended to guide temperature correction of data obtained by Decagon ECH$_2$O soil moisture sensors. Although we used CS655 sensors in this study, their functionality is similar to the ECH$_2$O sensors. Both sensor types derive VWC data from measurements of permittivity, which is temperature dependent as described above. Neither Decagon Devices nor Campbell Scientific noted either sensor to be sensitive to soil temperature changes. We feel confident that application of this temperature correction method to the CS655 data discussed here is justified.

The Cobos and Campbell [2007] method proved ineffective for temperature-correction of the diurnal signal in the MPS-6 tension data. Instead, we designed a 4th order low-pass Butterworth filter with a 40-hour cutoff period, which effectively removed

all data with a period lower than this cutoff value. Virtually no data were removed other than those with a 24-hour period as shown in Figure 6. This method eliminated the diurnal signal in the tension data (Figure 7). Inconsistencies between the original and filtered data occurred during periods of rapid wetting or drying. We considered the corrected data suitable for subsequent analysis because these periods did not coincide with isotope sampling. For more information on the use of Butterworth filters refer to Roberts and Roberts [1978].

There is speculation that diurnal fluctuations in VWC and matric potential are tied to plant water uptake during the day and hydraulic redistribution at night [Mares et al., 2016]. However, our data show an increase in VWC and matric potential during the daytime (Figures 4 and 8). This observation runs counter to the idea that plants are inducing a diurnal decrease in both VWC and matric potential due to daytime transpiration. Therefore, we feel confident that removal of diurnal signals in both datasets is justified.

VWC Data Processing and Generation of Characteristic Curves

We noticed that the 5 and 20 cm sensors reported temperatures at or below 0° C for some of the winter months. This coincided with a noticeable decrease in recorded VWC values during this period (Figure 9). As such, we removed all VWC values for which soil temperature was reported as 0.1° C or lower for any analyses that used the entire dataset. This processing step disregarded all data from the 5 cm sensor from early December 2016 to early March 2017. We also disregarded all data from the 20 cm sensor from late December to early February. The three lower sensors remained above 0° C

throughout the study period. The processed VWC data were plotted in a histogram to determine field capacity and plant extraction limit as described by Chandler et al. [2017].

We plotted VWC data against the matric potential data for each of the paired sensors to generate characteristic curves. These plots were compared to the results from Rosetta to assess their ability to produce accurate predictions of water retention behavior.

RESULTS

VWC Trends

General soil moisture trends (Figure 9) were consistent with previous observations of seasonal precipitation in the Boise Foothills (DCEW, 2017). The 5 and 20 cm sensors showed sensitivity to large-scale precipitation events. The 45, 70, and 100 cm sensors showed steady dry-down in summer, followed by steady wet-up in winter before dry-down began again in early summer 2017. A steady dry-down of all VWC sensors marked the summer months. A single significant infiltration event (July 10th, 2016) occurred between mid-May and late-September. Occasional storms of light intensity and duration (< 2 mm per hour for 1-2 hours) occurred over this period (Figure 9). However, the July 10th infiltration event only affected the 5 and 20 cm VWC sensors. Progressive wet-up of the hillslope soil profile occurred beginning in late September with the 5 and 20 cm sensors. The wetting front did not reach the 70 and 100 cm sensors until mid-winter 2017. The hillslope location was snow-covered from at least December 19th, 2016 to March 11th, 2017. All snow cover after this point was intermittent.

Riparian VWC trends differed strikingly from hillslope trends, reflecting a much wetter environment (Figure 10). Both 5 and 25 cm sensors were above 0.4 in early May 2016. The 5 cm sensor dried to 0.17 by September while the 25 cm sensor remained around 0.4 due to the influence of the water table. The 5 cm riparian VWC sensor malfunctioned from October 2016 to May 2017 while VWC increased to almost 0.45 at 25 cm over the winter months.

Estimation of Field Capacity and Plant Extraction Limit

Estimated values for field capacity and plant extraction limit derived from the frequency analysis method in Chandler et al. [2017] are shown in Figure 11 and Table 3**.** Plant extraction limit is much more clearly defined in the frequency analysis than field capacity. Plant extraction limit values from frequency analysis show mostly good agreement with those derived from in situ characteristic curves. Plant extraction limit derived from the Rosetta model were systematically higher than those from frequency analysis. Plant extraction limit from frequency analysis corresponds to the lowest VWC values recorded over the study, with values ranging from 0.01 to 0.04.

We used -33 kPa for estimating field capacity from the in situ characteristic curves since the wettest VWC values clustered around -10 kPa, making it difficult to distinguish an appropriate value. Field capacity ranged from 0.10 – 0.14 for the five sensor depths and values show good agreement with those derived from the Rosetta model, but relatively poor agreement with the values from the characteristic curves. These values appear less constrained than plant extraction limit from frequency analysis, with multiple spikes for several sensors. As noted previously, a subset of the 5 and 20 cm VWC data was removed due to complications from below freezing soil temperatures. The timing of these complications was unfortunate as VWC was expected to stabilize during this period and would have helped constrain field capacity estimates. Despite this issue, these field capacity estimations provide adequate baselines for further analysis.

VWC at the hillslope soil profile was at or above field capacity at 5, 20 and 45 cm on May 10, 2016. However, VWC at all sensor depths remained below field capacity from mid-June to mid-October. By late summer, all sensors approached plant extraction

limit. The soil profile drained quickly back to or near field capacity during infiltration events (< 1 week), even during periods when there was likely little or no transpiration, such as early spring 2017.

Matric Potential Trends

Soil matric potential generally tracked changes in VWC (Figure 9). Matric potential at 45 and 70 cm showed a very steady dry-down from -10 kPa in May 2016 to less than -5000 kPa in September 2016. Dry conditions were assumed to exist through early winter but were not recorded due to sensor failure. A very rapid increase in matric potential in December (45 cm) and February (70 cm) occurred when the wetting front reached these sensors, as corroborated by the VWC data. Summer dry-down began again in May 2017. The 5 cm and 20 cm data were more variable than the deeper sensors and experienced repeated shallow infiltration events and evaporation cycles. During summer 2016 and 2017 dry-down, matric potential decreased at a slower rate for the 5 and 20 cm sensors versus those at 45 and 70 cm, and much higher values were recorded at deeper sensors in early fall (~ -5000 kPa vs. -2000 kPa). Fall rains increased matric potential for the 5 and 20 cm sensors to ~ -10 kPa, where it remained until the summer 2017 dry-down began in May.

Grain Size Analysis and Rosetta Results

Grain size analysis showed the soils of the hillslope profile to be relatively homogenous, with low silt percentages (6-11%) and sand percentages from 87-93% (Table 4). The hillslope profile had a very thin (< 1 cm) layer of newly deposited and decomposing organic material. Organic carbon percentages were highest in the 5 cm layer at nearly 5%. The A-horizon persisted down to 40-45 cm and consisted of loamy

sand with organic carbon from 1.5 – 2.9 %. The B-horizon was weakly formed where it existed at all. Virtually no clay (1% or less) was detected in the soil samples corresponding to the locations of our sensors. Below 40-45 cm, coarse pebbles and small cobbles of the parent granitics were occasionally encountered. The 70 cm layer was mostly composed of saprolite and had organic carbon percentages at or below 1 % and contained 91-93% sand-sized particles.

Riparian soils were categorized as sands with low silt content (< 7%) and virtually no clay content (<1%). Organic carbon levels were several percentage points higher at the riparian site than at the hillslope site.

Characteristic curves generated from VWC and MP data show hysteresis in wetting and drying limbs at all depths (Figure 12). The data from 5 and 20 cm show multiple wetting and drying cycles and drying limbs do not always overlap one another. The 45 and 70-cm curves show only one wetting and one drying cycle, though these main wetting and drying limbs occupy different areas of the plot and do not overlap. Wetting curves of the two deepest sensors are characterized by large decreases in tension with very small (< 0.01) increases in VWC in winter 2017. The 5-cm curve is shifted left relative to the other sensors, likely due to underestimation of VWC as discussed previously in the Methods section.

Modelled characteristic curves from each paired-sensor depth at the hillslope location are shown in Figure 13. We attempted to isolate a steadily drying subset for each sensor depth. All modelled curves predicted lower matric potentials for a given VWC than were observed in the field data. Poor agreement between the 5 and 20 cm sensors is evident due to considerable hysteresis as we were unable to isolate a prolonged drying

period at these depths. The curves from the 45 and 70 cm depths showed much better agreement, though matric potential was consistently underestimated.

Isotopic Trends in Precipitation, Stream and Groundwater

Precipitation samples plot along the LMWL with no significant deviations as shown in Figure 14. The mean δ^2H and $\delta^{18}O$ values were -104.62 (σ = 32.44) and -14.06 (σ = 3.61), respectively. Winter samples plot lower on the MWL than do spring and early summer samples. However, they are not arranged linearly with time of precipitation. For example, the 4-9-17 rain/snow mix plots higher up the MWL than does the 6-19-17 rain event.

Like previous ecohydrologic separation studies [Bowling et al., 2016; Brooks et al., 2010; Oshun et al., 2016], stream and groundwater samples clustered tightly on the MWL and varied little seasonally (Figure 14). Mean δ^2H and $\delta^{18}O$ for stream water was -121.53 (σ = 2.74) and -16.26 (σ = 0.48), respectively. Mean δ^2H and $\delta^{18}O$ for groundwater was -122.54 (σ = 3.22) and -16.14 (σ = 0.54), respectively.

Isotopic Trends in Soil Water

Mean δ^2H and $\delta^{18}O$ for all soil water was -121.90 (σ = 16.48) and -15.47 (σ = 2.93). Mean δ^2H and $\delta^{18}O$ for hillslope soil water was -122.55 (σ = 17.53) and -15.41 (σ = 3.07). Upper soil layers showed considerably more variation relative to lower layers through summer 2016 (Figure 15). This phenomenon was also observed by Song et al., [2009], McCutcheon et al., [2017], and Zhao et al., [2013]. Lc-excess became increasingly negative in the upper 40 cm through rain-free periods in the summer months. The most negative lc-excess values in the 5 and 10 cm layers were observed in August and early September 2016. Soil layers below 40 cm mostly retain lc-excess values above

-10, indicating minimal effects from evaporation or movement of high lc-excess water lower in the soil profile. Increased precipitation and VWC in fall 2016 coincided with lc-excess values near zero at all depths from October 2016 through March 2017 (Figure 15). 5 cm water from 3-14-17 is highly enriched, possibly due to the last melt input from an enriched snowpack.

Hillslope soil profiles from late spring 2017 (Figure 15) show more isotopic variability with decreasing depth as observed by Ma et al. [2017], Song et al., [2009] and Zhao et al., [2013]. As shown in Figure 9, the months of March and April 2017 were the wettest period of the study. No soil layers have highly negative (< -20) lc-excess values until June 8th, and these are restricted to the 5 cm layer. Subsequent rain storms on June 11-12th dilute this signal in the 5 and 10 cm layers of the June 19th profile. Curiously, shallow layers (< 30 cm) occasionally show negative lc-excess values between -20 and -10 ‰.

Riparian soil water varied less than hillslope soil water in both δ^2H and $\delta^{18}O$ (Figure 16). Mean δ^2H and $\delta^{18}O$ for riparian soil water was -124.25 (σ = 11.47) and -16.36 (σ = 1.87). Evaporative enrichment was restricted to the 5 cm layer but lc-excess values never exceeded -40 ‰ (Figure 17). The enriched signal at 5 cm was absent in the December 19th profile (Figure 17). A highly enriched signal at 20 and 25 cm (lc-excess > -20) emerged on March 14th, 2017 but was absent on March 23rd, at least down to 20 cm. Riparian soil isotopes from late spring to early summer had lc-excess values generally less negative than -10 ‰ (Figure 17).

When plotted in dual isotope space, soil water from May 10th, 2016 shows definitive structure with all samples on the MWL and upper layers progressively more

enriched on the MWL than lower layers (Figure 18). Shallow soil water from late summer 2016 shows a trend along an evaporation line (Figure 18) as observed in many studies including McCutcheon et al. [2017] and simulations by Sprenger et al. [2016]. Considering the findings of Benettin et al. [2018], we refer to an apparent soil evaporation line, but make no inferences from it regarding source water. As the summer months progress, the deepest (> 70 cm) soil water generally occupies the same location on dual isotope plots, with minimal movement up and down the MWL and no movement off it (Figure 19). By 12-19-16, all soil water plots on the MWL, but without the linear structure observed on 5-10-2016. Soil water clusters at its lowest point on the MWL on February 17, 2016 and moves up the MWL from late winter through early spring. Spring 2017 was very wet, with alternating rain and quickly-melting snow storms. The resulting soil water plots change dramatically between sample dates over this period, particularly in the shallowest layers. Shallow soil water from a few sampling dates plot outside of the 95% CI for the MWL. For the March 31st and April 9th profiles (Figure 20), these unexpected compositions may be the result of precipitation that falls on a MWL with a steeper slope in the winter months as observed by Tappa [2013].

Deep (> 20 cm) riparian soil water plots near stream and groundwater for the duration of the study period (Figure 21), except for the anomaly from March 14th, 2017 (Figure 17).

Isotopic Trends in Hillslope Plant Water

Plant water isotopic evolution varied with species and sampling location (Figure 22). Mean δ^2H, $\delta^{18}O$, and lc-excess for hillslope Douglas Fir was -131.67 (σ = 5.64), -16.67 (σ = 1.23) and -8.2 (σ = 9.09). Mean δ^2H, $\delta^{18}O$, and lc-excess for hillslope

sagebrush was -125.05 (σ = 7.55), -14.33 (σ = 1.7) and -19.77 (σ = 10.36). McCutcheon et al. [2017] also noted the least negative lc-excess values in Douglas Fir versus sagebrush and deciduous species in DCEW. Dual isotope plots of plant water reveal that hillslope Douglas Fir water plots within or just below the LMWL 95% CI from May 10th to October 21st, 2016 (Figure 23), similar to the trend observed by McCutcheon et al. [2017] and Gierke et al. [2016]. Sagebrush water plots inside the LMWL 95% CI through the June 15th sampling date but moves off beginning July 9th through October 21st. Sagebrush water makes a distinct move back towards the LMWL on 12-19-17 and 2-11-17 but maintains an enriched composition.

The 2-11-17 and 4-9-17 hillslope Douglas Fir water plots off the LMWL with lc-excess values around -20 (Figure 23). Similarly, the 4-9-17 sagebrush water possesses higher lc-excess values (-33 and -35) than Douglas Fir, plotting well right of the LMWL. This date is also the first sampling date for chokecherry, which had lc-excess values below -30 as well. Mean δ^2H, δ^{18}O, and lc-excess for hillslope chokecherry was -131.81 (σ = 11.39), -15.64 (σ = 2.79) and -16.39 (σ = 11.25).

Isotopic composition of hillslope plants from April to July 2017 show a different trend than May to July 2016 (Figure 23). Douglas Fir plotted right of the LMWL and below soil water from May 8th through the end of the study period on July 6th. Sagebrush remained off the LMWL and maintained higher lc-excess values than soil water until June 19th. Chokecherry water vacillates between the LMWL and the lower envelope occupied by Douglas Fir water over this period.

Isotopic Trends in Riparian Plant Water

Mean δ^2H, $\delta^{18}O$, and lc-excess for riparian Douglas Fir was -128.27 (σ = 8.64), -16.28 (σ = 1.54), and -7.92 (σ = 9.74), respectively. Mean δ^2H and $\delta^{18}O$ for riparian water birch was -127.15 (σ = 9.31), -14.92 (σ = 2.21), and -17.22 (σ = 10.56), respectively. Dual isotope plots show that both species plot mostly right of the LMWL but within the 95% CI from 5-10-16 to 8-6-16. A weak evaporative signal emerged in water birch (lc-excess > -20 ‰) until September 30th when lc-excess averaged -27.4 (Figure 24). The strongest evaporative signal was found on 2-11-17, 4-9-17 and 5-8-17 for both species, though there was considerable variance in the Douglas Fir samples from the February 11th sampling date (Figure 24). Lc-excess from a single limb ranged from -25.83 to -0.53 ‰. In contrast to the 2016 riparian growing season, both species occupied the lower envelope below riparian soil water and right of the CI for the LMWL from 5-24-16 through 7-6-17 (Figure 24).

DISCUSSION

The Relationship Between Mobility and Isotopic Composition

To assess the relationship between isotopic composition and soil water mobility, we plotted lc-excess of soil water sampled at each sensor depth against matric potential (Figure 25). Strong positive relationships exist at 5 and 20 cm as matric potential decreases with increasingly negative lc-excess. Examination of the seasonal evolution of isotopic content and matric potential at 5 and 20 cm reveals that the highest lc-excess and lowest matric potentials at these depths occurred in late summer 2016 (Figures 26 and 27). Early summer 2017 samples suggest the continuation of this trend.

No relationship exists between isotopic composition and matric potential at the 45 and 70 cm depths (Figures 28 and 29). Matric potentials at these depths were systematically higher than shallower depths over the same period, but isotopic enrichment was restricted to lc-excess values below -20 and mostly below -10 ‰. These results are similar to the observations by McCutcheon et al. [2017] of waters with similar isotopic composition held at varying tensions.

However, defining mobility strictly by matric potential is complicated in this case by the fact that samples gathered above or near field capacity cluster around the assumed -10 kPa threshold for field capacity (Figures 26-29). Using VWC instead of matric potential to define field capacity and the mobile/immobile threshold can improve interpretation of the relationship between mobility and isotopic composition. The relationship between VWC and lc-excess varies with depth as with matric potential and

lc-excess (Figure 30). The r-squared values are slightly lower at 5 and 20 cm, but still show moderate strength. Negligible relationships exist at 45 and 70 cm.

Individual plots from each sensor depth reveal fundamental differences in the mobility/isotope relationship at a given depth. To better visualize the four possible combinations of mobility and isotopic composition, Figures 31-34 are broken into quadrants as follows: I- enriched/mobile, II- unenriched/mobile, III- unenriched/immobile, IV- enriched/immobile. At 5 cm, 7 of 17 samples are considered isotopically enriched and plot in Quadrant IV, representing high lc-excess, immobile water present during dry, hot summers at shallow depths (Figure 31). However, the existence of enriched, mobile waters in Quadrant I suggest that high lc-excess water is not always held below field capacity. In this instance, the assumption that an enriched isotopic signal is necessarily associated with immobile soil water would lead to an erroneous interpretation. Oshun et al. [2016] observed similar results in shallow soil water with some enriched water occurring when VWC ~0.20 (field capacity was not reported).

Mobile soil water with high lc-excess values (Quadrant I) is virtually absent in the 20 cm plot (Figure 32), and completely absent in the 45 and 70 cm plots (Figures 33 and 34). This could mean that the conditions for the creation of enriched mobile water (VWC > field capacity, high evaporative demand) were only present for a brief period at the 5 cm sensor during our study. This interpretation is supported by the VWC data showing rapid draining at the 5 and 20 cm sensors. Samples from 45 and 70 cm were mostly unenriched and immobile, suggesting lack of evaporative influence. These relationships

could vary significantly in other environments. Poorly drained soils with high VWC and high evaporative demand could coincide for longer periods in hot, humid climates.

Depth of Evaporative Front as a Control On Mobility and Soil Water Isotopes

The isotope data from summer 2016 suggests a maximum depth of evaporative influence of 45 cm at the hillslope site. Figure 18 supports this interpretation, showing highly enriched waters at 5 cm and lc-excess values becoming less negative with depth on August 23rd. All waters below 45 cm do not differ significantly from the LMWL. Maximum enrichment depth was < 45 cm for subsequent sampling dates in summer 2016.

The drying curves from spring 2017 support the idea of negligible evaporative influence at or below 45 cm (Figure 35). In April and early May, drying curves for the top three sensors appear to have similar slopes. Water is likely lost as drainage during periods where VWC > field capacity and transpiration is assumed to be zero or negligible. However, the two infiltration and drying events in mid-May and mid-June show the 5 and 20 cm sensors record a steeper drying curve than the 45 cm sensor. We interpret this pattern to mean that greater rates of evapotranspiration occur at 5 and 20 cm. While the relative contribution of evaporation and transpiration is not explored here, soil temperatures are much greater at the shallowest depths during the growing season, as shown in Figure 36.

The 45 cm layer is likely a lower bound for depth of the evaporative front. Transport of high lc-excess water from shallow layers to deeper layers has been observed in previous studies [Ma et al., 2017; Zhao et al., 2013], but the piston flow mechanism seems unlikely given the lack of precipitation in summer 2016. Downward transport of

enriched water to 45 cm and below is theoretically possible at the hillslope site, though all soil layers were below field capacity for much of the growing season. Twarakavi et al. [2009] note that drainage does not fully stop below field capacity. Rather, the authors found that a drainage rate -0.01 cm/day was an adequate definition upper bound for drainage below field capacity. At this low rate, enriched water would take 500 days to move only 5 cm. We believe this supports the idea that evaporative influence at the hillslope site was restricted to depths less than 45 cm, and only reached this depth in late summer. As noted previously, the soil layers below 45 cm were composed mostly of saprolite. Oshun et al. [2016] also noted that evaporative enrichment ceased below the top of a saprolite layer at their California study site. This finding underscores the utility of complementary soil texture information. While our soil profile was relatively homogenous with regards to sand content, soil water mobility relationships were profoundly affected below the saprolite layer.

Based on the previous assessment, we suggest that evaporation is the primary driver of the relationship between soil water mobility and isotopic composition at our hillslope study location. Soil water mobility generally decreases with increasingly negative lc-excess values at 5, 20 and to a lesser extent, 45 cm. This effect is strongly associated with depth of evaporative demand during the summer months. Below this critical depth, the soil water isotope/mobility relationship breaks down due to the lack of evaporated soil water.

Figure 37 further illustrates the relationship between soil water depth, evaporative enrichment, and mobility. VWC and matric potential steadily decrease in both the shallow subsurface and at depths > 70 cm from May to early September 2016. Both

layers experience similar decreases in mobility but the rate of decrease is much greater in the shallow soils than at depth. As discussed previously, we attribute this to the combined effects of evaporation and transpiration in the shallowest layers, while water loss below 70 cm occurs only via transpiration. As mobility decreases in both soil layers, only the shallow soil water becomes enriched. Furthermore, the relatively mobile, unenriched soil water from May 10th is isotopically similar to the immobile, unenriched deep soil water from late summer. If we assumed that isotopic composition implied mobility, one could erroneously conclude that both these waters were immobile.

Infiltration Mechanism and Mixing in the Subsurface

The flow mechanism associated with infiltration events can have important implications for soil water isotope profiles. The orderly placement of soil water in Figure 18 suggests that progressively warmer spring storms pushed earlier, more depleted storms deeper into the soil profile via piston flow. Unfortunately, we do not have precipitation data to confirm this explanation. VWC data from this study also suggest piston flow predominated at the hillslope site. Visual analysis of VWC data shows that shallow sensors recorded increased VWC before deeper sensors for all infiltration events (Figure 38). This is indicative of a steadily descending wetting front associated with piston flow. Similarly, the first major rains in October 2016 did not reach the 45 cm sensor until December. These initial fall infiltration events contributed to storage in the unsaturated zone rather than to stream flow or groundwater, as noted by Brooks et al. [2010] and Oshun et al. [2016] in a similar geologic environment to DCEW.

The soil water isotope data from the hillslope profile suggests that preferential flow occurred under certain conditions during our study. A 22 mm rain storm on July

10th, 2016 infiltrated through high lc-excess water at 5 and 20 cm, but VWC data suggests that this event water did not reach 45 cm. However, the soil water isotope profile from July 22nd shows significantly enriched water (lc-excess = -13.18 ‰) at 50 cm where none existed on July 9th or previous profiles (Figure 39). No other previously unenriched soil layers show this effect. Though restricted to a single depth, this enriched signal suggests the movement of some of the enriched water from the shallowest layers to greater depth via preferential flow as observed by Ma et al. [2017]. Piston flow can be disregarded since layers just above 50 cm showed no evidence of enriched water before or after infiltration. Furthermore, VWC at the 5 cm sensor increased from ~0.02 to over 0.11 during the July 10th storm. Though we do not have the precipitation isotopic composition from this storm, we would expect the shallow soil water to move much closer to the LMWL if precipitation and antecedent soil water mixed completely. Shallow soil water lc-excess does decrease but to a smaller extent than expected. This observation is consistent with the idea that very immobile water existed in shallow soil layers pre-storm and was generally not displaced. Some mixing has occurred to transmit the evaporated signal to the 50 cm layer. This effect is consistent with observations by Gazis and Feng [2014] and Piayda et al. [2017]. Gazis and Feng [2014] successfully constrained the amount of water that remained after infiltration. However, the authors were not able to assess whether antecedent water remained compartmentalized or mixed completely with event water.

A series of infiltration events occurred in similar antecedent conditions between the September 30th and October 21st sampling dates (Figure 40). The C1E meteorological station recorded 53 mm of rain over this period and only the 5 and 20 cm VWC sensors

registered this event water. High lc-excess soil water at shallow depths (< 30 cm) moved closer to the LMWL, with the shallowest layers moving the farthest. In contrast to the July rain event, no high lc-excess water appears below 30 cm. However, water from 35-65 cm shifts noticeably up the LMWL, despite no indication from the VWC data that the wetting front reached below 45 cm. Considered together, these isotopic changes in tandem suggest the combined effects of piston and preferential flow. A wetting front pushed below 20 but above 45 cm, mixing with the antecedent high lc-excess water there. Preferential flow paths could have moved event water into the 35-65 layers without first mixing with enriched shallow layers. Unfortunately, since precipitation isotopic composition is unknown, this hypothesis is difficult to verify.

The sampling scales involved in our study may help explain some of the inconsistencies noted between isotopic profiles, VWC, and matric potential data. VWC and matric potential were measured in a single profile, but not the *exact* same profile. In addition, the sampling area of the VWC sensors was much larger than for the matric potential sensors. Small scale heterogeneity could account for some discrepancies between the two data sources. Similarly, in an effort not to disturb the soil pits, we sampled isotopes on a plot scale. This almost certainly introduced some error in the form of differential soil water inputs as well as varying preferential flow paths for each profile. Mueller et al. [2014] notes that rock fragments, partially frozen soil, animal burrows can encourage preferential flow and all were observed at the hillslope site at some point in the study.

Evidence for Plant Water Source and Connections to Mobility

Assessing mobility of plant water sources is complicated by several factors in addition to those discussed above. VWC and matric potential data help establish how these parameters vary with depth, but unsampled regions in our soil profile inevitably remain. In addition, accurate matric potential thresholds for plant water uptake are extremely limited. Root physiology is more constrained for our sample species, but determination of which roots are active is not possible given our methods. Finally, soil water isotopes were sampled within several meters of study plants and not at the soil-root interface. As such, precise sampling of plant water sources was impossible.

Considering these limitations and the previously discussed relationship between isotopic composition and mobility, we are still able to make limited inferences regarding the mobility of plant water sources. Figure 23 shows that hillslope Douglas Fir samples do not deviate from the LMWL through summer 2016, and overlap with the deepest soil water (Figure 19). Matric potential at 45 and 70 cm reaches -1500 kPa by August 1st and over -3000 kPa by August 20th. Transpiration theoretically stops at this point. However, VWC at 45, 70, and 100 cm declines over this period by .007, .006, and .012 m^3/m^3, respectively. If our previously established evaporation threshold of 45 cm is accurate, we can attribute most of this decrease to transpiration since drainage at such low VWC is negligible. Sap flux data from Geisler [2016] supports this idea, as transpiration declines steadily, but continues through the summer months (Figure 41). Thus, the water source for Douglas Fir appears to be mostly deeper than 45 cm, since a limited evaporative signal is only observed in late summer and in the winter months as noted previously. Since VWC at all sampled depths was < field capacity for virtually all of summer 2016,

these data suggest that Douglas Fir utilized mostly immobile water or an unsampled source.

Hillslope sagebrush appear to be more reliant on shallow water than Douglas Fir in summer 2016. Early summer sagebrush water occupies a similar location to Douglas Fir, nearest to the deep soil water and on the LMWL. As all sensors were below field capacity as of June 15th, this water was unenriched and immobile or from an unsampled source. Figure 23 shows that sagebrush water displays increasingly negative lc-excess values beginning on July 9th. These samples sometimes overlap with evaporatively enriched shallow soil water from the same sample date (Figure 42). More often, they plot just below the soil evaporation line but off the LMWL, in between the shallow, enriched soil water and the deepest, unenriched layers. This could indicate that sagebrush utilizes both shallow and deep water sources concurrently. Matric potential at 5 and 20 cm increases due to the infiltration event on July 10th and mostly remains below -1000 until September 1st. Since matric potential deeper in the profile is much lower over this period, shallow soil water may be energetically easier to obtain. Herve-Fernandez et al. [2016] observed similar opportunistic behavior in *Eucalyptus nitens*, as these plants utilized both mobile and immobile sources, depending on season. Plants in DCEW may be conditioned to capitalize on the few infiltration events that occur in summer. Smith [2010] noted that late spring or early summer rains play an outsized role in plant uptake due to limited water storage potential in the soil.

Winter Enrichment of Plant Water

We noted winter enrichment of plant water, as observed by numerous ecohydrologic separation studies [McCutcheon et al., 2017; Oerter and Bowen, 2017].

Figure 23 shows that both sagebrush and Douglas Fir samples move off the LMWL from December 2016 to April 2017. Enriched plant water in early spring has been interpreted as residual water taken up the previous fall. The trend in these data suggests this explanation is unlikely, but increased winter sampling would be necessary to confirm this. Other research has shown that Douglas Fir can transpire in the winter months in a similar seasonally-dry environment [Link et al., 2014]. Could Douglas Fir transpire highly negative lc-excess water through the winter months? This explanation seems unlikely given that shallow bulk soil water had high VWC values through winter and early spring and the evaporative signal was absent or extremely diluted. Similar winter plant water trends have been attributed to evaporative enrichment of stagnant xylem water that remains after transpiration ceases [Bowling et al., 2016; McCutcheon et al., 2017; Oerter and Bowen, 2017]. This interpretation seems most applicable here.

Plant Water Uptake in Xerophytes

Recent studies attribute plant water deviations from the MWL to selective isotopic uptake by the plants themselves, which contradicts earlier findings by Allison et al., [1984], Zimmerman et al. [1967a] and Zhang et al. [2010]. Vargas et al. [2017] observed preferential uptake of lighter isotopes by avocado plants in a controlled lab experiment. This process would partially explain the fact that sagebrush water frequently plots below soil water in Figure 42. Ellsworth and Williams [2007] showed that selective uptake may be common among halophytes and xerophytes, including sagebrush. However, their results identified only a 1 - 2 ‰ difference between sagebrush xylem and source δ^2H, the second lowest among the 16 plants in the study. The other plants in our

study do not fall into the category of halophytes or xerophytes. This effect cannot completely explain our results.

Limitations and Issues with Cryogenic Vacuum Distillation

Cryogenic vacuum distillation remains a popular way to extract water from soils and plant matter, but recent studies have raised questions about the influence of soil type on extraction accuracy. A cryogenic vacuum distillation experiment by Orlowski et al. [2016] successfully recovered spiked water composition in a sandy soil but failed to do so in silty and clayey soils, including a loamy sand. Araguas-Araguas et al. [1995] reported similar extraction issues in clayey soils. Oerter et al. [2014] and Oshun et al. [2016] suggest that high clay content and weathered bedrock can lead to depleted free water in the subsurface due to binding of heavier isotopes with cations. The findings of Orlowski et al. [2016] are encouraging for sandy soils and somewhat concerning for sandy loam. The clay content of the sandy loam from Orlowski et al. [2016] was not reported, but sandy loams can contain up to 20 % clay. The loamy sands and sands for our study had virtually no clay at either site. Interpolation from the results from Newberry et al., [2017b] show that soils with sand components of 85% or greater results in an extraction error of -0.25 ‰ or less for $\delta^{18}O$. In addition, the modified vacuum extraction method from Koeniger et al. [2011] had good success recovering the isotopic composition of spiked water in sandy soils. We are optimistic that the miniscule clay content and high sand content of our soil samples limited any extraction issues related to soil type.

Regardless of soil type, cryogenic vacuum distillation does not ultimately sample the precise water source used by plant roots due to obvious spatial restrictions. Furthermore, the breadth of pore sizes associated with plant uptake is sometimes several

orders of magnitude smaller than that associated with cryogenic vacuum distillation methods [Evaristo et al., 2016]. New in-situ soil water sampling methods may represent a solution to this issue. Volkmann et al. [2016] and Oerter and Bowen [2017] illustrate the promise of this method, which relies on real-time isotopic measurements of soil water vapor. Though the question of isotopic heterogeneity at the pore scale remains, the ability to sample at high temporal frequency makes this advancement intriguing.

CONCLUSIONS

In this study, we assessed the relationship between soil and plant water isotopes and two indicators of soil water mobility, volumetric water content and matric potential. We found that depth of evaporation was a strong control on the relationship between soil water mobility and soil water isotopic composition. In shallow layers, soil water became evaporatively enriched as mobility declined. Deeper soil water became less mobile with no evaporative enrichment, suggesting transpiration and drainage as the only sources of water loss. Despite a strong relationship between mobility and isotopic composition in shallow layers, waters with highly negative lc-excess were frequently, but not always immobile. Conversely, immobile water took on a breadth of isotopic compositions throughout the soil profile. This indicates that soil water isotopic composition is not necessarily a reliable indicator of mobility. Our results suggest differential uptake patterns between conifers, sagebrush and deciduous species in water-stressed environments. We found that VWC and matric potential data are indispensable to constrain mobility thresholds and corroborate interpretations of soil water dynamics and plant water uptake.

Further research is necessary to explore the relationship between soil water mobility and soil water isotopic composition, particularly in regions where high VWC is concurrent with high evaporative demand. Further work to determine the influence of plant uptake on soil and xylem water isotopic content is also necessary. These relationships are vital to ongoing examinations of plant uptake and water storage in the

vadose zone. Issues with cryogenic vacuum distillation of plant and soil samples must be addressed, as this technique plays a central role in the exploration of the plant-soil-atmosphere continuum. Advances in in situ instrumentation that measures soil and xylem water isotopic content may solve problems of accuracy, sampling frequency and sample destruction associated with other extraction methods.

REFERENCES

Aishlin, P. and J. P. McNamara (2011), Bedrock infiltration and mountain block recharge accounting using chloride mass balance. *Hydrological Processes*, 25(12), 1934-1948. http://dx.doi.org/10.1002/hyp.7950

Allison, G. B., C.J. Barnes, and M.W. Hughes (1983), The distribution of deuterium and O-18 in dry soils. *Experimental Journal of Hydrology*, 64(1–4), 377–397.

Allison, G.B., C.J. Barnes, M.W. Hughes, and F.W.J. Leaney (1984), Effect of climate and vegetation on oxygen-18 and deuterium profiles in soils. Isotopes Hydrology, IAEA, Vienna, 105-122.

Araguas-Araguas L., Rozanski K, Gonfiantini R, Louvat D. (1995), Isotope effects accompanying vacuum extraction of soil water for stable isotope analyses. Journal of Hydrology168: 159– 171.

Arslan, H., M. Tasan, D. Yildirim, E.S. Koksal, and B. Cemek (2014). Predicting field capacity, wilting point, and the other physical properties of soils using hyperspectral reflectance spectroscopy: two different statistical approaches. *Environmental Monitoring and Assessment*, 186(8), 5077-5088.

Assouline, S. and D. Or (2014) The concept of field capacity revisited: Defining intrinsic static and dynamic criteria for soil internal drainage dynamics. *Water Resources Research*, 50(6), 4787-4802.

Ball, D.F. (1964), Loss-on-ignition as an estimate of organic matter and organic carbon in non-calcareous soils. *Journal of Soil Science*, 15, 84–92.

Barnes, C. and G. Allison (1988), Tracing of water movement in the unsaturated zone using stable isotopes of hydrogen and oxygen. *Journal of Hydrology*, 100, 143-176.http://dx.doi.org/10.1016/0022-1694(88)90184-9.

Beier, C. and K. Hansen (1992), Evaluation of porous cup soil-water samplers under controlled field conditions: comparison of ceramic and PTFE cups. *European Journal of Soil Science*, 43(2), 261-271.

Benettin, P., T.H.M. Volkmann, J. von Freyberg, J. Frentress, D. Penna, T. Dawson and J.W. Kirchner (2018) Effects of climatic seasonality on the isotopic composition of evaporating soil waters. *Hydrology and Earth System Sciences Discussions*, under review.

Berry, Z.C., J. Evaristo, G. Moore, M. Poca, K. Steppe, L. Verrot, H. Asbjornsen, L. Borma, M. Bretfeld, P. Hervé-Fernández, M. Seyfried, L. Schwendenmann, K. Sinacore, L. De Wispelaere, J. McDonnell (2017), The two water worlds hypothesis: Addressing multiple working hypotheses and proposing a way forward. *Ecohydrology*, e1843.10.1002/eco.1843.

Beven, K., and P. Germann (1982), Macropores and water flow in soils, Water Resources Research, 18 (5), 1311–1325. doi:10.1029/WR018i005p01311.

Beven, K., and P. Germann (2013), Macropores and water flow in soils revisited, Water Resources Research, 49, 3071–3092. doi:10.1002/wrcr.20156.

Beyer, M., P. Koeniger, M. Gaj, J.T. Hamutoko, H. Wanke, and T. Himmelsbach (2016), A deuterium-based labeling technique for the investigation of rooting depths, water uptake dynamics and unsaturated zone water transport in semiarid environments. *Journal of Hydrology*, 533, 627-643.

Bouyoucos, G.J. (1962), Hydrometer method improved for making particle size analysis of soils. Agronomy Journal, 54, 464-465.

Bowling, D.R., E.S. Schulze, and S.J. Hall (2017), Revisiting streamside trees that do not use stream water: can the two water worlds hypothesis and snowpack isotopic effects explain a missing water source? *Ecohydrology*, 10(1), 1771.

Briggs, L.J., and H. L. Shantz (1912) The wilting coefficient and its indirect determination. *Botanical Gazette*, 53 (1), 20-37.

Brooks, J.R., H.R. Barnard, R. Coulombe, and J.J. McDonnell (2010), Ecohydrologic separation of water between trees and streams in a Mediterranean climate. *Nature Geoscience* 3 (2), 100-104.

Brunel, J.P., G. R. Walker, C. D. Walker, J. C. Dighton, and A. Kennett-Smith (1991) Using stable isotopes of water to trace plant water uptake. *Stable isotopes in plant nutrition, soil fertility and environmental studies*, 543-51.

Campbell Scientific (2017), CS650 and CS655 Water Content Reflectometers: Instruction Manual.

Chandler, D., Seyfried, M., McNamara J., and Hwang, K. (2017) Inference of soil hydrologic parameters from electronic soil moisture records. *Frontiers in Earth Science,* 5.

Cobos, D. and C. Campbell (2007), Correcting temperature sensitivity of ECH2O soil moisture sensors, Decagon Devices, Pullman, WA.

Collins, R., A. Jenkins, and M.A. Harrow (2000), The contribution of old and new water to a storm hydrograph determined by tracer addition to a whole catchment, *Hydrological Processes*, 14 (4), 701-711.

Craig, H., L. I. Gordon, and Y. Horibe (1963), Isotopic exchange effects in the evaporation of water: Low-temperature experimental results, Journal of Geophysical Research, 68(17), 5079–5087. doi:10.1029/JZ068i017p05079.

Dahlke H.E., Z.M. Easton, S.W. Lyon, G. Destouni, M.T. Walter and T.S. Steenhuis (2012), Dissecting the variable source area concept - Subsurface flow pathways and water mixing processes in a hillslope. *Journal of Hydrology*, 420421, 125-141.

Dawson, T.E. (1996), Determining water use by trees and forests from isotopic, energy balance and transpiration analyses: the roles of tree size and hydraulic lift. *Tree Physiology*, 16(1-2), 263-272.

DCEW (2017), Watershed Description, Retrieved from http://earth.boisestate.edu/drycreek/watershed-description/

Decagon Devices, Inc. (2017) MPS-2 & MPS-6 Dielectric Water Potential Sensors Operator's Manual.

De Smedt, F., and P. J. Wierenga (1984), Solute transfer through columns of glass beads, *Water Resources Research*, 20(2), 225–232. doi:10.1029/WR020i002p00225.

Dingman, S.L., (2015) *Physical Hydrology*. Waveland Press.

Ehleringer, J. R. and T. E. Dawson (1992), Water uptake by plants: perspectives from stable isotope composition. *Plant, Cell & Environment*, 15: 1073–1082. doi:10.1111/j.1365-3040.1992.tb01657.x

Ellsworth, P.Z. and D.G. Williams (2007), Hydrogen isotope fractionation during water uptake by woody xerophytes. *Plant and Soil*, 291(1-2), 93-107.

Evaristo, J., S. Jasechko, J.J. McDonnell (2015), Global separation of plant transpiration from groundwater and streamflow. *Nature*, 525 (7567), 91-94.

Evaristo, J., J.J. McDonnell, M.A. Scholl, L.A. Bruijnzeel, and K.P. Chun (2016), Insights into plant water uptake from xylem-water isotope measurements in two tropical catchments with contrasting moisture conditions. *Hydrological Processes*, 30(18), 3210-3227.

Gaines, K.P., J.W. Stanley, F.C. Meinzer, K.A. McCulloh, D.R. Woodruff, W. Chen, T.S. Adams, H. Lin, and D.M. Eissenstat (2016), Reliance on shallow soil water in a mixed-hardwood forest in central Pennsylvania. *Tree Physiology*, 36 (4), 444-458. doi: 10.1093/treephys/tpv113

Gat, J.R. (1996), Oxygen and hydrogen isotopes in the hydrologic cycle. *Annual Review of Earth and Planetary Sciences*, 24(1), 225-262.

Gat, J.R. and Y. Tzur (1967), Modification of the isotopic composition of rainwater by processes which occur before groundwater recharge. *Proceedings of the Symposium on Isotopes in Hydrology*. International Atomic Energy Agency in

Co-operation with the International Union of Geodesy and Geophysics, Vienna, Austria, 4.

Gaudet, J. P., H. Jégat, G. Vachaud, and P. J. Wierenga (1977), Solute transfer, with exchange between mobile and stagnant water, through unsaturated sand. *Soil Science Society of America Journal*, 41, 665-671.doi:10.2136/sssaj1977.03615995004100040009x

Gazis, C., and X. Feng (2004), A stable isotope study of soil water: Evidence for mixing and preferential flow paths, *Geoderma*, 119(1-2),97–111. doi:10.1016/S0016-7061(03)00243-X.

Gehrels, J.C., E.M. Peeters, J.J. De Vries, and M. Dekkers (1998), The mechanism of soil water movement as inferred from ^{18}O stable isotope studies. *Hydrologic Science Journal*, 43, 579 – 594.

Geisler, E.T. (2016), Riparian zone evapotranspiration using streamflow diel signals. Boise State University Theses and Dissertations. 1090.

Geris, J., Tetzlaff, D., McDonnell, J., Anderson, J., Paton, G., and Soulsby, C. (2015) Ecohydrological separation in wet, low energy northern environments? A preliminary assessment using different soil water extraction techniques. *Hydrological Processes*, 29: 5139–5152. doi: 10.1002/hyp.10603.

Geris, J., Tetzlaff, D., McDonnell, J., and Soulsby, C. (2017) Spatial and temporal patterns of soil water storage and vegetation water use in humid northern catchments. *Science of the Total Environment*, Oct 1; 595:486-493. doi: 10.1016/j.scitotenv.2017.03.275.

Gierke, C., B. Newton, and F. Phillips (2016), Soil-water dynamics and tree water uptake in the Sacramento Mountains of New Mexico (USA): a stable isotope study, *Hydrogeology Journal*, 24(4), 805–818.

Goldin, A. (1997), Reassessing the use of loss-on-ignition for estimating organic matter content in noncalcareous soils. *Communications in Soil Science and Plant Analysis*, 18, 1111–1116.

Goldsmith, G.R., L.E. Muñoz-Villers, F. Holwerda, J.J. McDonnell, (2011) Stable isotopes reveal linkages among ecohydrological processes in a seasonally dry tropical montane cloud forest. *Ecohydrology*, 5 (6), 779-790.

Good, S.P., D. Noone, G. J. Bowen (2015) Hydrologic connectivity constrains partitioning of global terrestrial water fluxes. *Science*. Vol. 349, p 175 – 177. doi:10.1126/science.aaa5931

Gouet-Kaplan, M., G. Arye, and B. Berkowitz (2012), Interplay between resident and infiltrating water: Estimates from transient water flow and solute transport, *Journal of Hydrology*, 458, 40–50. doi:10.1016/j.jhydrol.2012.06.026.

Gribb, M. M., I. Forkutsa, A. Hansen, D.G. Chandler, and J.P. McNamara (2009), The effect of various soil hydraulic property estimates on soil moisture simulations. *Vadose Zone Journal*, 8(2), 321-331.

Guber, A.K. and Y.A. Pachepsky (2010), Multimodeling with pedotransfer functions: Documentation and user manual for PTF Calculator (CalcPTF), version 3.0. USDA Rep., Beltsville Agricultural Research Center, Beltsville, Md.

Hales, S. (1727) Vegetable Staticks: Or an Account of Some Statical Experiments on the Sap in Vegetables Being an Overview Essay Towards a Natural History of Vegetation. London, 441. Available at: https://archive.org/details/mobot31753000812500.

Hervé-Fernández, P., C. Oyarzún, C. Brumbt, D. Huygens, S. Bodé, N.E.C. Verhoest, and P. Boeckx (2016), Assessing the 'two water worlds' hypothesis and water sources for native and exotic evergreen species in south-central Chile. *Hydrological Processes*, 30, 4227–4241. doi: 10.1002/hyp.10984.

Hewlett, J.D. and A.R. Hibbert (1967), Factors Affecting the Response of Small Watersheds to Precipitation in Humid Areas. In: Sopper, W.E. and Lull, H.W., Eds., Proceedings of the International Symposium on Forest Hydrology, Pergamon, Pennsylvania State University, New York, 275-290.

Horton, J.H. and R.H. Hawkins (1964), The importance of capillary pores in rainwater percolation to the ground water table (No. DPSPU-64-30-23). Du Pont de Nemours (EI) and Co., Aiken, SC Savannah River Plant.

Jasechko, S., Z.D. Sharp, J.J. Gibson, S.J. Birks,Y. Yi, P.J. Fawcett (2013), Terrestrial water fluxes dominated by transpiration. *Nature,* 496, 347–350. doi:10.1038/nature11983

Jia, G., X. Yu, W. Deng, Y. Liu, and Y. Li (2012). Determination of minimum extraction times for water of plants and soils used in isotopic analysis. *Journal of Food, Agriculture and Environment,* 10, 1035-1040.

Johnson, K.M., R.S. Lewis, E.H. Bennett, and T.H. Kiilsgaard (1988), Cretaceous and Tertiary intrusive rocks of south-central Idaho. *Guidebook to the Geology of Central and Southern Idaho,* Idaho Geologic Survey, Bulletin 27, pp. 55-86.

Koeniger, P., M. Gaj., M. Beyer, and T. Himmelsbach (2016) Review on soil water isotope-based groundwater recharge estimations. *Hydrological Processes,* 30: 2817–2834. doi: 10.1002/hyp.10775.

Koeniger, P., C. Leibundgut, T. Link, and J.D. Marshall (2010), Stable isotopes applied as water tracers in column and field studies. *Organic Geochemistry*, 41, 31–40.

Koeniger, P., J.D. Marshall, T. Link, and A. Mulch (2011), An inexpensive, fast, and reliable method for vacuum extraction of soil and plant water for stable isotope analyses by mass spectrometry. *Rapid Communications in Mass Spectrometry*, 25(20), 3041-3048.

Landon, M.K., G.N. Delin, S.C. Komor, and C.P. Regan (1999), Comparison of the stable-isotopic composition of soil water collected from suction lysimeters, wick samplers, and cores in a sandy unsaturated zone. *Journal of Hydrology,* 224, 45–54. http://dx.doi.org/10.1016/S0022-1694(99)00120-1.

Landwehr, J. M., and T. B. Coplen (2006), Line-conditioned excess: A new method for characterizing stable hydrogen and oxygen isotope ratios in hydrologic systems, *International Conference on Isotopes in Environmental Studies*, 132–135, IAEA, Vienna.

Link, P., K. Simonin, H. Maness, J. Oshun, T. Dawson, and I. Fung (2014), Species differences in the seasonality of evergreen tree transpiration in a Mediterranean climate: Analysis of multiyear, half-hourly sap flow observations. *Water Resources Research*, 50(3), 1869-1894.

Liu, Y.H., F.D. Liu, Z. Xu, J.P. Zhang, L.X. Wang, and S.Q. An (2015), Variations of soil water isotopes and effective contribution times of precipitation and throughfall to alpine soil water, in Wolong Nature Reserve, China. *Catena*, 126, 201–208. doi.org/10.1016/j.catena.2014.11.008

Lu, M., J. Kapilaratne and I. Kaihotsu (2015), A data-driven method to remove temperature effects in TDR-measured soil water content at a Mongolian site. *Hydrological Research Letters*, 9(1), 8–13 DOI: 10.3178/hrl.9.8

Ma, B., X. Liang, S. Liu, M. Jin, J.R. Nimmo, and J. Li (2017), Evaluation of diffuse and preferential flow pathways of infiltrated precipitation and irrigation using oxygen and hydrogen isotopes, *Hydrogeology Journal*, 25(3), 675-688.

Mares, R., H.R. Barnard, , D. Mao, A. Revil, and K. Singha (2016). Examining diel patterns of soil and xylem moisture using electrical resistivity imaging. *Journal of Hydrology*, 536, 327-338.

Mathieu, R., and T. Bariac (1996), An Isotopic Study (2H and 18O) of Water Movements in Clayey Soils Under a Semiarid Climate, *Water Resources Research*, 32(4), 779–789. doi:10.1029/96WR00074.

McCutcheon, R. (2015) Stable isotopes reveal a disconnect between biotic and abiotic hydrological processes in a seasonally-dry, semi-arid watershed. Boise State University Theses and Dissertations.

McCutcheon R., J. McNamara, M. Kohn, and S. Evans (2017). An evaluation of the ecohydrological separation hypothesis in a semiarid catchment. *Hydrological Processes*, DOI: 10.1002/hyp.11052

McDonnell J. (2014), The two water worlds hypothesis: ecohydrological separation of water between streams and trees? *WIREs Water*, 1, 323-329.

McDonnell, J.J., M.K. Stewart and I.F. Owens (1991), Effect of catchment-scale subsurface mixing on stream isotopic response. *Water Resources Research*, 27(12), 3065-3073.

Miller, R.D., and J.L. McMurdie (1953). Field capacity in laboratory columns. *Soil Science Society of America Journal*, 17, 191–195.

Mohanty, M., N.K. Sinha, D.K. Painuli, K.K. Bandyopadhyay, K.M. Hati, K.S. Reddy, and R.S. Chaudhary (2015), Modelling soil water contents at field capacity and permanent wilting point using artificial neural network for Indian soils. *National Academy Science Letters*, 38(5), 373-377.

Mueller, M.H., A. Alaoui, C. Kuells, H. Leistert, K. Meusburger, C. Stumpp, M. Weiler, and C. Alewell (2014), Tracking water pathways in steep hillslopes by $\delta^{18}O$ depth profiles of soil water. *Journal of Hydrology*, 519, 340-352.

Newberry, S., D. Nelson, and A. Kahmen (2017a), Cryogenic vacuum artifacts do not affect plant water-uptake studies using stable isotope analysis, *Ecohydrology*, accepted. 10.1002/eco.1892

Newberry, S.L., U.E. Prechsl, M. Pace, and A. Kahmen (2017b), Tightly bound soil water introduces isotopic memory effects on mobile and extractable soil water pools. *Isotopes in Environmental and Health Studies*, 53(4), 368-381.

Nimmo, J. R (2005) Unsaturated zone flow processes, *Encyclopedia of Hydrological Sciences: part 13 Groundwater*, edited by: Anderson, M. G. and Bear, J., Wiley, Chichester, UK, 2299–2322.

Oerter, E.J., and R. Amundson, R. (2016), Climate controls on spatial and temporal variations in the formation of pedogenic carbonate in the western Great Basin of North America. *Geological Society of America Bulletin*, 128, 1095-1104.

Oerter E.J. and G. Bowen (2017), In situ monitoring of H and O stable isotopes in soil water reveals ecohydrologic dynamics in managed soil systems. *Ecohydrology*. e1841. https://doi.org/10.1002/eco.1841

Oerter, E., K. Finstad, J. Schaefer, G. R. Goldsmith, T. Dawson, and R. Amundson (2014), Oxygen isotope fractionation effects in soil water via interaction with

cations (Mg, Ca, K, Na) adsorbed to phyllosilicate clay minerals, *Journal of Hydrology*, 515, 1–9.

Or, D., P. Lehmann, E. Shahraeeni, and N. Shokri (2013), Advances in soil evaporation physics—A review. *Vadose Zone Journal*, 12(4).

Orlowski, N., Breuer, L., and McDonnell, J. J. (2016), Critical issues with cryogenic extraction of soil water for stable isotope analysis. *Ecohydrology*, 9: 1–5. doi: 10.1002/eco.1722.

Orlowski, N., H. Frede, N. Brüggemann and L. Breuer (2013), Validation and application of a cryogenic vacuum extraction system for soil and plant water extraction for isotope analysis. *Journal of Sensors and Sensor Systems*, 2, 179-193.

Oshun, J., W. E. Dietrich, T. E. Dawson, and I. Fung (2016), Dynamic, structured heterogeneity of water isotopes inside hillslopes, *Water Resources Research*, 52, 164–189. doi:10.1002/2015WR017485.

Parham, W. B., (2015) Spatial and temporal storage dynamics moderate the ecohydrologic significance of evapotranspiration in semi-arid, mountainous terrain. Boise State University Theses and Dissertations. 946.

Peel, M. C, B. L. Finlayson, and T. A. McMahon, (2007), Updated world map of the Koppen-Geiger climate classification, *Hydrology and Earth System Sciences*, 11, 1633–1644.

Pionke, H. B., and D. R. DeWalle (1992), Intra- and inter-storm ^{18}O trends for selected rainstorms in Pennsylvania, *Journal of Hydrology*, 138 (1–2), 131–143.doi:10.1016/0022-1694(92)90160-W.

Piayda, A., M. Dubbert, R. Siegwolf, M. Cuntz, and C. Werner (2017) Quantification of dynamic soil–vegetation feedbacks following an isotopically labelled precipitation pulse. *Biogeosciences*, 14, 2293-2306.

Radulovich, R., P. Baveye, P. Sollins and E. Solorzano (1992), Bypass water flow through unsaturated microaggregated tropical soils. *Soil Science Society of America Journal*, 56(3), 721-726.

Roberts, J. and Roberts, T.D. (1978). Use of the Butterworth low-pass filter for oceanographic data. *Journal of Geophysical Research: Oceans*, 83(C11), 5510-5514.

Robertson, Sarah (2011) Direct estimation of organic matter by loss on ignition: methods. Simon Fraser University, 1-11

Roden J.S. and J.R. Ehleringer (2000). Hydrogen and oxygen isotope ratios of tree-ring cellulose for field grown riparian trees. *Oecologia*, 123, 481–89.

Romano, N., and A. Santini (2002), Field, in Methods of Soil Analysis. Part 4, Physical Methods, Soil Science Society of America Book Series, vol. 5, edited by J. H. Dane, and G. C. Topp, 721–738, Madison, Wisconsin.

Rothfuss, Y., S. Merz, J. Vanderborght, N. Hermes, A. Weuthen, A. Pohlmeier, H. Vereecken, and N. Brüggemann (2015), Long-term and high-frequency non-destructive monitoring of water stable isotope profiles in an evaporating soil column, *Hydrology of Earth Systems Sciences*, 19(10), 4067–4080. doi:10.5194/hess-19-4067-2015

Rozanski, K., L. Araguas-Araguas, R. Gonfiantini (1992), Relation between long-termtrends of oxygen-18 isotope compostion of precipitation and climate. *Science*, 258, 981-985.

Sacchi, E., J. L. Michelot, H. Pitsch, P. Lalieux, and J. F. Aranyossy (2000), Extraction of water and solutes from argillaceous rocks for geochemical characterisation: Methods, processes, and current understanding, *Hydrogeology Journal*, 9, 17–33.

Schaap, M.G., F.L. Leij, and M.T. van Genuchten (1998). Neural network analysis for hierarchical prediction of soil hydraulic properties. *Soil Science Society of America Journal*, 62, 847–855.

Schaap, M.G., F.J. Leij, and M.T. van Genuchten (2001), Rosetta: A computer program for estimating soil hydraulic parameters with hierarchical pedo-transfer functions. Journal of Hydrology, 251, 163–176.

Seyfried, M.S., L.E. Grant, D. Marks, A. Winstral and J. McNamara (2009), Simulated soil water storage effects on streamflow generation in a mountainous snowmelt environment, Idaho, USA. *Hydrological Processes*, 23(6), 858-873.

Sklash, M.G., M.K. Stewart and A.J. Pearce (1986), Storm runoff generation in humid headwater catchments, 2. A case study of hillslope and low-order stream response*Water Resources Research*, 22 (8), 1273-1282.

Smith, T. (2010), Using soil moisture trends across topographic gradients to examine controls on semi-arid ecosystem dynamics. Boise State University Theses and Dissertations.

Song, X., S. Wang, G. Xiao, Z. Wang, X. Liu, and P. Wang (2009), A study of soil water movement combining soil water potential with stable isotopes at two sites of shallow groundwater areas in the North China Plain, *Hydrological Processes*, 23, 1376–1388. doi:10.1002/hyp.7267, 2009.

Sprenger, M., H. Leistert, K. Gimbel, and M. Weiler (2016), Illuminating hydrological processes at the soil-vegetation-atmosphere interface with water stable isotopes, *Reviews of Geophysics*, 54, 674–704. doi:10.1002/2015RG000515.

Sprenger, M., D. Tetzlaff, and C. Soulsby (2017), Stable isotopes reveal evaporation dynamics at the soil-plant-atmosphere interface of the critical zone, *Hydrology and Earth System Sciences Discussions*, in review. doi:10.5194/hess-2017-87

Stratton, B.T., V. Sridhar, M.M. Gribb, J.P. McNamara, and B. Narasimhan (2009), Modeling the spatially varying water balance processes in a semiarid mountainous watershed of Idaho. *Journal of the American Water Resources Association*, 45, 1390–1408. doi: 10.1111/j.1752-1688.2009.00371.x.

Stumpp, C. and P. Maloszewski (2010) Quantification of preferential flow and flow heterogeneities in an unsaturated soil planted with different crops using the environmental isotopes $\delta^{18}O$. *Journal of Hydrology*, 394,407 – 415.doi.org/10.1016/j.jhydrol.2010.09.014

Tappa, D.J., (2013), Isotopic composition of precipitation in a topographically complex, seasonally snow-dominated watershed: hydrometeorological controls and

variations from the Global Meteoric Water Line. *Boise State University Theses and Dissertations*. 369.

Twarakavi, N.K., M. Sakai, and J. Šimůnek (2009) An objective analysis of the dynamic nature of field capacity. *Water Resources Research*, 45(10).

USDA (1999). Soil taxonomy: a basic system of soil classification for making and interpreting soil surveys. N. R. C. Service. Washington, DC, U.S. Dept. of Agriculture, Soil Survey Staff, United States Government Printing Office. 436 - 869.

Van Genuchten, M.T. (1980), A closed-form equation for predicting the hydraulic conductivity of unsaturated soils. *Soil Science Society of America Journal*, 44, 892-898.

Van Genuchten, M. T., and P. J. Wierenga (1976), Mass transfer studies in sorbing porous media, I. Analytical solutions, *Soil Science Society of America Journal*, 40, 473-481.

Vargas, A. I., B. Schaffer, L. Yuhong, and L. d. S. L. Sternberg (2017), Testing plant use of mobile vs immobile soil water sources using stable isotope experiments. *New Phytologist*, 215, 582–594.

Veihmeyer, F.J. and A.H. Hendrickson (1931), The moisture equivalent as a measure of the field capacity of soils. *Soil Science*, 32(3), 181-194.

Volkmann, T. H. M., K. Haberer, A. Gessler and M. Weiler (2016), High-resolution isotope measurements resolve rapid ecohydrological dynamics at the soil–plant interface. *New Phytologist*, 210, 839–849. doi:10.1111/nph.13868.

Wassenaar L., M. Hendry, Chostner V., and G. Lis (2008) High resolution pore water ^{2}H and ^{18}O measurements by H_2O (liquid)-H_2O (vapor) equilibration laser spectroscopy. *Environmental Science and Technology*, 42(24), 9262–9267.

West, A.G., S.J. Patrickson, J.R. Ehleringer (2006), Water extraction times for plant and soil materials used in stable isotope analysis. *Rapid Communication in Mass Spectrometry*, 20,1317–1321.

White, J.W.C., E.R. Cook, J.R. Lawrence, and W.S. Broecker (1985), The D/H ratios of sap in trees: implications for water sources and tree ring D/H ratios. *Geochimica et Cosmochimica Acta*, 49, 237-246.

Wythers, K. R., W. K. Lauenroth, and J. M. Paruelo (1999), Bare-soil evaporation under semiarid field conditions. *Soil Science Society of America Journal*, 63, 1341-1349.

Zhang, S., X. Wen, J. Wang, G. Yu, and X. Sun (2010) The use of stable isotopes to partition evapotranspiration fluxes into evaporation and transpiration, *Acta Ecologica Sinica*, 30, 201-209. doi:10.1016/j.chnaes.2010.06.003.

Zhao, L., L. Wang, L.A. Cernusak, X. Liu, H. Xiao, M. Zhou, and S. Zhang (2016), Significant difference in hydrogen isotope composition between xylem and tissue water in Populus euphratica. *Plant, Cell & Environment*, 39(8), 1848-1857.

Zhao, P., X. Tang, P. Zhao, C. Wang, and J. Tang (2013), Identifying the water source for subsurface flow with deuterium and oxygen-18 isotopes of soil water collected from tension lysimeters and cores. *Journal of Hydrology*, 503, 1–10. 10.1016/j.jhydrol.2013.08.033

Zimmerman, U., D. Ehhalt, and K.O. Munnich (1967a), Soil Water Movement and Evapotranspiration: Changes in the Isotopic Composition of the Water. In: Isotopes in Hydrology, Proceedings of the Symposium, International Atomic Energy Agency (I.A.E.A.), Vienna, 567-584.

Zimmermann, U., K.O. Munnich, and W. Roether (1967b). Downward movement of soil moisture traced by means of hydrogen isotopes. Isotope techniques in the hydrologic cycle. *American Geophysical Union Geophysics Monograph Series*, 11, 28-36.

Table 1. Soil texture inputs for the Rosetta pedotransfer functions. HS = Hillslope Site, RS = Riparian Site.

Sample Location	Sample Depth [cm]	Mean Bulk Density [cm^3/cm^3]	Mean Sand %	Mean Silt %	Mean Clay %
HS	5	1.04	88.30	10.68	1.02
HS	20	1.03	89.36	9.72	0.92
HS	45	1.08	91.53	7.83	0.64
HS	70	1.08	92.39	6.80	0.81
RS	5	-	93.04	6.60	0.35
RS	20	-	94.25	5.75	0.00

Table 2. Rosetta model outputs of van Genuchten parameters. HS = Hillslope Site, RS = Riparian Site.

Sample Location	Sample Depth [cm]	θ_r [cm^3/cm^3]	θ_s [cm^3/cm^3]	α [1/cm]	*n*
HS	5	0.04171	0.51492	0.055294	1.756022
HS	20	0.04238	0.51991	0.056176	1.79399
HS	45	0.04386	0.50723	0.053973	2.001935
HS	70	0.04493	0.50924	0.05342	2.058638
RS	5	0.04467	0.38496	0.039218	3.197128
RS	20	0.04521	0.38464	0.038892	3.417197

Table 3. Predictions of field capacity and wilting point by frequency analysis of soil moisture data only ($FC_{freq.}$ and $PEL_{freq.}$), characteristic curves generated from in situ soil moisture plus matric potential data (FC_{cc} and PEL_{cc}) and the Rosetta pedotransfer function (FC_{ros} and PEL_{ros}) for the hillslope site. $FC_{freq.}$ and $PEL_{freq.}$ were derived from the histograms in Figure 11. FC_{cc} and FC_{ros} correspond to the VWC where matric potential = - 33 kPa and PEL_{cc} and PEL_{ros} correspond to VWC where matric potential = -1500 kPa on the drying limb of the characteristic curve in question. The 5 cm predictions from the use of soil moisture data only are likely an underestimation due to systematic underreporting of soil moisture.

	$FC_{freq.}$	FC_{cc}	FC_{ros}	$PEL_{freq.}$	PEL_{cc}	PEL_{ros}
5 cm	0.11	0.13800	0.1057	0.01	0.01178	0.07563
20 cm	0.14	0.10250	0.1291	0.03	0.03850	0.07296
45 cm	0.14	0.10450	0.1323	0.03	0.04848	0.05936
70 cm	0.11	0.08428	0.1018	0.04	0.03954	0.05786
100 cm	0.10	-	-	0.04	-	-

Table 4. Soil characteristics for VWC and matric potential sensor locations determined by the hydrometer method and loss on ignition. HS = Hillslope Site, RS = Riparian Site.

Sample Location	Sample Depth [cm]	Bulk Density [cm^3/cm^3]	Organic Carbon %	Sand %	Silt %	Clay %	USDA Classification
HS	5	0.99	4.57	88.22	10.73	1.05	Loamy Sand/Sand
HS	5	1.16	4.74	87.84	10.98	1.18	Loamy Sand/Sand
HS	5	0.95	4.84	88.83	10.33	0.84	Loamy Sand/Sand
HS	20	1.06	2.77	90.38	8.83	0.79	Loamy Sand/Sand
HS	20	1.05	2.69	87.18	11.77	1.05	Loamy Sand/Sand
HS	20	0.98	2.53	90.52	8.55	0.93	Loamy Sand/Sand
HS	45	1.24	1.50	91.18	8.10	0.71	Sand
HS	45	0.97	2.36	91.26	8.13	0.61	Sand
HS	45	1.02	2.94	92.14	7.25	0.61	Sand
HS	70	0.95	1.05	91.22	7.69	1.09	Sand
HS	70	1.04	0.79	93.32	5.93	0.75	Sand
HS	70	1.25	0.60	92.65	6.77	0.59	Sand
RS	5	-	7.64	93.04	6.60	0.35	Sand
RS	25	-	3.53	94.25	5.75	0.00	Sand

Table 5. $\delta^{2}H$, $\delta^{18}O$, and lc-excess values for all precipitation samples from Con 1.

Sample ID	δ2H [‰]	δ18O [‰]	lc-excess [‰]
RAIN/SNOW 12-16-16	-146.619	-18.704	-7.592
RAIN 2-21-17	-123.666	-15.845	-6.642
RAIN/SNOW 3-11-17	-120.094	-16.292	0.370
RAIN/SNOW 4-9-17	-77.651	-11.437	5.439
RAIN 5-7-17	-58.139	-8.751	4.274
RAIN 6-13-17	-101.569	-13.351	-3.744

Table 6. $\delta^{2}H$, $\delta^{18}O$, and lc-excess values for all Con 1 groundwater and stream samples. C1E = main branch of Con 1 stream, C1S = groundwater spring near Con 1.

Sample ID	δ2H [‰]	δ18O [‰]	lc-excess [‰]
C1E 16-05-30	-118.054	-16.235	1.971
C1E 16-06-15	-117.016	-16.363	3.995
C1E 16-06-24	-118.395	-16.393	2.842
C1E 16-07-09	-120.899	-16.152	-1.516
C1E 16-07-22	-120.694	-16.137	-1.424
C1E 16-08-06	-118.640	-15.960	-0.736
C1E 16-08-23	-120.743	-15.954	-2.883
C1E 16-09-09	-121.095	-16.235	-1.069
C1E 16-09-30	-121.092	-16.212	-1.248
C1E 16-10-21	-124.939	-17.099	1.736
C1E 16-12-13	-122.124	-15.864	-4.958
C1E 16-12-19	-122.118	-15.867	-4.927
C1E 17-01-31	-120.616	-16.317	0.042
C1E 17-02-11	-123.991	-16.940	1.457
C1E 17-02-21	-123.977	-16.975	1.745
C1E 17-02-26	-118.292	-15.971	-0.302
C1E 17-03-11	-127.915	-16.538	-5.556
C1E 17-03-14	-128.734	-16.501	-6.665
C1E 17-03-23	-122.568	-16.833	2.057
C1E 17-03-31	-122.771	-16.386	-1.582

C1E 17-04-09	-122.646	-16.854	2.141
C1E 17-04-21	-119.724	-15.077	-8.616
C1E 17-05-08	-121.767	-15.633	-6.375
C1E 17-05-24	-121.698	-15.731	-5.552
C1E 17-06-08	-119.529	-15.741	-3.304
C1E 17-06-19	-121.405	-16.063	-2.704
C1E 17-07-06	-119.741	-16.996	6.142
C1S 16-02-26	-117.527	-15.549	-2.782
C1S 16-07-22	-119.967	-15.757	-3.621
C1S 16-10-21	-118.326	-16.327	2.403
C1S 16-12-13	-119.720	-15.438	-5.835
C1S 16-12-19	-119.773	-15.432	-5.929
C1S 17-01-31	-121.658	-16.394	-0.411
C1S 17-02-11	-124.067	-16.494	-2.046
C1S 17-02-21	-129.132	-16.461	-7.369
C1S 17-03-11	-124.350	-16.752	-0.346
C1S 17-03-14	-125.243	-16.839	-0.569
C1S 17-03-23	-125.018	-16.922	0.293
C1S 17-03-31	-129.132	-16.424	-7.652
C1S 17-04-09	-123.555	-15.998	-5.357
C1S 17-04-21	-123.479	-16.958	2.114
C1S 17-05-08	-122.945	-15.982	-4.865
C1S 17-05-24	-122.433	-15.225	-10.183

C1S 17-06-08	-121.298	-15.721	-5.232
C1S 17-06-19	-120.947	-15.759	-4.591
C1S 17-07-06	-119.698	-16.167	-0.199

Table 7. $\delta^{2}H$, $\delta^{18}O$, and lc-excess values for all soil water samples. Pit 1 = hillslope site, Pit 2 = riparian site.

Sample ID	δ2H [‰]	δ18O [‰]	lc-excess [‰]
PIT 1 5 16-05-10	-90.814	-11.844	-4.595
PIT 1 5 16-05-30	-82.095	-7.515	-29.199
PIT 1 5 16-06-15	-61.508	-3.835	-36.943
PIT 1 5 16-06-24	-89.220	-6.755	-42.176
PIT 1 5 16-07-09	-95.483	-5.526	-57.899
PIT 1 5 16-07-22	-102.043	-8.193	-43.924
PIT 1 5 16-08-06	-94.017	-4.139	-67.110
PIT 1 5 16-08-23	-107.786	-3.292	-87.396
PIT 1 5 16-09-09	-103.620	-6.057	-61.947
PIT 1 5 16-09-30	-86.751	-6.287	-43.308
PIT 1 5 16-10-21	-94.126	-11.730	-8.779
PIT 1 5 16-12-19	-121.347	-15.760	-4.983
PIT 1 5 17-02-11	-142.046	-17.270	-14.054
PIT 1 5 17-02-17	-156.086	-20.648	-2.088
PIT 1 5 17-03-03	-139.580	-18.284	-3.780
PIT 1 5 17-03-14	-127.036	-12.980	-32.070
PIT 1 5 17-03-23	-93.025	-12.411	-2.441
PIT 1 5 17-03-31	-179.819	-22.267	-13.361
PIT 1 5 17-04-09	-164.942	-20.246	-14.042
PIT 1 5 17-04-21	-98.443	-12.181	-9.623

PIT 1 5 17-05-05	-145.172	-18.390	-8.557
PIT 1 5 17-05-08	-131.919	-15.201	-19.857
PIT 1 5 17-05-24	-127.534	-15.241	-15.162
PIT 1 5 17-06-08	-121.827	-12.980	-26.860
PIT 1 5 17-06-19	-112.086	-16.036	6.406
PIT 1 5 17-07-06	-105.279	-11.948	-18.254
PIT 1 10 16-05-10	-95.484	-12.670	-2.901
PIT 1 10 16-05-30	-82.094	-8.407	-22.326
PIT 1 10 16-06-24	-103.223	-10.173	-29.864
PIT 1 10 16-07-09	-84.499	-6.099	-42.502
PIT 1 10 16-07-22	-98.761	-9.221	-32.730
PIT 1 10 16-08-06	-100.469	-6.913	-52.205
PIT 1 10 16-08-23	-108.722	-6.311	-65.095
PIT 1 10 16-09-09	-106.470	-6.538	-61.096
PIT 1 10 16-09-30	-107.240	-9.712	-37.431
PIT 1 10 16-10-21	-88.919	-9.411	-21.423
PIT 1 10 16-12-19	-113.597	-14.795	-4.655
PIT 1 10 17-02-11	-146.444	-18.354	-10.110
PIT 1 10 17-02-17	-154.753	-20.462	-2.190
PIT 1 10 17-03-03	-142.156	-18.453	-5.058
PIT 1 10 17-03-23	-94.195	-13.312	3.324
PIT 1 10 17-03-31	-167.914	-20.583	-14.420
PIT 1 10 17-04-09	-173.257	-20.960	-16.862

PIT 1 10 17-05-05	-140.329	-18.425	-3.450
PIT 1 10 17-05-08	-147.999	-17.869	-15.397
PIT 1 10 17-05-24	-129.450	-15.823	-12.600
PIT 1 10 17-06-08	-132.157	-16.010	-13.868
PIT 1 10 17-06-19	-114.858	-15.768	1.572
PIT 1 10 17-07-06	-116.320	-13.533	-17.095
PIT 1 15 16-05-10	-96.783	-12.864	-2.707
PIT 1 15 16-05-30	-82.795	-9.873	-11.744
PIT 1 15 16-06-15	-82.327	-8.047	-25.331
PIT 1 15 16-06-24	-104.099	-12.639	-11.760
PIT 1 15 16-07-09	-89.005	-8.048	-32.002
PIT 1 15 16-07-22	-104.588	-10.470	-28.940
PIT 1 15 16-08-06	-116.883	-11.960	-29.767
PIT 1 15 16-08-23	-109.094	-6.593	-63.292
PIT 1 15 16-09-09	-99.194	-7.242	-48.396
PIT 1 15 16-09-30	-101.594	-9.535	-33.150
PIT 1 15 16-10-21	-87.077	-8.555	-26.176
PIT 1 15 16-12-19	-91.343	-12.110	-3.074
PIT 1 15 17-02-11	-145.563	-17.390	-16.646
PIT 1 15 17-02-17	-161.898	-20.502	-9.028
PIT 1 15 17-03-03	-134.632	-17.454	-5.226
PIT 1 15 17-03-14	-130.314	-16.275	-9.983
PIT 1 15 17-03-23	-92.556	-12.143	-4.035

PIT 1 15 17-03-31	-159.371	-19.501	-14.206
PIT 1 15 17-04-09	-179.525	-22.826	-8.765
PIT 1 15 17-04-21	-115.958	-14.961	-5.743
PIT 1 15 17-05-05	-144.678	-18.454	-7.574
PIT 1 15 17-05-08	-150.019	-17.716	-18.594
PIT 1 15 17-05-24	-131.025	-16.986	-5.218
PIT 1 15 17-06-08	-137.846	-16.846	-13.119
PIT 1 15 17-06-19	-119.259	-14.882	-9.654
PIT 1 15 17-07-06	-124.796	-14.787	-15.919
PIT 1 20 16-05-10	-90.807	-12.132	-2.368
PIT 1 20 16-05-30	-93.774	-11.606	-9.382
PIT 1 20 16-06-15	-95.854	-12.110	-7.588
PIT 1 20 16-06-24	-110.196	-14.068	-6.857
PIT 1 20 16-07-09	-94.819	-9.971	-23.017
PIT 1 20 16-07-22	-108.144	-12.369	-17.879
PIT 1 20 16-08-06	-121.741	-13.806	-20.419
PIT 1 20 16-08-23	-107.289	-7.807	-52.144
PIT 1 20 16-09-09	-104.291	-7.336	-52.774
PIT 1 20 16-09-30	-111.773	-11.703	-26.634
PIT 1 20 16-10-21	-95.733	-11.006	-15.960
PIT 1 20 16-12-19	-87.013	-11.368	-4.457
PIT 1 20 17-02-11	-148.031	-18.718	-8.894
PIT 1 20 17-02-17	-157.066	-20.821	-1.738

PIT 1 20 17-03-03	-140.695	-18.159	-5.862
PIT 1 20 17-03-14	-131.347	-16.811	-6.886
PIT 1 20 17-03-23	-101.869	-13.817	-0.458
PIT 1 20 17-03-31	-145.056	-18.477	-7.770
PIT 1 20 17-04-09	-171.037	-21.525	-10.287
PIT 1 20 17-04-21	-129.025	-16.196	-9.303
PIT 1 20 17-05-05	-123.643	-16.440	-2.043
PIT 1 20 17-05-08	-138.061	-16.596	-15.260
PIT 1 20 17-05-24	-123.051	-16.033	-4.581
PIT 1 20 17-06-08	-143.390	-17.173	-16.147
PIT 1 20 17-06-19	-118.974	-14.279	-14.007
PIT 1 20 17-07-06	-125.607	-14.037	-22.500
PIT 1 25 16-05-10	-103.987	-13.132	-7.853
PIT 1 25 16-05-30	-101.676	-12.684	-8.987
PIT 1 25 16-06-15	-99.366	-12.737	-6.268
PIT 1 25 16-06-24	-103.399	-13.408	-5.136
PIT 1 25 16-07-09	-97.767	-11.686	-12.760
PIT 1 25 16-07-22	-109.737	-12.159	-21.092
PIT 1 25 16-08-06	-118.503	-14.828	-9.307
PIT 1 25 16-08-23	-111.588	-11.683	-26.604
PIT 1 25 16-09-09	-113.946	-9.039	-49.318
PIT 1 25 16-09-30	-116.149	-12.961	-21.328
PIT 1 25 16-10-21	-99.483	-11.559	-15.458

PIT 1 25 16-12-19	-89.898	-11.727	-4.574
PIT 1 25 17-02-11	-154.477	-19.334	-10.598
PIT 1 25 17-02-17	-161.366	-20.554	-8.094
PIT 1 25 17-03-03	-139.367	-18.330	-3.213
PIT 1 25 17-03-14	-125.896	-16.270	-5.600
PIT 1 25 17-03-23	-119.152	-14.388	-13.345
PIT 1 25 17-03-31	-135.560	-17.369	-6.804
PIT 1 25 17-04-09	-163.348	-20.149	-13.191
PIT 1 25 17-04-21	-127.746	-15.744	-11.500
PIT 1 25 17-05-05	-124.850	-16.974	0.864
PIT 1 25 17-05-08	-140.907	-16.695	-17.339
PIT 1 25 17-05-24	-122.335	-16.104	-3.323
PIT 1 25 17-06-08	-137.887	-17.360	-9.201
PIT 1 25 17-06-19	-120.238	-14.101	-16.645
PIT 1 25 17-07-06	-133.129	-18.108	1.316
PIT 1 30 16-05-10	-106.003	-14.268	-1.122
PIT 1 30 16-05-30	-98.514	-12.420	-7.854
PIT 1 30 16-06-15	-102.350	-13.170	-5.919
PIT 1 30 16-06-24	-105.107	-14.063	-1.803
PIT 1 30 16-07-09	-102.905	-11.825	-16.831
PIT 1 30 16-07-22	-117.112	-12.985	-22.108
PIT 1 30 16-08-06	-110.911	-14.199	-6.561
PIT 1 30 16-08-23	-116.001	-12.687	-23.291

PIT 1 30 16-09-09	-129.632	-15.428	-15.818
PIT 1 30 16-09-30	-127.805	-16.581	-5.118
PIT 1 30 16-10-21	-104.385	-12.649	-11.964
PIT 1 30 16-12-19	-87.931	-11.463	-4.640
PIT 1 30 17-02-11	-151.073	-19.295	-7.495
PIT 1 30 17-02-17	-153.184	-20.242	-2.315
PIT 1 30 17-03-03	-140.385	-18.521	-2.762
PIT 1 30 17-03-14	-129.633	-16.293	-9.163
PIT 1 30 17-03-23	-123.539	-16.044	-4.988
PIT 1 30 17-03-31	-134.881	-17.296	-6.688
PIT 1 30 17-04-09	-159.936	-19.611	-13.920
PIT 1 30 17-04-21	-137.303	-16.897	-12.179
PIT 1 30 17-05-05	-126.693	-16.319	-6.023
PIT 1 30 17-05-08	-132.434	-16.335	-11.639
PIT 1 30 17-05-24	-123.085	-15.542	-8.396
PIT 1 30 17-06-08	-136.212	-16.567	-13.635
PIT 1 30 17-07-06	-131.300	-17.279	-3.238
PIT 1 35 16-05-10	-112.706	-14.970	-2.418
PIT 1 35 16-05-30	-99.074	-12.588	-7.122
PIT 1 35 16-06-15	-104.744	-13.898	-2.714
PIT 1 35 16-06-24	-102.814	-13.866	-1.027
PIT 1 35 16-07-09	-112.209	-12.908	-17.793
PIT 1 35 16-07-22	-127.210	-14.843	-17.898

PIT 1 35 16-08-06	-109.449	-12.249	-20.106
PIT 1 35 16-08-23	-118.351	-14.210	-13.914
PIT 1 35 16-09-09	-119.450	-12.721	-26.479
PIT 1 35 16-09-30	-127.417	-16.849	-2.664
PIT 1 35 16-10-21	-106.642	-12.161	-17.978
PIT 1 35 16-12-19	-91.165	-12.164	-2.478
PIT 1 35 17-02-11	-145.212	-18.317	-9.164
PIT 1 35 17-03-03	-143.242	-18.421	-6.393
PIT 1 35 17-03-14	-130.546	-16.816	-6.050
PIT 1 35 17-03-23	-121.000	-15.849	-3.949
PIT 1 35 17-03-31	-118.992	-15.306	-6.116
PIT 1 35 17-04-09	-149.601	-19.006	-8.248
PIT 1 35 17-04-21	-141.950	-18.324	-5.848
PIT 1 35 17-05-08	-124.150	-15.484	-9.911
PIT 1 35 17-05-24	-119.384	-15.214	-7.221
PIT 1 35 17-06-08	-136.038	-15.002	-25.503
PIT 1 35 17-06-19	-119.607	-16.963	6.019
PIT 1 35 17-07-06	-132.845	-17.835	-0.506
PIT 1 40 16-05-10	-104.388	-13.889	-2.426
PIT 1 40 16-05-30	-104.192	-13.855	-2.488
PIT 1 40 16-06-15	-105.371	-13.873	-3.532
PIT 1 40 16-06-24	-102.611	-14.141	1.295
PIT 1 40 16-07-09	-109.307	-13.447	-10.748

PIT 1 40 16-07-22	-122.660	-14.672	-14.672
PIT 1 40 16-08-06	-105.629	-14.683	2.444
PIT 1 40 16-08-23	-121.533	-15.035	-10.745
PIT 1 40 16-09-09	-125.364	-15.921	-7.760
PIT 1 40 16-09-30	-132.669	-17.510	-2.833
PIT 1 40 16-10-21	-108.673	-14.007	-5.799
PIT 1 40 16-12-19	-87.518	-11.507	-3.887
PIT 1 40 17-02-11	-136.590	-18.152	-1.806
PIT 1 40 17-02-17	-153.008	-20.504	-0.122
PIT 1 40 17-03-03	-136.020	-18.012	-2.316
PIT 1 40 17-03-14	-125.008	-15.823	-8.152
PIT 1 40 17-03-23	-128.765	-16.535	-6.428
PIT 1 40 17-03-31	-116.357	-15.109	-5.002
PIT 1 40 17-04-09	-136.594	-16.397	-15.322
PIT 1 40 17-04-21	-132.129	-16.782	-7.896
PIT 1 40 17-05-05	-127.281	-17.792	4.726
PIT 1 40 17-05-08	-125.748	-15.462	-11.671
PIT 1 40 17-05-24	-113.219	-14.668	-5.256
PIT 1 40 17-06-08	-135.571	-16.860	-10.738
PIT 1 40 17-06-19	-124.434	-15.458	-10.395
PIT 1 40 17-07-06	-132.656	-16.664	-9.328
PIT 1 45 16-05-10	-115.833	-15.330	-2.779
PIT 1 45 16-05-30	-111.645	-14.543	-4.649

PIT 1 45 16-06-15	-99.433	-13.269	-2.243
PIT 1 45 16-06-24	-110.931	-15.291	1.828
PIT 1 45 16-07-09	-111.249	-13.575	-11.700
PIT 1 45 16-07-22	-123.269	-14.423	-17.193
PIT 1 45 16-08-06	-111.361	-14.641	-3.610
PIT 1 45 16-08-23	-116.352	-14.345	-10.880
PIT 1 45 16-09-09	-122.537	-16.169	-3.020
PIT 1 45 16-09-30	-131.703	-16.945	-6.215
PIT 1 45 16-10-21	-110.789	-14.464	-4.398
PIT 1 45 16-12-19	-97.100	-12.650	-4.671
PIT 1 45 17-02-11	-137.503	-18.206	-2.308
PIT 1 45 17-02-17	-153.280	-20.273	-2.168
PIT 1 45 17-03-03	-140.092	-18.269	-4.413
PIT 1 45 17-03-14	-129.040	-16.958	-3.446
PIT 1 45 17-03-23	-130.995	-16.634	-7.901
PIT 1 45 17-03-31	-98.078	-12.642	-5.712
PIT 1 45 17-04-09	-139.008	-17.597	-8.496
PIT 1 45 17-04-21	-135.869	-17.302	-7.628
PIT 1 45 17-05-05	-113.224	-14.450	-6.940
PIT 1 45 17-05-08	-125.440	-15.169	-13.626
PIT 1 45 17-05-24	-114.052	-14.483	-7.514
PIT 1 45 17-06-08	-132.885	-15.588	-17.839
PIT 1 45 17-06-19	-125.757	-16.908	-0.556

PIT 1 45 17-07-06	-133.132	-17.235	-5.413
PIT 1 50 16-05-10	-122.837	-16.314	-2.203
PIT 1 50 16-05-30	-114.908	-14.902	-5.146
PIT 1 50 16-06-15	-108.186	-14.437	-2.004
PIT 1 50 16-06-24	-113.130	-15.269	-0.545
PIT 1 50 16-07-09	-111.083	-13.460	-12.420
PIT 1 50 16-07-22	-117.195	-12.672	-24.602
PIT 1 50 16-08-06	-113.932	-15.144	-2.310
PIT 1 50 16-08-23	-131.048	-17.667	0.001
PIT 1 50 16-09-09	-117.381	-16.191	2.306
PIT 1 50 16-09-30	-137.141	-18.237	-1.702
PIT 1 50 16-10-21	-108.460	-14.219	-3.955
PIT 1 50 16-12-19	-87.000	-11.449	-3.817
PIT 1 50 17-02-11	-134.167	-17.941	-1.012
PIT 1 50 17-02-17	-149.525	-19.620	-3.444
PIT 1 50 17-03-03	-142.988	-17.875	-10.340
PIT 1 50 17-03-14	-130.901	-17.390	-1.984
PIT 1 50 17-03-23	-137.091	-17.458	-7.651
PIT 1 50 17-03-31	-100.854	-13.020	-5.580
PIT 1 50 17-04-09	-133.150	-17.464	-3.664
PIT 1 50 17-04-21	-134.473	-17.502	-4.693
PIT 1 50 17-05-05	-116.456	-15.283	-3.763
PIT 1 50 17-05-08	-124.998	-15.694	-9.139

PIT 1 50 17-05-24	-113.061	-14.781	-4.230
PIT 1 50 17-06-08	-130.317	-16.662	-7.003
PIT 1 50 17-06-19	-121.753	-15.312	-8.837
PIT 1 50 17-07-06	-134.313	-17.080	-7.783
PIT 1 55 16-05-10	-131.147	-17.826	1.124
PIT 1 55 16-05-30	-114.163	-14.960	-3.952
PIT 1 55 16-06-15	-116.288	-15.567	-1.409
PIT 1 55 16-06-24	-119.058	-15.994	-0.891
PIT 1 55 16-07-09	-121.089	-14.401	-15.186
PIT 1 55 16-07-22	-127.613	-14.763	-18.918
PIT 1 55 16-08-06	-116.142	-15.280	-3.467
PIT 1 55 16-08-23	-125.904	-16.189	-6.235
PIT 1 55 16-09-09	-120.950	-16.246	-0.840
PIT 1 55 16-09-30	-132.243	-17.501	-2.471
PIT 1 55 16-10-21	-114.240	-15.096	-2.983
PIT 1 55 16-12-19	-87.838	-11.473	-4.470
PIT 1 55 17-02-11	-132.178	-17.738	-0.586
PIT 1 55 17-02-17	-144.929	-19.505	0.264
PIT 1 55 17-03-03	-137.033	-18.037	-3.135
PIT 1 55 17-03-14	-129.614	-16.622	-6.613
PIT 1 55 17-03-23	-133.485	-16.698	-9.895
PIT 1 55 17-03-31	-99.473	-13.191	-2.885
PIT 1 55 17-04-09	-135.806	-17.351	-7.190

PIT 1 55 17-05-05	-128.939	-17.556	1.258
PIT 1 55 17-05-08	-121.478	-15.519	-6.967
PIT 1 55 17-05-24	-117.376	-15.453	-3.369
PIT 1 55 17-06-08	-129.645	-16.661	-6.342
PIT 1 55 17-06-19	-126.110	-17.075	0.378
PIT 1 55 17-07-06	-136.155	-17.494	-6.443
PIT 1 60 16-05-10	-122.209	-16.506	-0.102
PIT 1 60 16-05-30	-117.137	-15.184	-5.202
PIT 1 60 16-06-15	-110.343	-14.580	-3.061
PIT 1 60 16-07-09	-120.142	-14.262	-15.307
PIT 1 60 16-07-22	-123.037	-14.332	-17.661
PIT 1 60 16-08-06	-116.915	-15.267	-4.345
PIT 1 60 16-08-23	-125.212	-16.651	-1.984
PIT 1 60 16-09-09	-153.978	-21.663	7.828
PIT 1 60 16-09-30	-132.026	-17.620	-1.337
PIT 1 60 16-10-21	-114.855	-15.175	-2.994
PIT 1 60 16-12-19	-92.528	-12.212	-3.470
PIT 1 60 17-02-11	-128.763	-16.942	-3.300
PIT 1 60 17-02-17	-149.675	-19.785	-2.321
PIT 1 60 17-03-03	-139.581	-18.213	-4.329
PIT 1 60 17-03-14	-128.656	-16.643	-5.495
PIT 1 60 17-03-23	-134.889	-17.277	-6.844
PIT 1 60 17-03-31	-102.303	-13.038	-6.888

PIT 1 60 17-04-21	-133.075	-16.450	-11.398
PIT 1 60 17-05-05	-125.054	-16.023	-6.659
PIT 1 60 17-05-08	-120.646	-15.071	-9.583
PIT 1 60 17-05-24	-119.304	-15.083	-8.148
PIT 1 60 17-06-08	-127.801	-15.346	-14.624
PIT 1 60 17-06-19	-130.278	-15.758	-13.926
PIT 1 60 17-07-06	-143.197	-17.770	-11.359
PIT 1 65 16-05-10	-124.002	-16.864	0.862
PIT 1 65 16-05-30	-121.278	-15.717	-5.238
PIT 1 65 16-06-15	-112.636	-15.265	-0.077
PIT 1 65 16-06-24	-116.952	-15.981	1.120
PIT 1 65 16-07-09	-116.582	-14.012	-13.672
PIT 1 65 16-07-22	-119.669	-13.455	-21.048
PIT 1 65 16-08-06	-115.556	-15.045	-4.690
PIT 1 65 16-08-23	-122.942	-16.034	-4.464
PIT 1 65 16-09-09	-131.236	-16.169	-11.719
PIT 1 65 16-09-30	-135.717	-18.152	-0.934
PIT 1 65 16-10-21	-115.868	-15.082	-4.716
PIT 1 65 17-02-11	-124.976	-16.657	-1.705
PIT 1 65 17-03-03	-137.335	-18.168	-2.430
PIT 1 65 17-03-14	-137.914	-17.936	-4.796
PIT 1 65 17-03-31	-108.007	-14.208	-3.586
PIT 1 65 17-04-21	-133.706	-17.260	-5.795

PIT 1 65 17-05-05	-133.385	-17.035	-7.206
PIT 1 65 17-05-08	-123.050	-15.578	-8.082
PIT 1 65 17-05-24	-127.204	-16.699	-3.605
PIT 1 65 17-06-08	-124.596	-15.137	-13.025
PIT 1 65 17-06-19	-133.731	-16.832	-9.111
PIT 1 65 17-07-06	-139.886	-18.025	-6.081
PIT 1 70 16-05-10	-127.943	-17.447	1.409
PIT 1 70 16-05-30	-116.606	-15.414	-2.901
PIT 1 70 16-06-15	-124.609	-16.522	-2.377
PIT 1 70 16-06-24	-125.127	-16.950	0.402
PIT 1 70 16-07-09	-124.085	-14.470	-17.649
PIT 1 70 16-08-06	-117.951	-15.400	-4.353
PIT 1 70 16-08-23	-126.097	-16.660	-2.800
PIT 1 70 16-09-09	-129.467	-16.252	-9.312
PIT 1 70 16-09-30	-134.040	-17.928	-0.981
PIT 1 70 16-12-19	-92.988	-12.151	-4.401
PIT 1 70 17-02-11	-126.409	-15.602	-11.258
PIT 1 70 17-03-03	-139.583	-18.672	-0.800
PIT 1 70 17-03-14	-143.190	-19.110	-1.034
PIT 1 70 17-03-23	-134.030	-17.197	-6.601
PIT 1 70 17-03-31	-113.251	-14.605	-5.775
PIT 1 70 17-04-21	-137.018	-19.019	4.437
PIT 1 70 17-05-05	-137.372	-17.353	-8.744

PIT 1 70 17-05-08	-120.371	-15.064	-9.363
PIT 1 70 17-05-24	-128.536	-16.611	-5.619
PIT 1 70 17-06-08	-125.676	-15.627	-10.330
PIT 1 70 17-06-19	-134.598	-17.008	-8.623
PIT 1 70 17-07-06	-143.481	-17.977	-10.045
PIT 1 75 16-05-10	-125.255	-17.038	0.948
PIT 1 75 16-06-15	-119.345	-15.918	-1.762
PIT 1 75 16-07-09	-126.859	-14.834	-17.623
PIT 1 75 16-08-06	-120.872	-15.791	-4.264
PIT 1 75 16-08-23	-130.351	-16.963	-4.722
PIT 1 75 16-09-09	-129.784	-17.569	0.509
PIT 1 75 16-09-30	-137.519	-18.911	3.102
PIT 1 75 16-12-19	-103.361	-14.021	-0.379
PIT 1 75 17-02-11	-121.586	-15.145	-9.951
PIT 1 75 17-03-03	-138.550	-18.341	-2.314
PIT 1 75 17-03-23	-137.893	-17.764	-6.095
PIT 1 75 17-03-31	-112.963	-14.892	-3.276
PIT 1 75 17-04-21	-127.345	-17.433	1.903
PIT 1 75 17-05-05	-131.724	-16.030	-13.280
PIT 1 75 17-05-08	-123.714	-16.049	-5.120
PIT 1 75 17-05-24	-134.415	-17.411	-5.338
PIT 1 80 16-05-10	-128.335	-17.616	2.318
PIT 1 80 16-06-15	-119.208	-15.817	-2.402

PIT 1 80 16-07-09	-123.308	-14.363	-17.696
PIT 1 80 16-08-06	-123.921	-16.101	-4.930
PIT 1 80 16-08-23	-132.016	-16.847	-7.284
PIT 1 80 16-09-30	-128.770	-17.224	-1.136
PIT 1 80 16-12-19	-121.847	-15.776	-5.359
PIT 1 80 17-02-11	-115.720	-13.731	-14.969
PIT 1 80 17-03-03	-138.312	-18.661	0.391
PIT 1 80 17-03-23	-135.796	-17.094	-9.157
PIT 1 80 17-03-31	-117.772	-15.464	-3.683
PIT 1 80 17-04-09	-108.473	-15.037	2.327
PIT 1 80 17-04-21	-118.113	-14.826	-8.934
PIT 1 80 17-05-08	-124.752	-15.945	-6.964
PIT 1 80 17-05-24	-138.626	-17.852	-6.156
PIT 1 80 17-06-19	-136.538	-17.096	-9.884
PIT 1 80 17-07-06	-140.613	-18.238	-5.170
PIT 1 85 16-05-10	-127.052	-17.330	1.400
PIT 1 85 16-06-15	-114.949	-15.239	-2.591
PIT 1 85 16-07-09	-122.855	-14.597	-15.441
PIT 1 85 16-12-19	-123.623	-16.577	-0.966
PIT 1 85 17-02-11	-111.998	-13.367	-14.053
PIT 1 85 17-03-03	-150.929	-19.932	-2.446
PIT 1 85 17-03-23	-136.361	-17.093	-9.729
PIT 1 85 17-03-31	-130.126	-17.348	-1.538

PIT 1 85 17-04-09	-105.852	-14.449	0.422
PIT 1 85 17-05-08	-129.275	-16.497	-7.233
PIT 1 85 17-05-24	-135.193	-17.968	-1.831
PIT 1 90 16-05-10	-125.541	-16.938	-0.103
PIT 1 90 16-08-06	-126.370	-16.940	-0.915
PIT 1 90 16-12-19	-124.278	-16.511	-2.131
PIT 1 90 17-02-11	-105.983	-12.584	-14.061
PIT 1 90 17-03-23	-135.671	-16.736	-11.793
PIT 1 90 17-03-31	-130.768	-16.790	-6.474
PIT 1 90 17-04-09	-106.782	-14.732	1.670
PIT 1 90 17-05-24	-136.343	-17.260	-8.428
PIT 1 90 17-06-19	-134.629	-17.735	-3.061
PIT 1 95 16-05-10	-125.064	-17.075	1.427
PIT 1 95 16-08-06	-129.313	-17.136	-2.353
PIT 1 95 16-12-19	-119.762	-15.901	-2.308
PIT 1 95 17-02-11	-106.248	-12.468	-15.221
PIT 1 95 17-03-23	-137.926	-18.131	-3.307
PIT 1 95 17-03-31	-135.914	-17.610	-5.309
PIT 1 95 17-04-09	-106.162	-14.589	1.189
PIT 1 95 17-05-24	-135.732	-17.568	-5.446
PIT 1 100 16-05-10	-127.588	-17.702	3.726
PIT 1 100 16-08-06	-130.286	-17.290	-2.143
PIT 1 100 16-12-19	-124.096	-16.820	0.433

PIT 1 100 17-02-11	-113.467	-13.188	-16.901
PIT 1 100 17-03-23	-134.970	-17.922	-1.959
PIT 1 100 17-03-31	-137.153	-17.266	-9.195
PIT 1 100 17-04-09	-110.955	-15.208	1.161
PIT 1 100 17-05-24	-132.672	-17.270	-4.680
PIT 1 100 17-06-19	-129.952	-19.428	14.654
PIT 1 100 17-07-06	-124.450	-15.970	-6.469
Pit 2 5 16-05-30	-93.661	-10.867	-14.964
PIT 2 5 16-06-15	-109.893	-14.164	-5.813
PIT 2 5 16-06-24	-127.641	-16.499	-5.584
PIT 2 5 16-07-09	-128.072	-14.493	-21.456
PIT 2 5 16-07-22	-110.254	-10.149	-37.080
PIT 2 5 16-08-06	-134.078	-17.478	-4.482
PIT 2 5 16-08-23	-120.964	-13.270	-23.765
PIT 2 5 16-09-09	-124.335	-14.467	-17.921
PIT 2 5 16-09-30	-120.182	-13.499	-21.221
PIT 2 5 16-10-21	-105.409	-12.493	-14.188
PIT 2 5 16-12-19	-101.794	-13.470	-3.057
PIT 2 5 17-02-11	-153.625	-20.570	-0.232
PIT 2 5 17-03-14	-122.644	-16.438	-1.057
PIT 2 5 17-03-23	-133.291	-17.758	-1.540
PIT 2 5 17-03-31	-137.647	-17.704	-6.318
PIT 2 5 17-04-21	-112.634	-14.362	-7.028

PIT 2 5 17-05-08	-120.329	-14.829	-11.126
PIT 2 5 17-05-24	-115.028	-15.207	-2.920
PIT 2 5 17-06-08	-116.851	-13.049	-21.351
PIT 2 5 17-06-19	-102.423	-14.415	3.588
PIT 2 5 17-07-06	-103.810	-12.500	-12.540
PIT 2 10 16-05-10	-153.851	-20.652	0.173
Pit 2 10 16-05-30	-102.221	-13.278	-4.962
PIT 2 10 16-06-15	-119.351	-16.113	-0.267
PIT 2 10 16-06-24	-115.168	-15.631	0.208
PIT 2 10 16-07-09	-125.913	-14.438	-19.726
PIT 2 10 16-07-22	-120.560	-13.669	-20.290
PIT 2 10 16-08-06	-124.326	-15.973	-6.318
PIT 2 10 16-08-23	-117.582	-14.841	-8.291
PIT 2 10 16-09-09	-124.869	-15.587	-9.834
PIT 2 10 16-09-30	-128.330	-16.238	-8.283
PIT 2 10 16-10-21	-103.951	-12.729	-10.916
PIT 2 10 16-12-19	-122.343	-16.299	-1.827
PIT 2 10 17-02-11	-152.748	-19.245	-9.554
PIT 2 10 17-03-14	-134.141	-17.922	-1.130
PIT 2 10 17-03-23	-127.893	-17.758	3.851
PIT 2 10 17-03-31	-133.612	-17.250	-5.774
PIT 2 10 17-04-21	-118.491	-16.598	4.328
PIT 2 10 17-05-08	-121.660	-15.812	-4.895

PIT 2 10 17-05-24	-117.536	-15.517	-3.040
PIT 2 10 17-06-08	-120.078	-15.059	-9.108
PIT 2 10 17-06-19	-109.554	-15.314	3.376
PIT 2 10 17-07-06	-122.563	-15.536	-7.916
PIT 2 15 16-05-10	-142.821	-19.753	4.284
Pit 2 15 16-05-30	-111.070	-14.701	-2.855
PIT 2 15 16-06-15	-118.978	-16.082	-0.130
PIT 2 15 16-06-24	-120.075	-16.262	0.160
PIT 2 15 16-07-09	-123.168	-14.839	-13.891
PIT 2 15 16-07-22	-121.877	-14.240	-17.207
PIT 2 15 16-08-06	-124.614	-16.396	-3.352
PIT 2 15 16-08-23	-122.842	-16.205	-3.050
PIT 2 15 16-09-09	-129.157	-17.323	-0.759
PIT 2 15 16-09-30	-129.107	-16.776	-4.920
PIT 2 15 16-10-21	-111.686	-14.399	-5.799
PIT 2 15 16-12-19	-107.158	-14.090	-3.643
PIT 2 15 17-02-11	-147.503	-19.716	-0.681
PIT 2 15 17-03-14	-137.549	-17.757	-5.812
PIT 2 15 17-03-23	-130.834	-17.086	-4.262
PIT 2 15 17-03-31	-129.186	-17.378	-0.363
PIT 2 15 17-04-21	-121.038	-18.000	12.576
PIT 2 15 17-05-08	-121.863	-16.387	-0.666
PIT 2 15 17-06-08	-121.019	-15.950	-3.185

PIT 2 15 17-06-19	-113.886	-15.748	2.391
PIT 2 15 17-07-06	-121.827	-16.494	0.187
PIT 2 20 16-05-10	-130.186	-18.072	3.980
Pit 2 20 16-05-30	-117.343	-15.681	-1.583
PIT 2 20 16-06-15	-119.064	-16.205	0.726
PIT 2 20 16-06-24	-121.279	-16.482	0.648
PIT 2 20 16-07-09	-123.017	-14.935	-12.999
PIT 2 20 16-07-22	-125.187	-14.902	-15.425
PIT 2 20 16-08-06	-126.128	-16.626	-3.091
PIT 2 20 16-08-23	-127.550	-16.948	-2.034
PIT 2 20 16-09-09	-133.504	-18.093	0.821
PIT 2 20 16-09-30	-129.100	-17.329	-0.657
PIT 2 20 16-10-21	-118.480	-15.881	-1.184
PIT 2 20 16-12-19	-114.233	-15.321	-1.247
PIT 2 20 17-02-11	-138.842	-18.401	-2.147
PIT 2 20 17-03-14	-144.974	-15.534	-30.349
PIT 2 20 17-03-23	-134.940	-18.084	-0.683
PIT 2 20 17-04-21	-123.023	-16.248	-2.895
PIT 2 20 17-05-08	-123.071	-16.057	-4.415
PIT 2 20 17-05-24	-120.585	-16.910	4.634
PIT 2 20 17-06-08	-120.846	-15.719	-4.793
PIT 2 20 17-06-19	-119.810	-16.756	4.225
PIT 2 25 16-05-30	-146.456	-20.293	4.805

PIT 2 25 16-06-15	-150.386	-21.277	8.455
PIT 2 25 16-06-24	-120.661	-16.532	1.650
PIT 2 25 16-07-09	-134.554	-15.850	-17.496
PIT 2 25 16-07-22	-119.625	-15.014	-8.997
PIT 2 25 16-08-06	-122.270	-16.077	-3.461
PIT 2 25 16-08-23	-118.932	-16.483	2.999
PIT 2 25 16-09-09	-127.458	-17.259	0.447
PIT 2 25 16-09-30	-127.748	-17.177	-0.472
PIT 2 25 16-10-21	-118.388	-15.754	-2.068
PIT 2 25 17-02-11	-130.134	-17.015	-4.106
PIT 2 25 17-03-14	-139.639	-16.388	-18.434
PIT 2 30 16-05-30	-153.982	-21.074	3.289
PIT 2 30 16-06-15	-123.638	-17.074	2.842
PIT 2 30 16-06-24	-119.046	-16.346	1.834
PIT 2 30 16-07-09	-121.485	-14.421	-15.423
PIT 2 30 16-07-22	-124.087	-14.933	-14.083
PIT 2 30 16-08-06	-121.393	-16.066	-2.672
PIT 2 30 16-09-09	-126.772	-17.111	-0.008
PIT 2 30 16-09-30	-130.447	-17.519	-0.540
PIT 2 30 17-02-11	-133.131	-17.603	-2.579
PIT 2 30 17-03-14	-133.315	-18.964	7.716

Table 8. δ^2H, $\delta^{18}O$, and lc-excess values for all plant samples. CC = hillslope chokecherry, DF1 = hillslope Douglas Fir, DF2 = riparian Douglas Fir, SB2 = hillslope sagebrush, WB1 = riparian water birch.

Sample ID	δ2H [‰]	δ18O [‰]	lc-excess [‰]
CC 17-04-09 A	-117.360	-11.889	-30.789
CC 17-04-09 B	-120.009	-11.888	-33.446
CC 17-04-21 A	-109.923	-10.054	-37.483
CC 17-04-21 B	-105.742	-10.252	-31.773
CC 17-05-05 A	-134.572	-16.775	-10.387
CC 17-05-05 B	-152.695	-19.660	-6.304
CC 17-05-08 A	-133.113	-15.736	-16.929
CC 17-05-24 A	-134.514	-16.295	-14.030
CC 17-05-24 B	-135.417	-15.603	-20.256
CC 17-05-24 C	-132.716	-16.294	-12.239
CC 17-06-08 A	-137.986	-18.423	-1.119
CC 17-06-08 B	-135.802	-18.473	1.452
CC 17-06-08 C	-136.862	-17.442	-7.546
CC 17-06-19 A	-135.666	-16.386	-14.484
CC 17-06-19 B	-135.532	-16.370	-14.468
CC 17-07-06 A	-138.462	-15.654	-22.911
CC 17-07-06 B	-138.962	-16.523	-16.723
CC 17-07-06 C	-137.159	-17.728	-5.644
DF1 16-05-10 A	-125.247	-15.832	-8.327

DF1 16-05-10 B	-123.795	-15.933	-6.100
DF1 16-05-10 C	-124.553	-15.857	-7.441
DF1 16-05-30 A	-124.665	-18.004	8.975
DF1 16-05-30 B	-124.364	-17.439	4.931
DF1 16-05-30 C	-126.861	-18.195	8.252
DF1 16-06-15 A	-132.267	-18.405	4.462
DF1 16-06-15 B	-138.272	-19.732	8.671
DF1 16-06-15 C	-133.636	-19.052	8.074
DF1 16-06-24 A	-123.917	-17.198	3.523
DF1 16-06-24 B	-121.082	-16.088	-2.191
DF1 16-07-09 A	-133.364	-15.235	-21.038
DF1 16-07-09 B	-131.619	-15.161	-19.861
DF1 16-07-09 C	-134.503	-15.831	-17.591
DF1 16-07-22 A	-131.137	-15.143	-19.518
DF1 16-07-22 B	-134.063	-14.984	-23.670
DF1 16-07-22 C	-135.553	-16.215	-15.683
DF1 16-08-06 A	-123.698	-15.017	-13.050
DF1 16-08-06 B	-126.811	-15.765	-10.404
DF1 16-08-06 C	-127.839	-15.679	-12.093
DF1 16-08-23 A	-135.357	-17.278	-7.301
DF1 16-08-23 B	-137.794	-17.463	-8.320
DF1 16-08-23 C	-135.705	-17.216	-8.127
DF1 16-09-09 A	-138.987	-16.574	-16.354

DF1 16-09-09 B	-136.513	-17.207	-9.003
DF1 16-09-09 C	-136.756	-17.714	-5.349
DF1 16-09-30 A	-138.292	-17.755	-6.571
DF1 16-09-30 B	-138.759	-17.737	-7.172
DF1 16-09-30 C	-138.252	-17.484	-8.614
DF1 16-10-21 A	-125.960	-16.316	-5.313
DF1 16-10-21 B	-125.787	-16.548	-3.353
DF1 16-10-21 C	-127.329	-15.962	-9.403
DF1 16-12-19 A	-122.930	-16.625	0.099
DF1 16-12-19 B	-124.275	-16.363	-3.264
DF1 16-12-19 C	-123.316	-16.251	-3.171
DF1 17-02-11 A	-125.628	-15.969	-7.653
DF1 17-02-11 B	-125.369	-14.243	-20.681
DF1 17-02-11 C	-127.172	-15.269	-14.584
DF1 17-04-09 A	-128.277	-14.417	-22.251
DF1 17-04-09 B	-128.648	-14.735	-20.173
DF1 17-04-21 B	-130.902	-18.042	3.031
DF1 17-05-05 A	-137.269	-18.014	-3.549
DF1 17-05-05 B	-138.616	-17.297	-10.414
DF1 17-05-08 A	-132.239	-14.283	-27.243
DF1 17-05-08 B	-133.077	-13.941	-30.715
DF1 17-05-08 C	-134.480	-15.446	-20.527
DF1 17-05-24 A	-132.300	-15.956	-14.427

DF1 17-05-24 B	-136.037	-17.099	-9.362
DF1 17-05-24 C	-134.330	-16.119	-15.201
DF1 17-06-08 A	-139.438	-15.806	-22.717
DF1 17-06-08 B	-139.578	-15.705	-23.631
DF1 17-06-19 A	-136.288	-16.592	-13.514
DF1 17-06-19 B	-136.112	-16.568	-13.524
DF1 17-07-06 A	-137.213	-16.760	-13.145
DF1 17-07-06 B	-139.085	-16.420	-17.638
DF1 17-07-06 C	-138.034	-17.084	-11.478
DF2 16-05-30 A	-106.110	-13.814	-4.722
DF2 16-05-30 B	-113.771	-14.835	-4.526
DF2 16-05-30 C	-115.860	-16.703	7.769
DF2 16-06-15 A	-127.773	-18.322	8.320
DF2 16-06-15 B	-128.025	-18.024	5.773
DF2 16-06-15 C	-123.521	-17.338	4.991
DF2 16-06-24 A	-134.081	-17.875	-1.434
DF2 16-06-24 B	-133.050	-18.138	1.621
DF2 16-06-24 C	-132.178	-17.732	-0.630
DF2 16-07-09 A	-124.951	-14.834	-15.709
DF2 16-07-09 C	-129.094	-15.262	-16.561
DF2 16-07-22 A	-129.315	-14.794	-20.384
DF2 16-07-22 B	-132.209	-16.679	-8.764
DF2 16-07-22 C	-127.389	-14.724	-18.999

DF2 16-08-06 A	-130.244	-16.429	-8.730
DF2 16-08-06 B	-128.860	-15.776	-12.366
DF2 16-08-23 A	-132.002	-16.225	-12.054
DF2 16-08-23 B	-131.959	-16.135	-12.707
DF2 16-08-23 C	-132.483	-16.902	-7.324
DF2 16-09-09 A	-140.334	-19.357	3.726
DF2 16-09-09 B	-138.743	-17.900	-5.899
DF2 16-09-09 C	-139.968	-18.246	-4.466
DF2 16-09-30 A	-140.577	-18.095	-6.233
DF2 16-09-30 B	-138.591	-18.604	-0.332
DF2 16-09-30 C	-141.529	-18.527	-3.863
DF2 16-10-21 A	-122.076	-16.095	-3.129
DF2 16-10-21 B	-120.266	-14.110	-16.604
DF2 16-10-21 C	-119.025	-14.990	-8.583
DF2 16-12-19 A	-112.706	-14.843	-3.400
DF2 16-12-19 B	-112.137	-15.143	-0.520
DF2 16-12-19 C	-111.690	-14.742	-3.157
DF2 17-02-11 A	-123.312	-14.349	-17.804
DF2 17-02-11 B	-115.265	-12.262	-25.827
DF2 17-02-11 C	-115.059	-15.521	-0.535
DF2 17-04-21 A	-132.639	-15.805	-15.928
DF2 17-04-21 B	-134.282	-16.104	-15.267
DF2 17-05-08 A	-134.253	-14.698	-26.057

DF2 17-05-08 B	-132.088	-15.287	-19.360
DF2 17-05-08 C	-132.689	-15.971	-14.700
DF2 17-05-24 A	-133.755	-15.370	-20.392
DF2 17-05-24 B	-135.226	-15.415	-21.514
DF2 17-05-24 C	-133.021	-15.952	-15.179
DF2 17-06-08 A	-135.758	-14.224	-31.217
DF2 17-06-08 B	-132.326	-14.752	-23.718
DF2 17-06-19 A	-126.048	-16.445	-4.410
DF2 17-06-19 B	-128.006	-16.008	-9.728
DF2 17-07-06 A	-131.333	-16.459	-9.582
DF2 17-07-06 B	-131.273	-15.067	-20.237
SB2 16-06-15 A	-118.709	-15.935	-0.995
SB2 16-06-15 B	-122.565	-16.514	-0.394
SB2 16-06-15 C	-124.925	-16.651	-1.698
SB2 16-06-24 A	-130.511	-17.187	-3.158
SB2 16-06-24 B	-127.588	-17.023	-1.500
SB2 16-06-24 C	-128.470	-16.975	-2.749
SB2 16-07-09 A	-125.971	-13.246	-28.957
SB2 16-07-09 B	-128.911	-14.670	-20.937
SB2 16-07-09 C	-127.280	-14.339	-21.855
SB2 16-07-22 A	-125.649	-13.223	-28.815
SB2 16-07-22 B	-126.124	-13.236	-29.187
SB2 16-07-22 C	-125.925	-13.445	-27.380

SB2 16-08-06 A	-122.629	-13.169	-26.204
SB2 16-08-06 B	-122.603	-13.698	-22.107
SB2 16-08-23 A	-128.939	-14.841	-19.648
SB2 16-08-23 B	-117.831	-11.709	-32.647
SB2 16-08-23 C	-129.271	-14.822	-20.128
SB2 16-09-09 A	-132.185	-14.851	-22.816
SB2 16-09-09 B	-129.348	-15.442	-15.426
SB2 16-09-09 C	-142.541	-15.013	-31.924
SB2 16-09-30 A	-130.612	-15.183	-18.684
SB2 16-09-30 B	-129.339	-15.173	-17.492
SB2 16-09-30 C	-126.659	-14.487	-20.092
SB2 16-10-21 A	-103.647	-10.870	-24.925
SB2 16-10-21 B	-105.616	-11.272	-23.794
SB2 16-10-21 C	-103.532	-11.094	-23.086
SB2 16-12-19 A	-119.650	-14.846	-10.321
SB2 16-12-19 B	-115.047	-13.546	-15.722
SB2 17-02-11 A	-120.124	-13.022	-24.836
SB2 17-02-11 B	-115.745	-14.477	-9.254
SB2 17-04-09 A	-124.983	-12.251	-35.631
SB2 17-04-09 B	-132.686	-12.975	-37.754
SB2 17-04-21 A	-121.603	-12.965	-26.752
SB2 17-04-21 B	-122.960	-12.746	-29.794
SB2 17-05-05 A	-121.256	-11.783	-35.505

SB2 17-05-05 B	-122.476	-11.434	-39.407
SB2 17-05-08 A	-120.478	-12.959	-25.671
SB2 17-05-08 B	-123.067	-13.256	-25.974
SB2 17-05-24 A	-130.158	-14.488	-23.581
SB2 17-05-24 B	-131.314	-14.686	-23.211
SB2 17-06-08 A	-129.572	-14.294	-24.488
SB2 17-06-08 B	-125.386	-12.556	-33.682
SB2 17-06-08 C	-129.508	-12.921	-34.996
SB2 17-06-19 A	-128.182	-15.759	-11.818
SB2 17-06-19 B	-127.665	-15.061	-16.682
SB2 17-07-06 A	-134.577	-15.759	-18.220
SB2 17-07-06 B	-133.509	-15.635	-18.103
SB2 17-07-06 C	-134.847	-16.109	-15.797
WB1 16-05-10 A	-118.056	-14.696	-9.883
WB1 16-05-10 B	-118.596	-15.154	-6.892
WB1 16-05-10 C	-120.035	-14.843	-10.722
WB1 16-05-30 A	-124.803	-15.814	-8.016
WB1 16-05-30 B	-118.592	-14.991	-8.141
WB1 16-05-30 C	-125.590	-16.468	-3.770
WB1 16-06-15 A	-131.886	-18.259	3.718
WB1 16-06-15 B	-127.426	-16.313	-6.798
WB1 16-06-15 C	-132.157	-18.245	3.343
WB1 16-06-24 A	-128.025	-16.832	-3.403

WB1 16-06-24 B	-128.730	-16.371	-7.658
WB1 16-06-24 C	-131.872	-16.360	-10.887
WB1 16-07-09 A	-128.121	-14.511	-21.366
WB1 16-07-09 B	-129.927	-14.636	-22.216
WB1 16-07-09 C	-130.007	-14.949	-19.885
WB1 16-07-22 A	-131.225	-14.355	-25.675
WB1 16-07-22 B	-125.582	-14.194	-21.273
WB1 16-08-06 A	-134.412	-16.320	-13.733
WB1 16-08-06 B	-131.416	-15.381	-17.967
WB1 16-08-06 C	-131.249	-15.491	-16.956
WB1 16-08-23 A	-136.542	-16.652	-13.306
WB1 16-08-23 B	-135.507	-16.467	-13.697
WB1 16-08-23 C	-135.540	-16.505	-13.434
WB1 16-09-09 A	-141.824	-17.354	-13.183
WB1 16-09-09 B	-142.276	-17.168	-15.072
WB1 16-09-09 C	-142.879	-17.513	-13.017
WB1 16-09-30 A	-132.364	-14.651	-24.531
WB1 16-09-30 B	-131.158	-13.992	-28.399
WB1 16-09-30 C	-132.413	-14.039	-29.294
WB1 16-10-21 A	-124.585	-14.630	-16.918
WB1 16-10-21 B	-127.011	-14.816	-17.914
WB1 16-10-21 C	-122.901	-13.872	-21.071
WB1 16-12-19 A	-107.561	-11.538	-23.698

WB1 16-12-19 B	-109.487	-11.566	-25.408
WB1 16-12-19 C	-109.258	-11.585	-25.032
WB1 17-02-11 A	-115.622	-11.458	-32.368
WB1 17-02-11 B	-112.968	-11.145	-32.126
WB1 17-02-11 C	-114.970	-10.414	-39.757
WB1 17-04-21 A	-110.944	-10.321	-36.442
WB1 17-04-21 B	-108.599	-10.421	-33.332
WB1 17-05-08 A	-120.400	-11.406	-37.548
WB1 17-05-08 B	-116.042	-10.916	-36.963
WB1 17-05-08 C	-114.879	-10.964	-35.428
WB1 17-05-24 A	-135.141	-15.497	-20.801
WB1 17-05-24 B	-133.508	-15.246	-21.097
WB1 17-05-24 C	-134.372	-15.395	-20.814
WB1 17-06-08 A	-135.571	-16.025	-17.166
WB1 17-06-08 B	-135.649	-15.654	-20.100
WB1 17-06-08 C	-137.408	-16.876	-12.449
WB1 17-06-19 A	-130.670	-16.053	-12.049
WB1 17-06-19 B	-132.823	-15.858	-15.700
WB1 17-07-06 A	-136.197	-15.642	-20.738

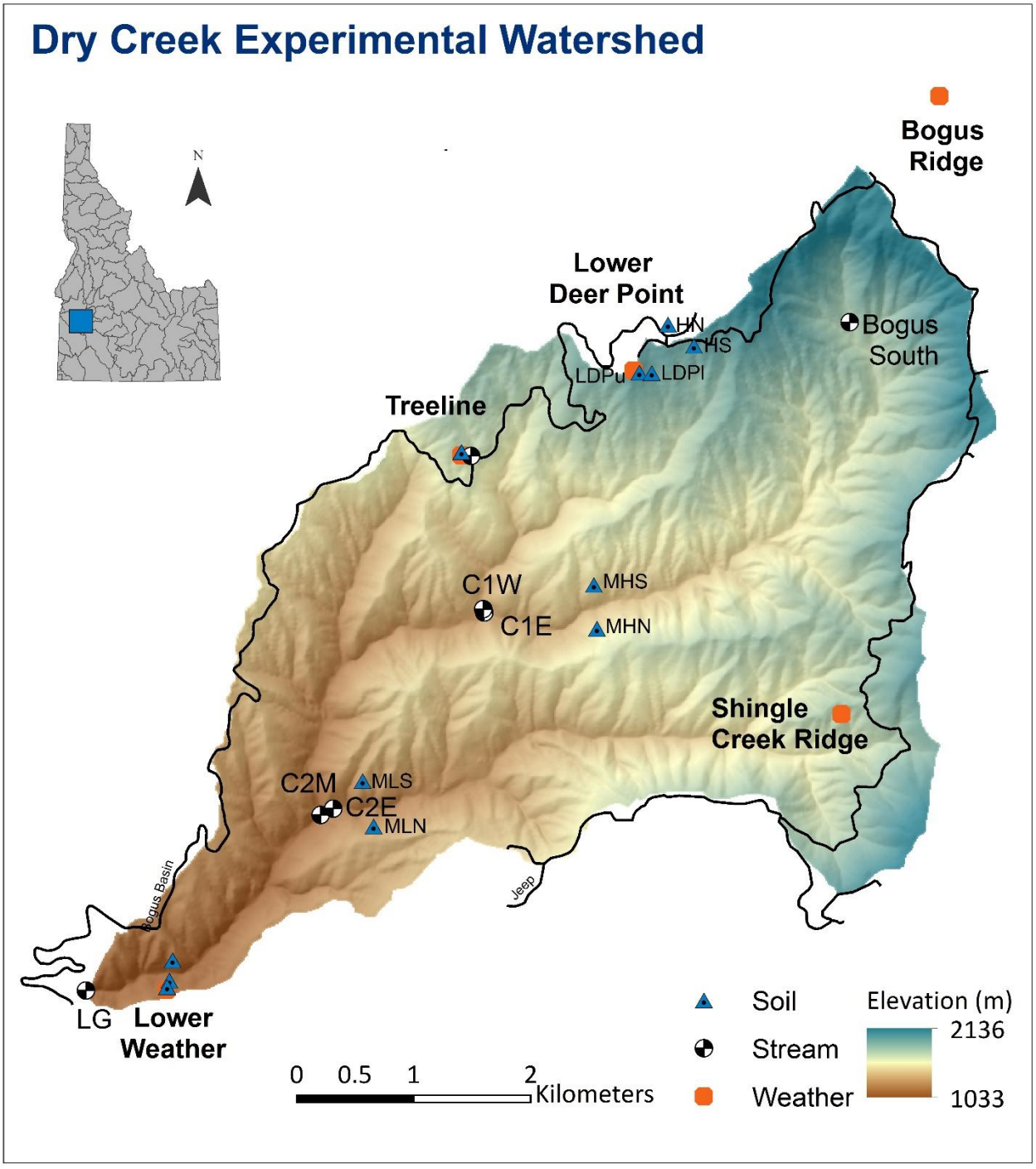

Figure 1. Dry Creek Experimental Watershed. From *DCEW* [2017].

Figure 2. Instrumentation at Con 1 study site. Image taken from *Geisler* [2016]. Our hillslope pit was located next to Con 1 Sap Flow and the riparian pit was located next to Con 1 East Gauge.

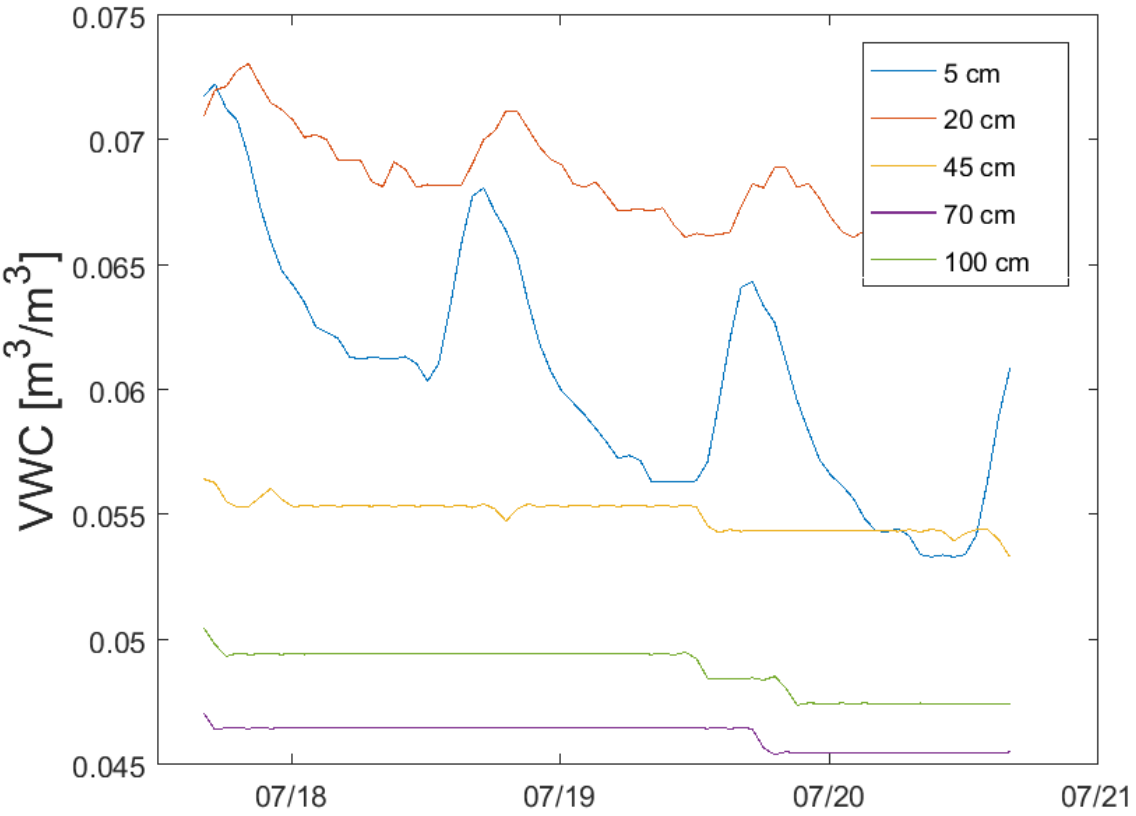

Figure 3. VWC data subset with diurnal signal. These signals were present in the data from the 5 and 20 cm sensors, but not those deeper in the soil profile.

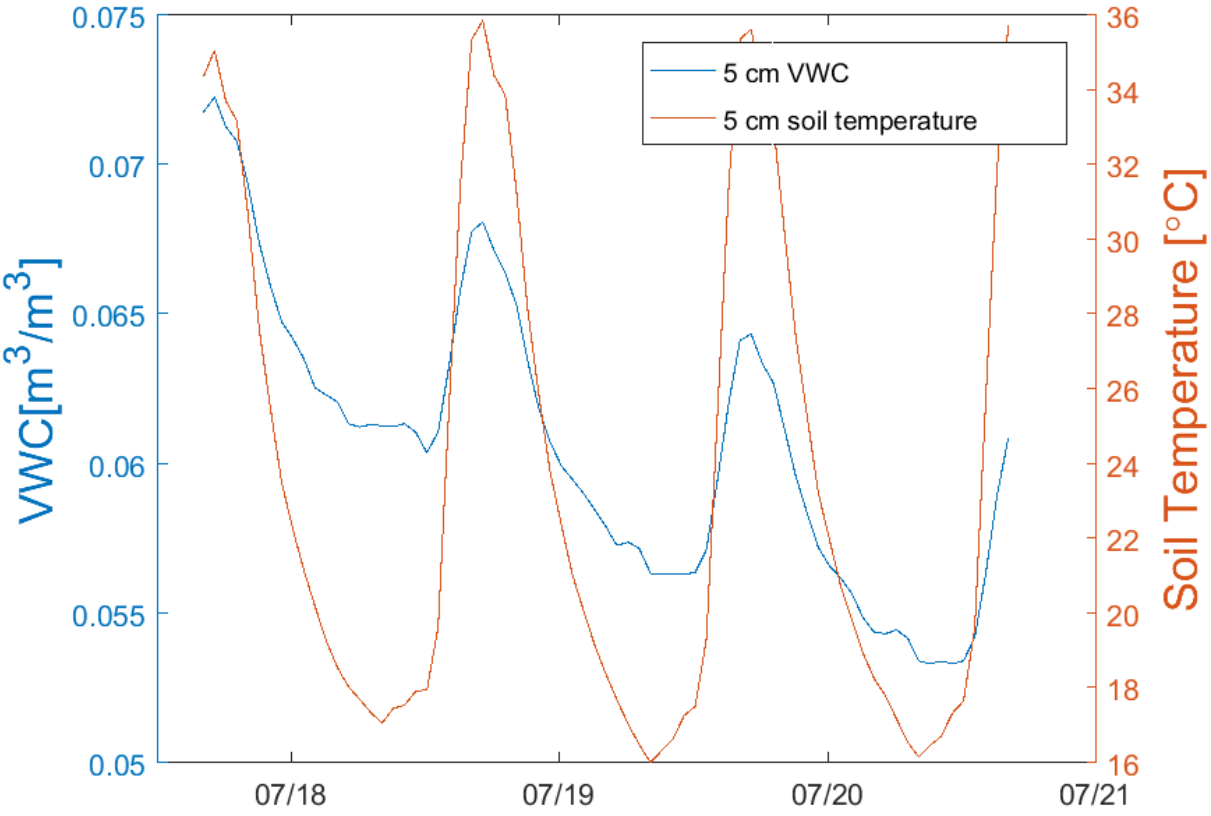

Figure 4. VWC and soil temperature subset. VWC diurnal fluctuations are in-phase with and controlled by fluctuations in soil temperature.

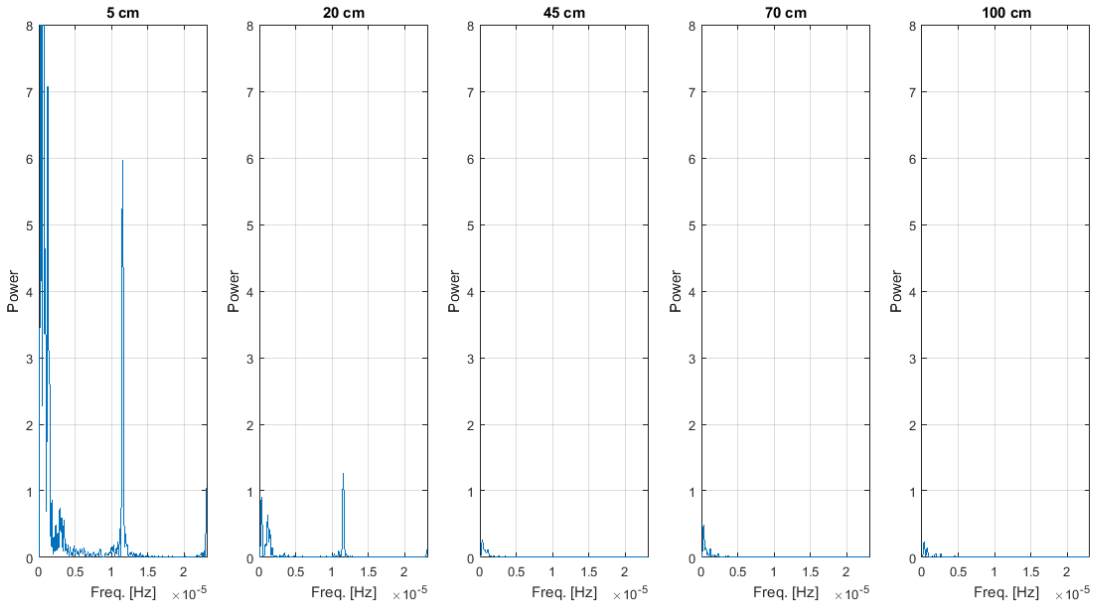

Figure 5. Periodogram of VWC subset. Strong power spikes in 5 and 20 cm at 1.157 x 10^{-5} Hz correspond to a 24-hour period, confirming that the signal in these data is diurnal.

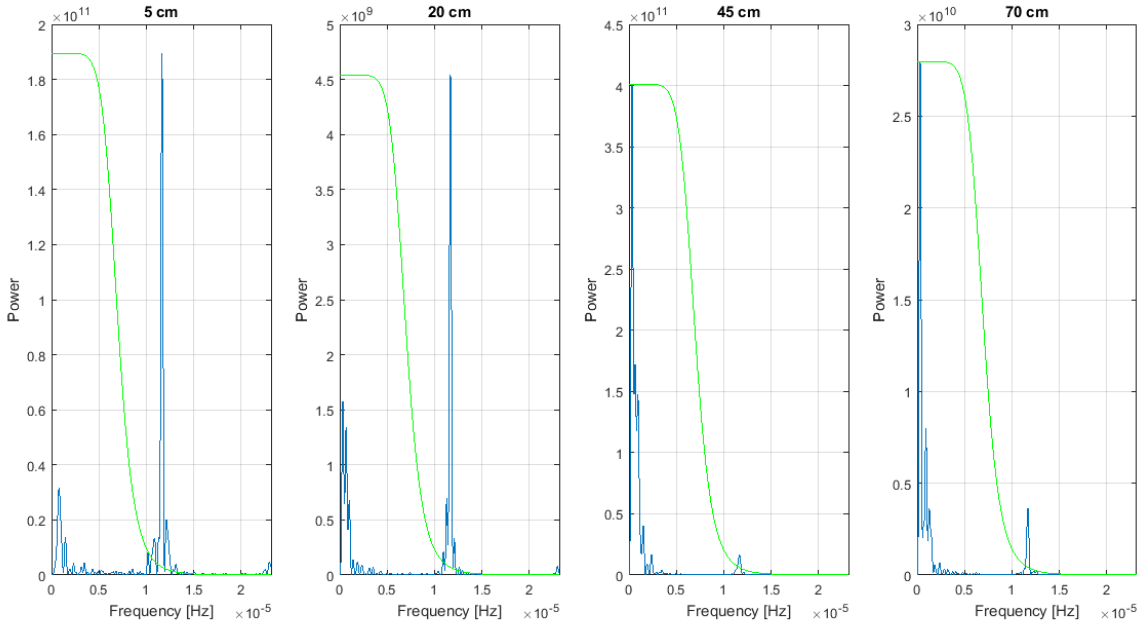

Figure 6. Periodogram of matric potential subset with low-pass filter. All data left of the filter cutoff were conserved.

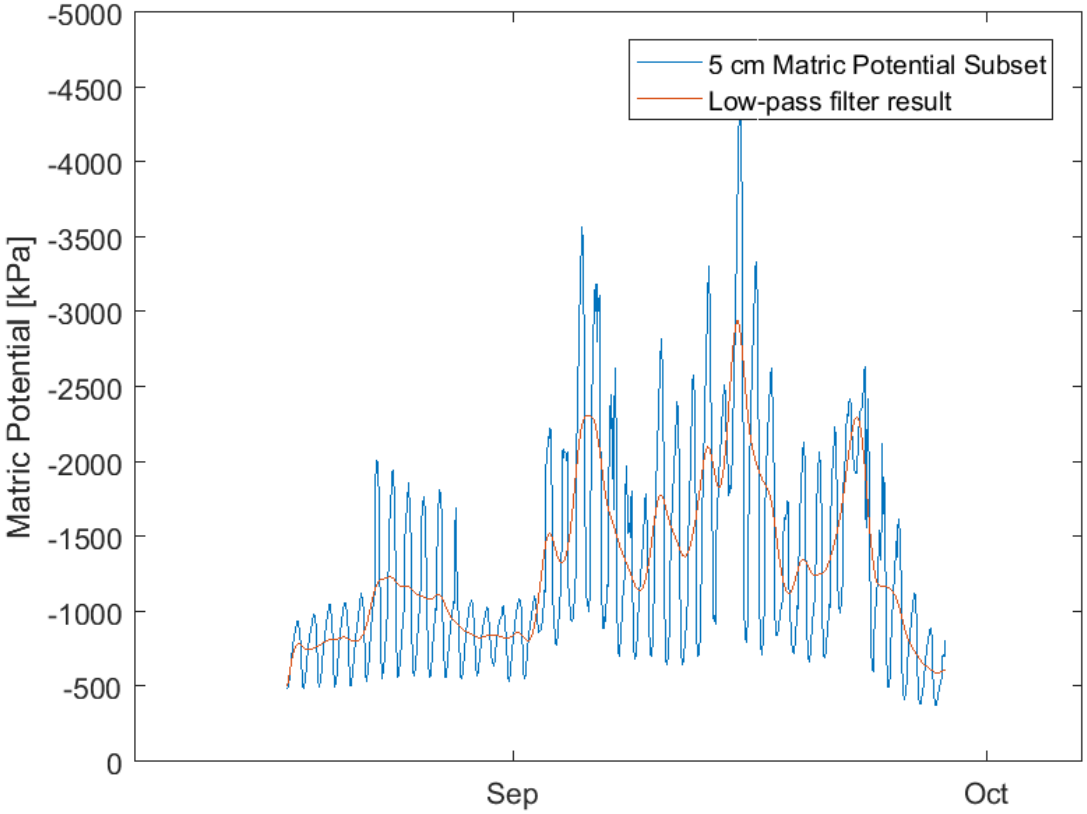

Figure 7. Subset of 5 cm matric potential data with results of low-pass filter.

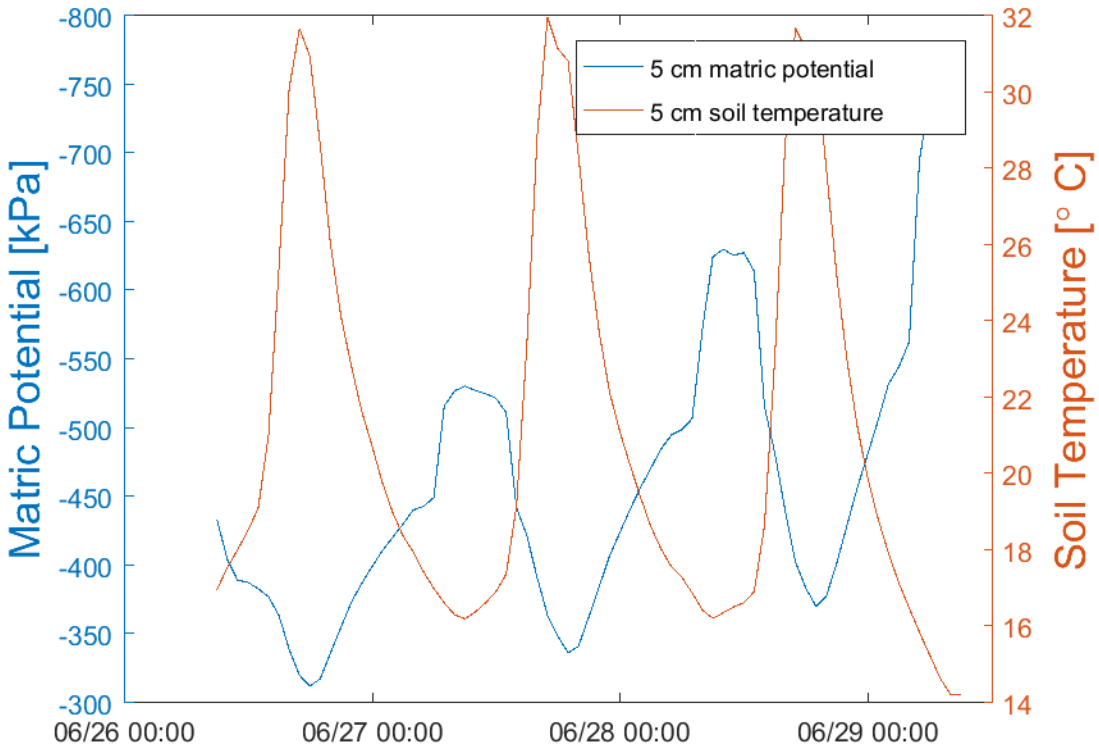

Figure 8. Subset of matric potential and soil temperature. The two data sources are out of phase.

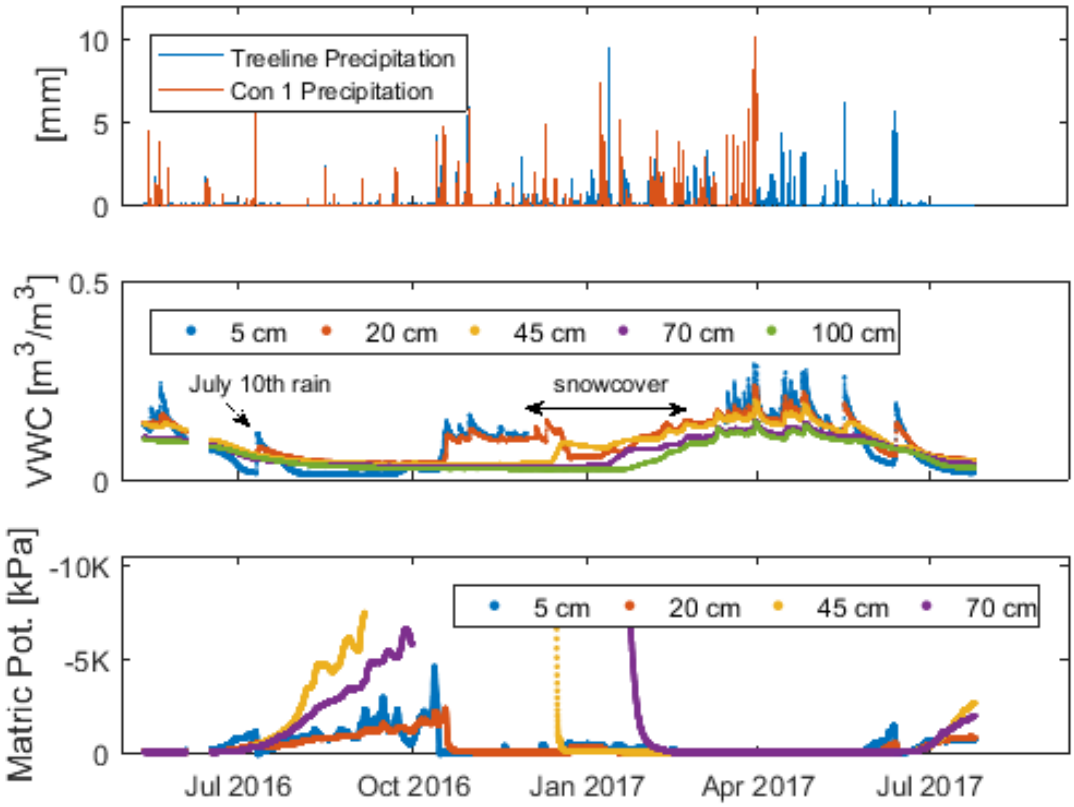

Figure 9. Precipitation at Treeline hydrometerological station from March 1st, 2016 to July 31st, 2017 and at C1E station from March 1st, 2016 to April 1st, 2017 (top panel). No data was recorded after 4-1-2017 at C1E due to power issues. After this date, hydrometeorological data from the Treeline station were used as proxy. Time series of soil moisture and matric potential at the hillslope pit from May 2016 to July 2017 appear in the middle and bottom panels. The data gap in mid-June 2016 is due to power supply issues. The data gap in the 5 cm sensor and the drop in VWC in the 20 cm sensor in January 2017 is due to freezing soil conditions. Note that very small (0.001-0.002) residual diurnal fluctuations remain after temperature correction of VWC data. The 45 and 70 cm matric potential sensors recorded no data from late fall 2016 to mid-winter 2017, presumably due to poor contact with the soil matrix due to dry conditions.

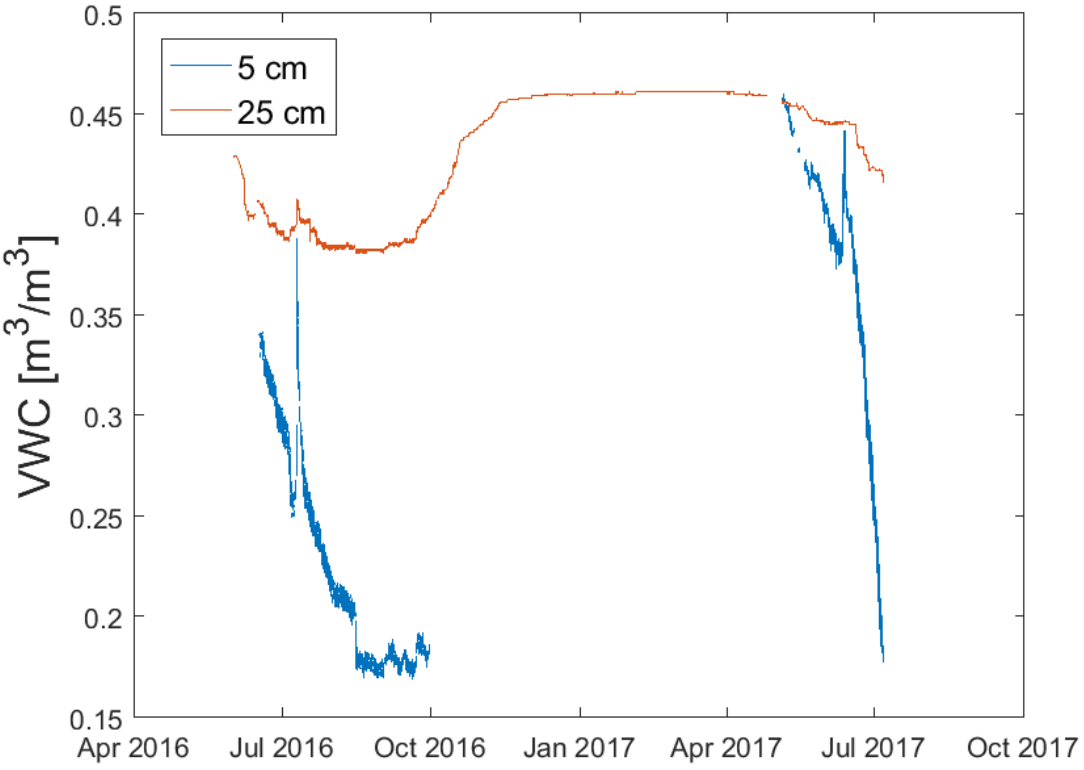

Figure 10. Time series of VWC at the riparian soil pit. Sensor malfunction, particularly at 5 cm, resulted in missing data in late 2016 and early 2017.

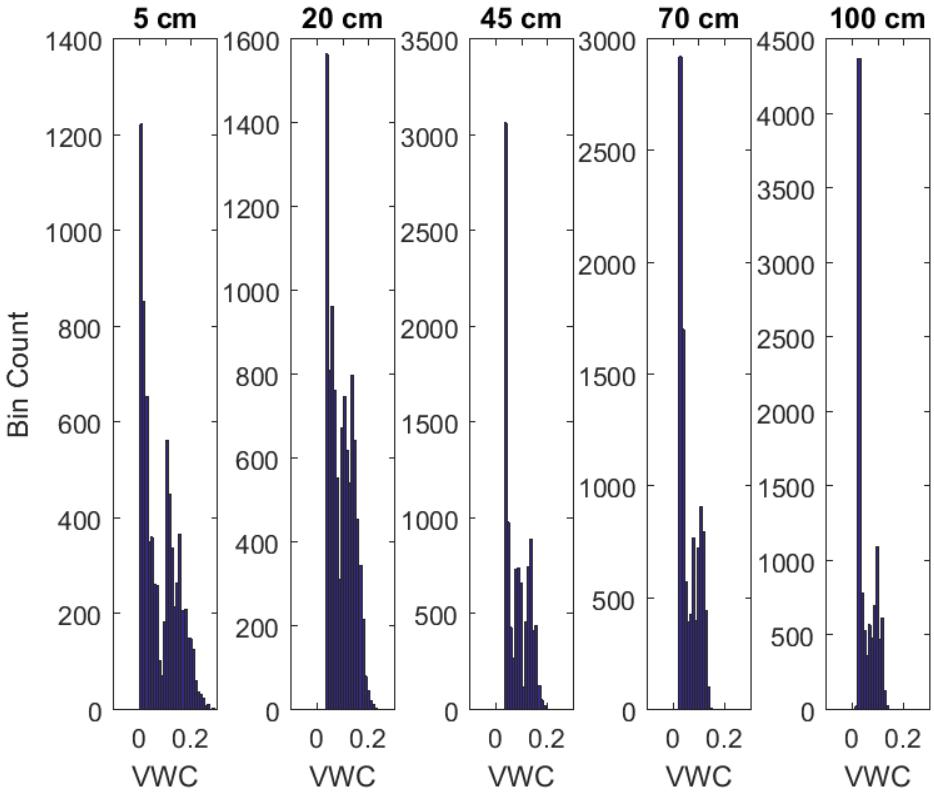

Figure 11. Histograms of VWC sensor data. Bin count spikes at low VWC (< 0.05) correspond to plant extraction limit. Bin count spikes at intermediate VWC (.10-.14) correspond to FC. Numeric results are reported in Table 1.

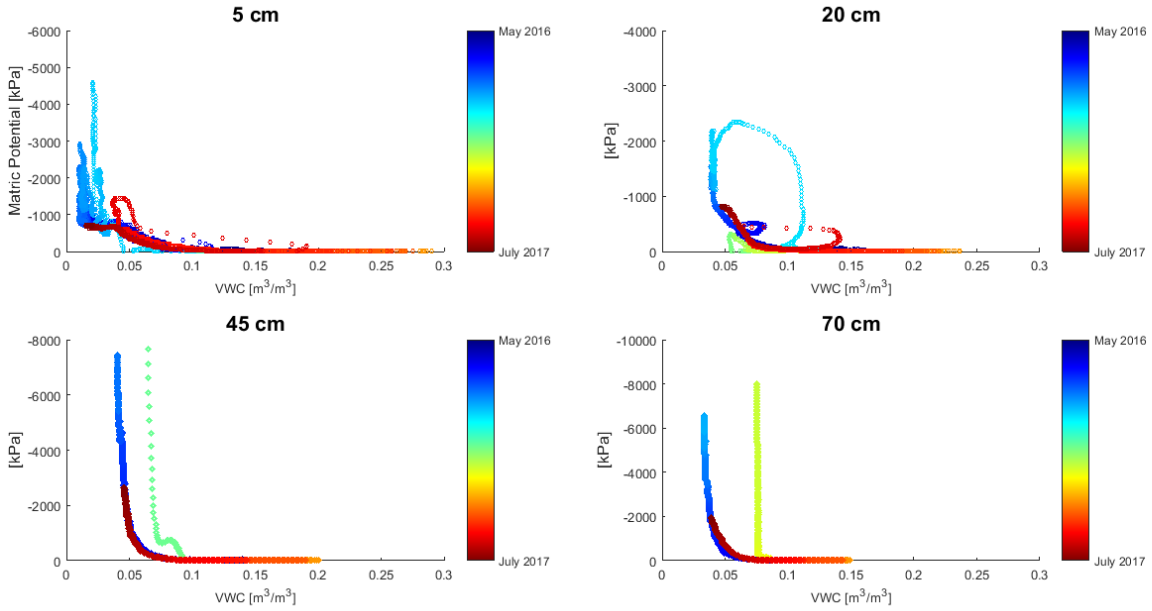

Figure 12. Characteristic moisture release curves generated by hillslope VWC and matric potential data.

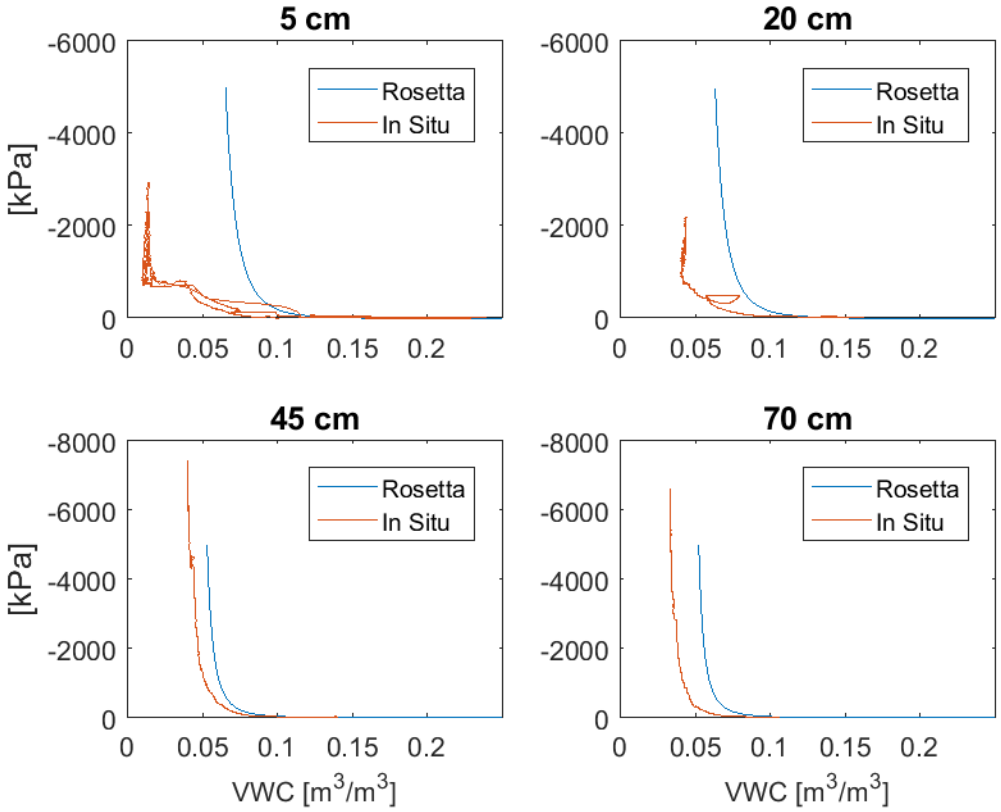

Figure 13. Characteristic curves generated from the Rosetta pedotransfer function and in situ data.

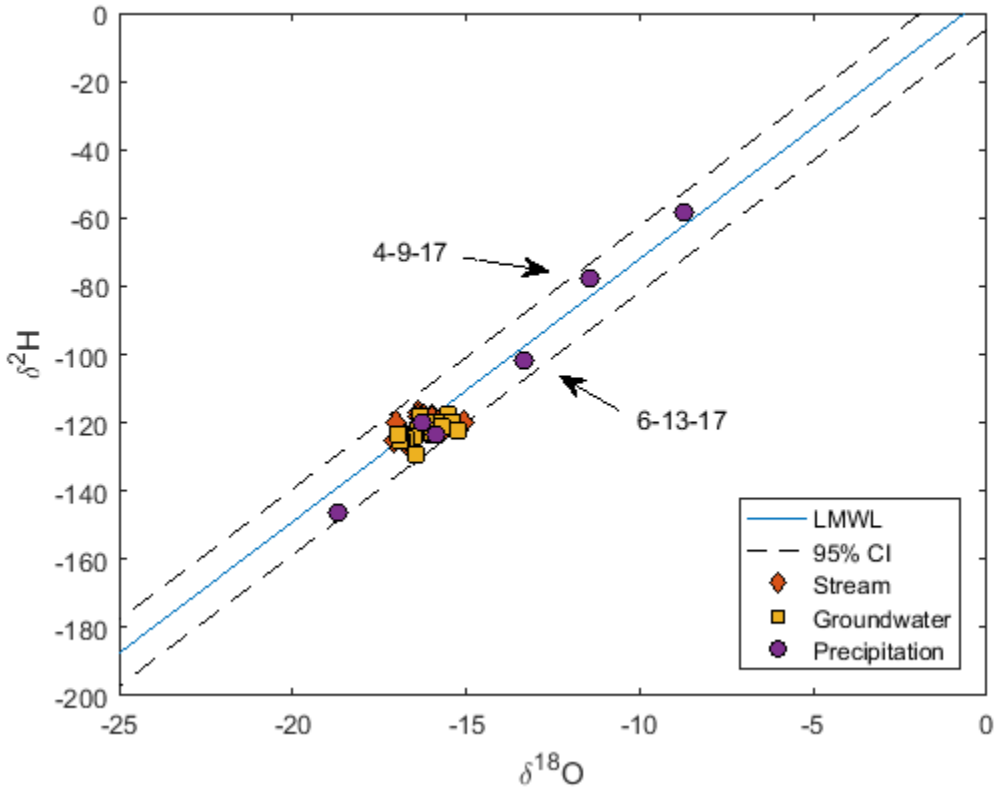

Figure 14. δ^2H and δ^{18}O values for stream and groundwater sampled from 5-10-2016 to 7-6-17. Precipitation was sampled from 12-19-2016 to 6-13-17.

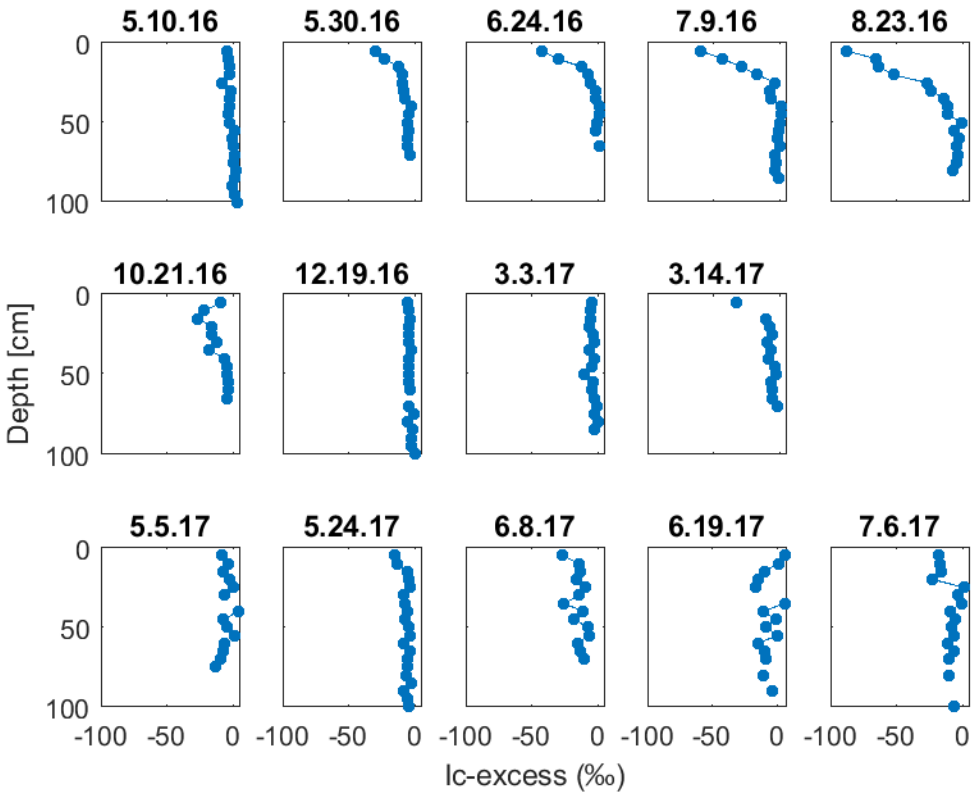

Figure 15. Lc-excess values for hillslope soil water in summer 2016 (top row), fall/winter 2016/2017 (middle row), and summer 2017 (bottom row). Note that some sampling dates are omitted from this figure to highlight general trends.

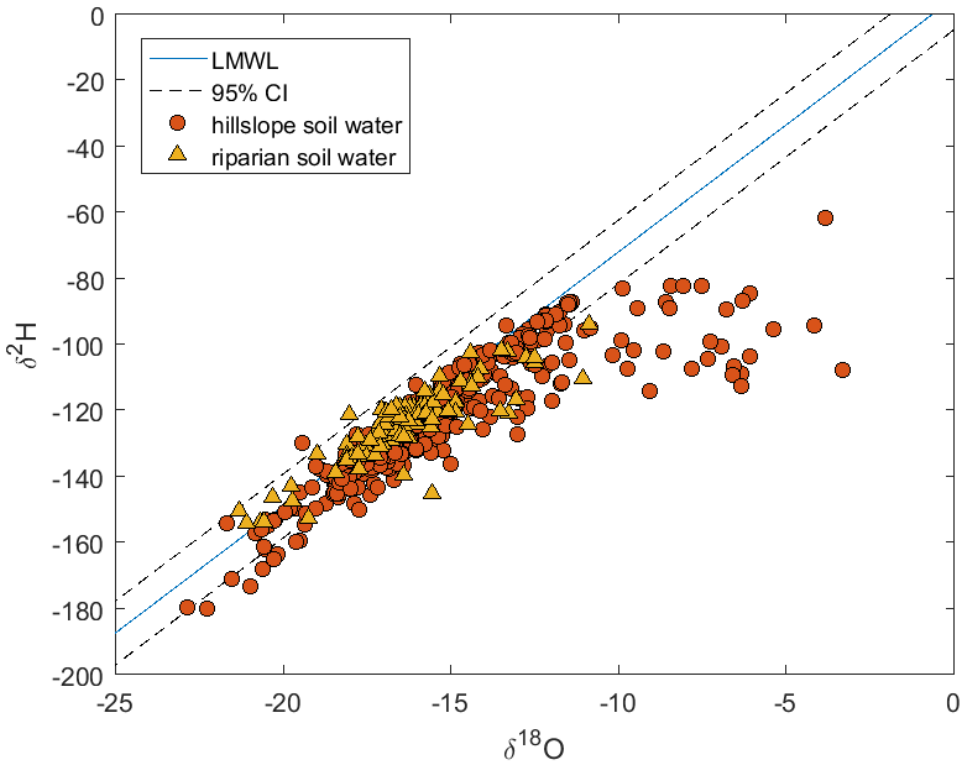

Figure 16. δ^2H and δ^{18}O values for hillslope and riparian soil water.

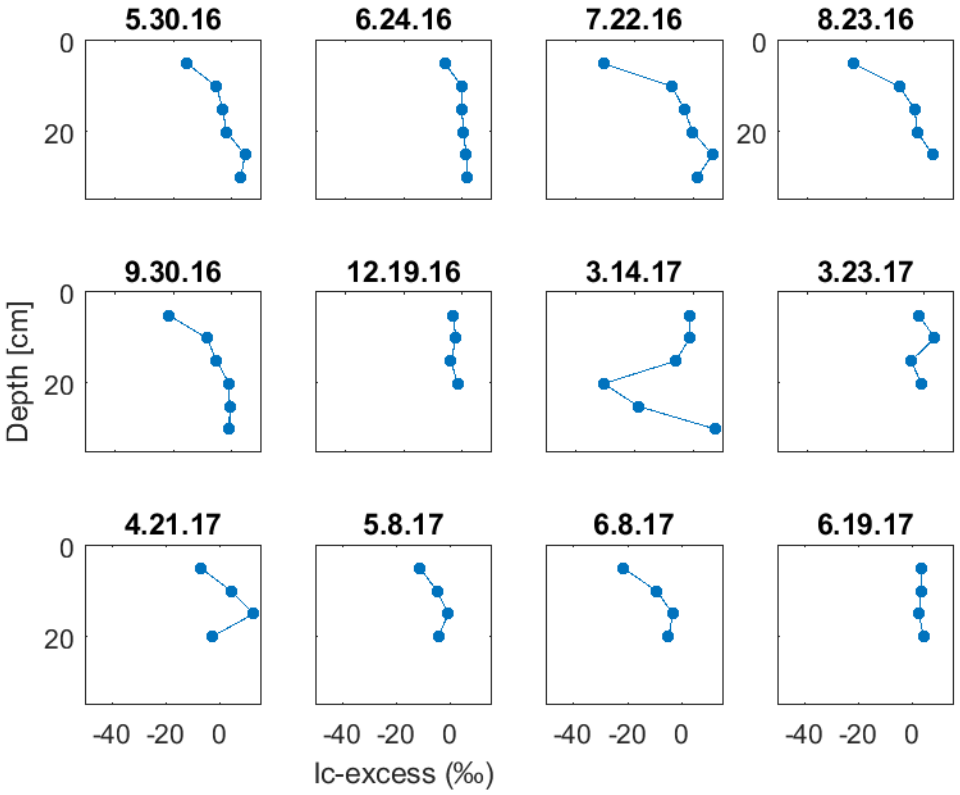

Figure 17. Lc-excess values for riparian soil water in summer 2016 (top row), fall/winter 2016/2017 (middle row), and spring 2017 (bottom row). Enriched lc-excess values are mostly restricted to the 5 cm layer. An enriched signal emerges at 20 and 25 cm on March 14th, 2017. This is likely due to extraction or sampling error.

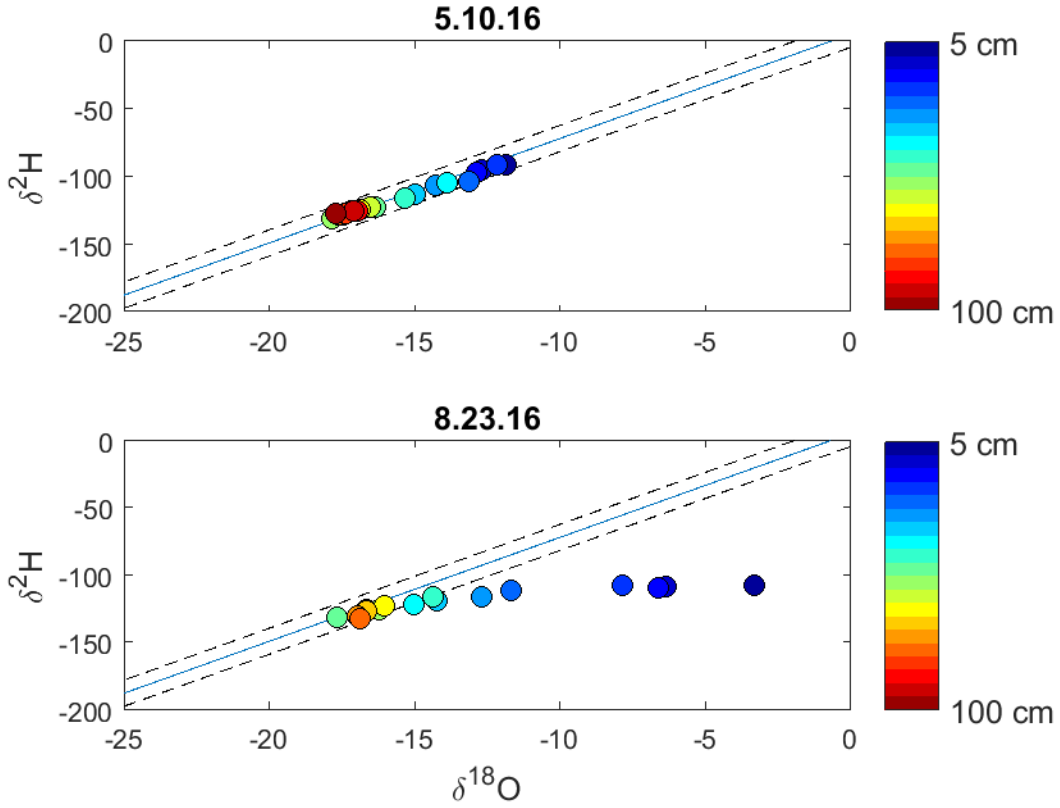

Figure 18. δ^2H and $\delta^{18}O$ for hillslope soil water on May 10 and August 23, 2016.

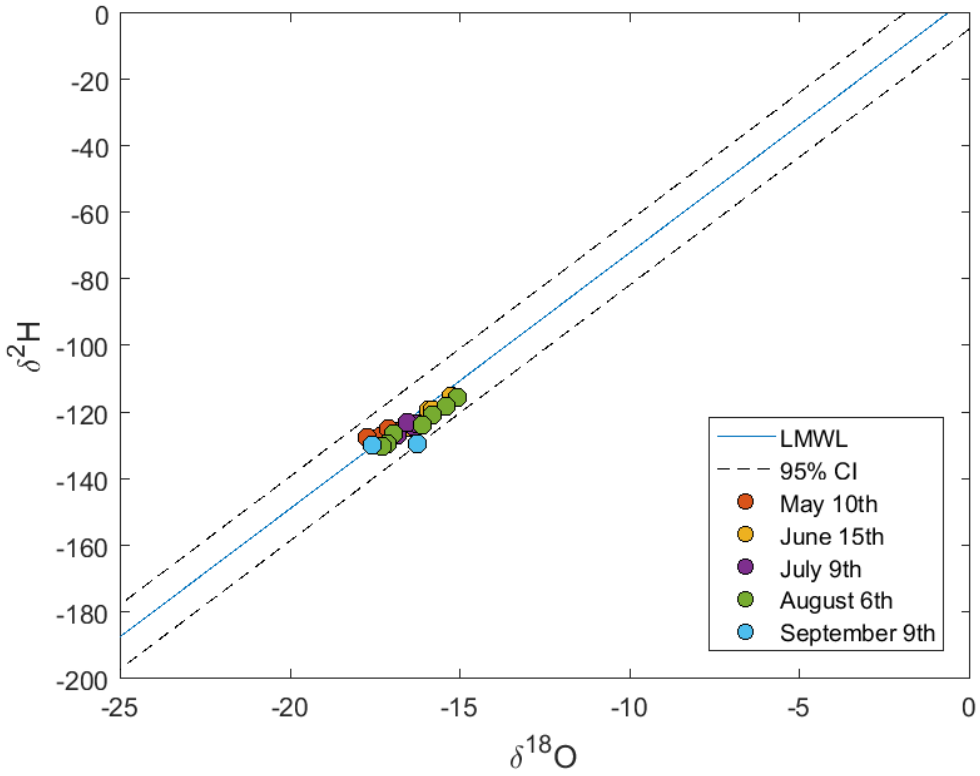

Figure 19. δ^2H and δ^{18}O for hillslope soil water at 70 cm or below during summer 2016. These data tightly cluster and do not move off the MWL over the growing season, suggesting minimal influence from more enriched layers higher in the soil column. These data overlap well with the groundwater data in Figure 14.

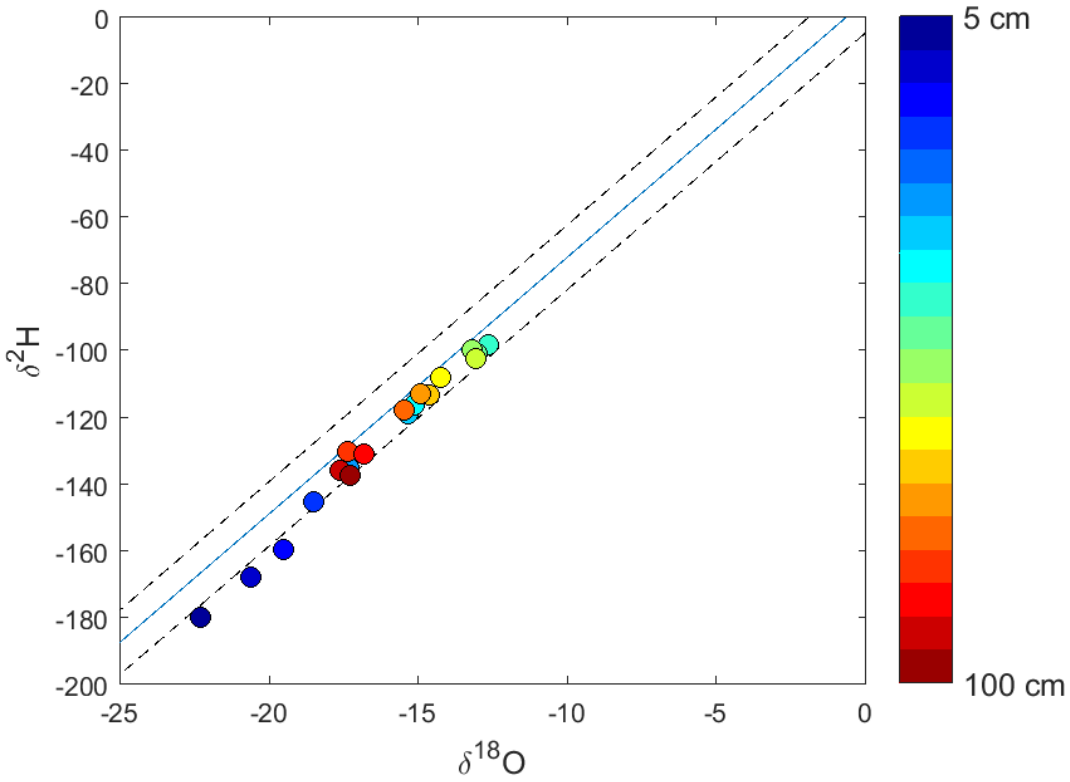

Figure 20. δ^2H and $\delta^{18}O$ for hillslope soil water on March 31st, 2017.

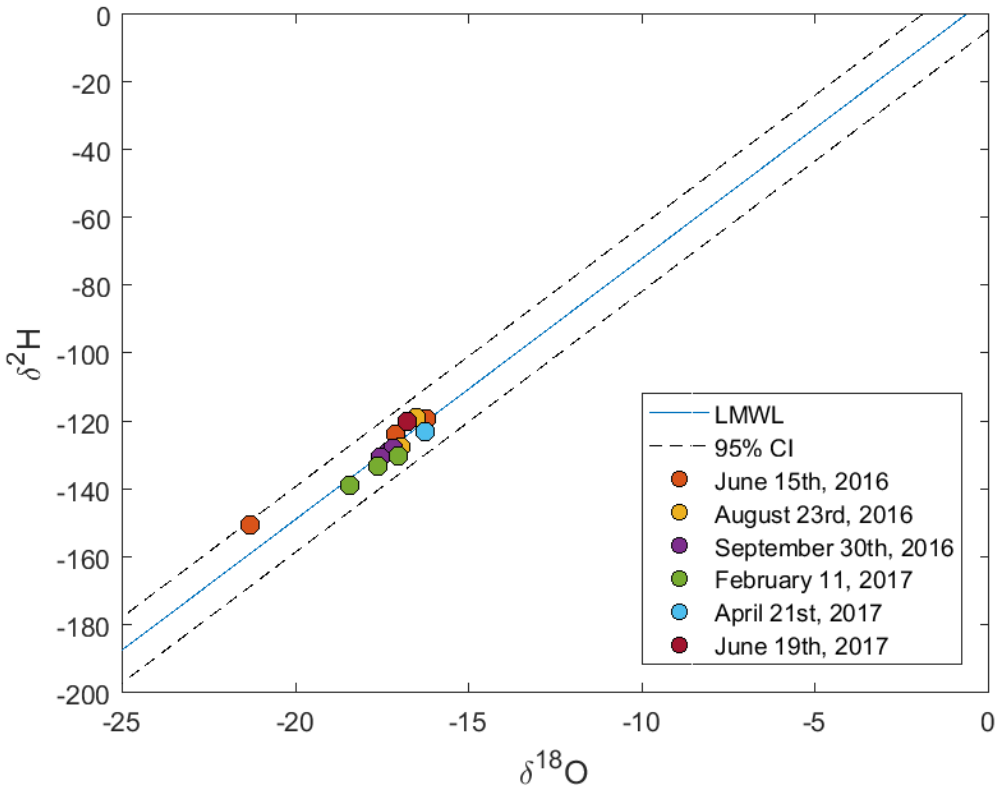

Figure 21. δ^2H and $\delta^{18}O$ for riparian soil water at 20 cm or below at selected dates throughout the study period. Water at these depths do not move significantly about the plot over the growing season and overlap with stream and groundwater, suggesting minimal influence from more enriched layers higher in the soil column. Upward movement of the water table to ~ 20 cm could also control isotopic composition in at these depths.

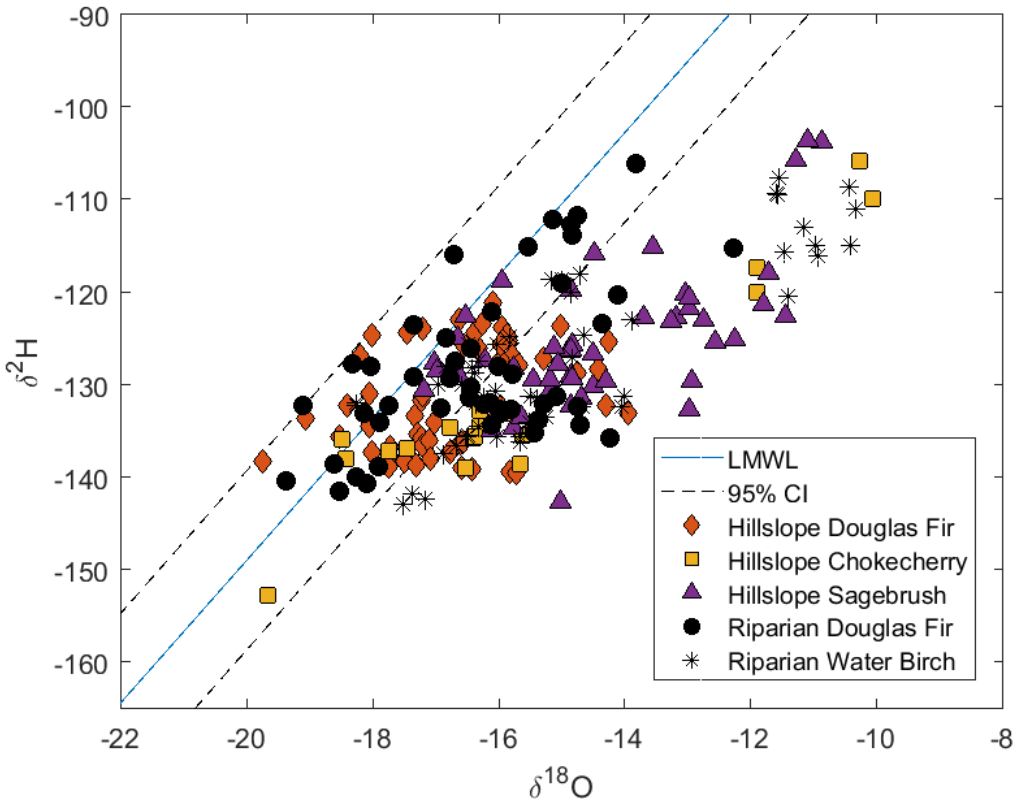

Figure 22. δ^2H and δ^{18}O for all plant species from May 2016 to July 2017.

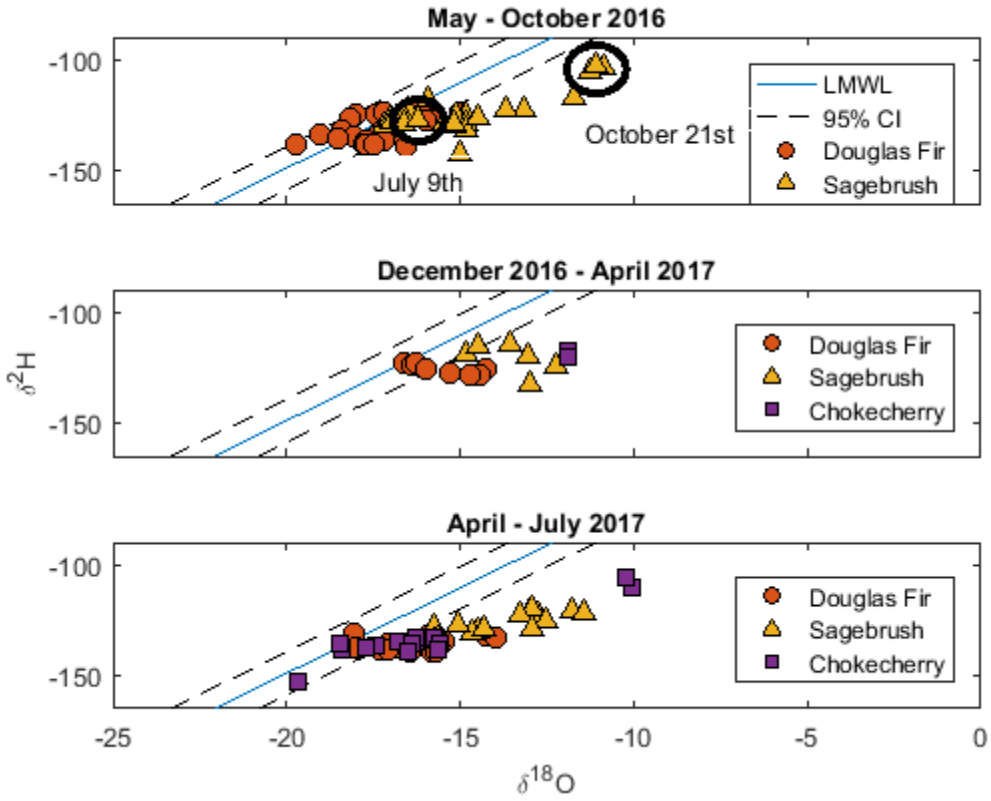

Figure 23. Top panel: δ^2H and δ^{18}O for hillslope Douglas Fir and sagebrush from May 10th through October 21st, 2016. Chokecherry was not sampled during this period. Middle panel: Hillslope Douglas Fir and sagebrush from December 19th, 2016, February 11th, and April 9th, 2017. Douglas Fir and sagebrush moved progressively off the LMWL with each subsequent sampling date. Chokecherry was sampled on April 9th. Bottom Panel: Hillslope Douglas Fir, sagebrush and chokecherry from April 21st to July 6th, 2017. No directional trend existed in the data for any of the three species. The chokecherry data points in the upper right corner are from April 21st, possibly a vestige of winter enrichment before transpiration began.

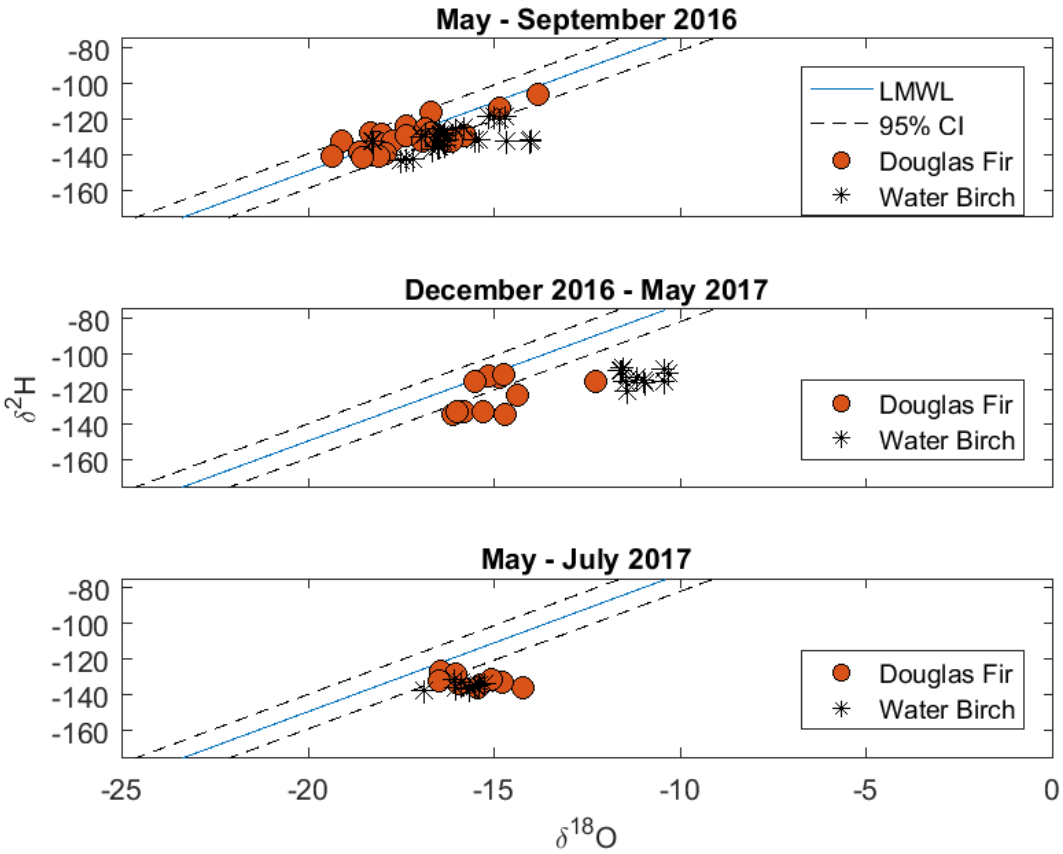

Figure 24. Top Panel: δ^2H and δ^{18}O for riparian Douglas Fir and water birch from May 10th to September 30th, 2016. Middle Panel: Riparian Douglas Fir and water birch from December 19, 2016 to May 8th, 2017. Both species' lowest lc-excess values occurred during this period. Bottom Panel: Riparian Douglas Fir and water birch from May 24th to July 6th, 2017.

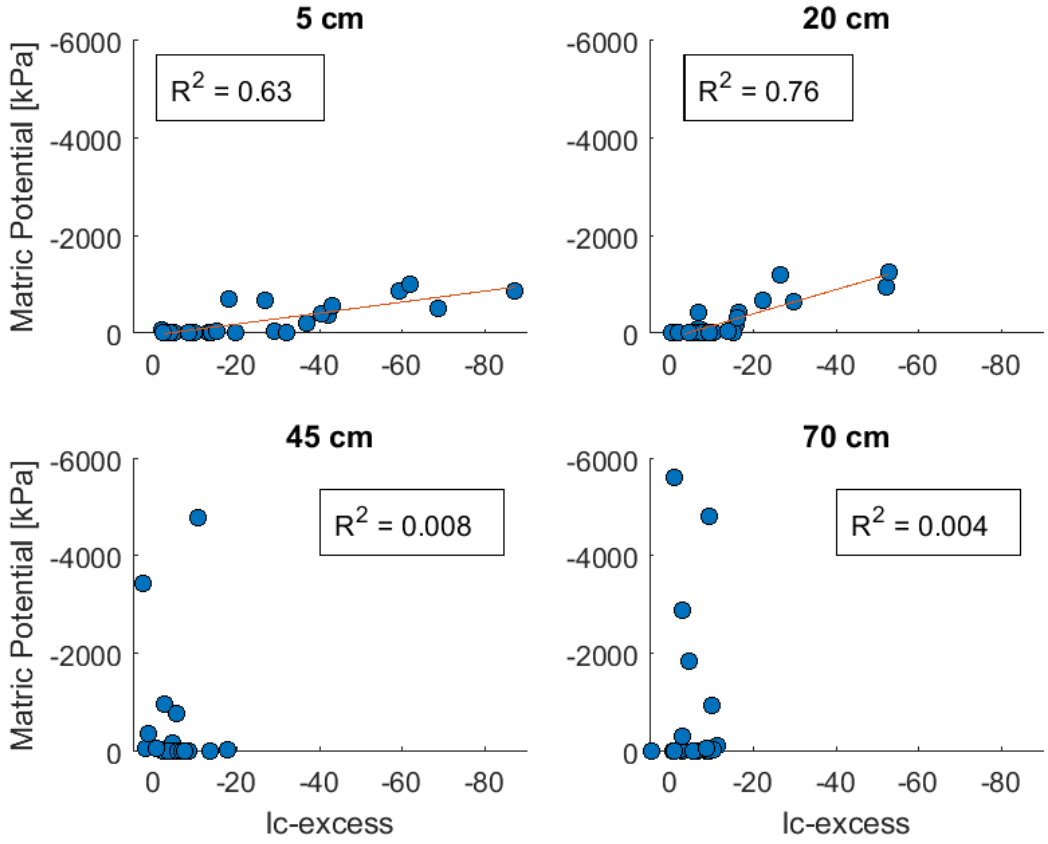

Figure 25. Matric potential versus lc-excess at each sensor depth. Strong relationships exist at 5 and 20 cm and virtually no relationship exists at the two lower depths.

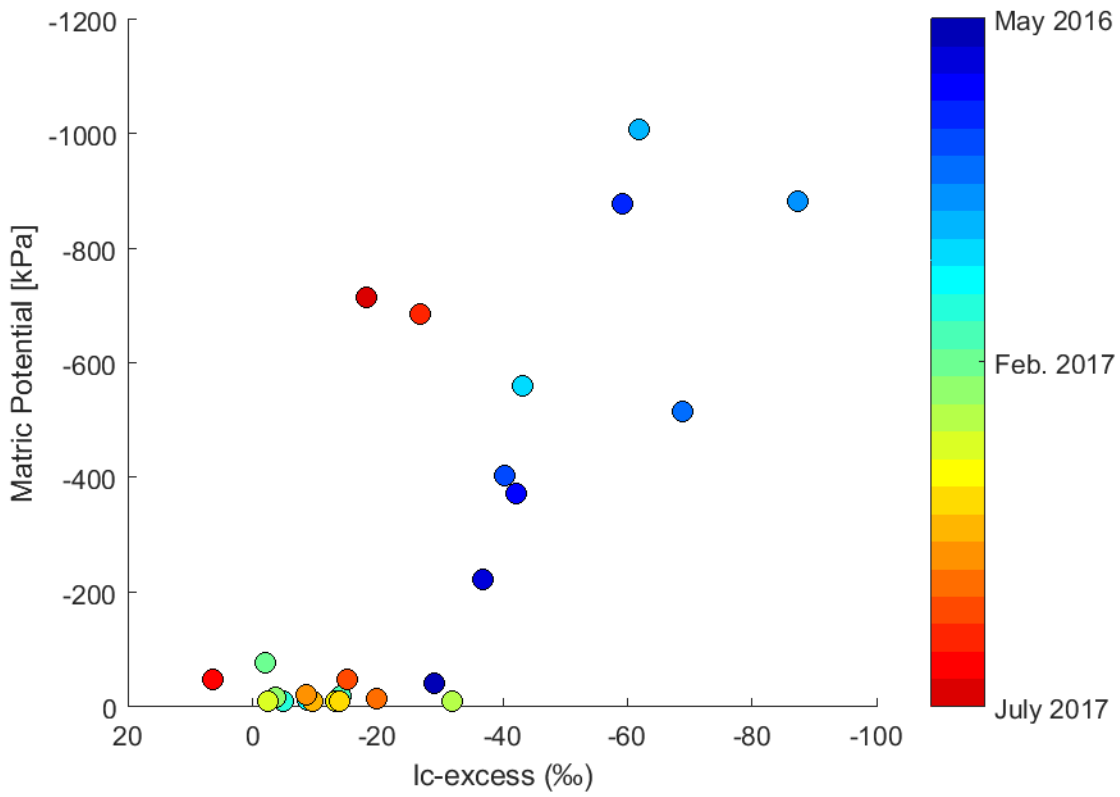

Figure 26. Temporal evolution of matric potential versus lc-excess at 5 cm at the hillslope pit. The most enriched soil water samples from summer 2016 are associated with the lowest matric potential values. The points along the x-axis suggest that elevated lc-excess (> -10 ‰) is not necessarily associated with lower matric potential, as some samples are associated with matric potential at or near estimated field capacity.

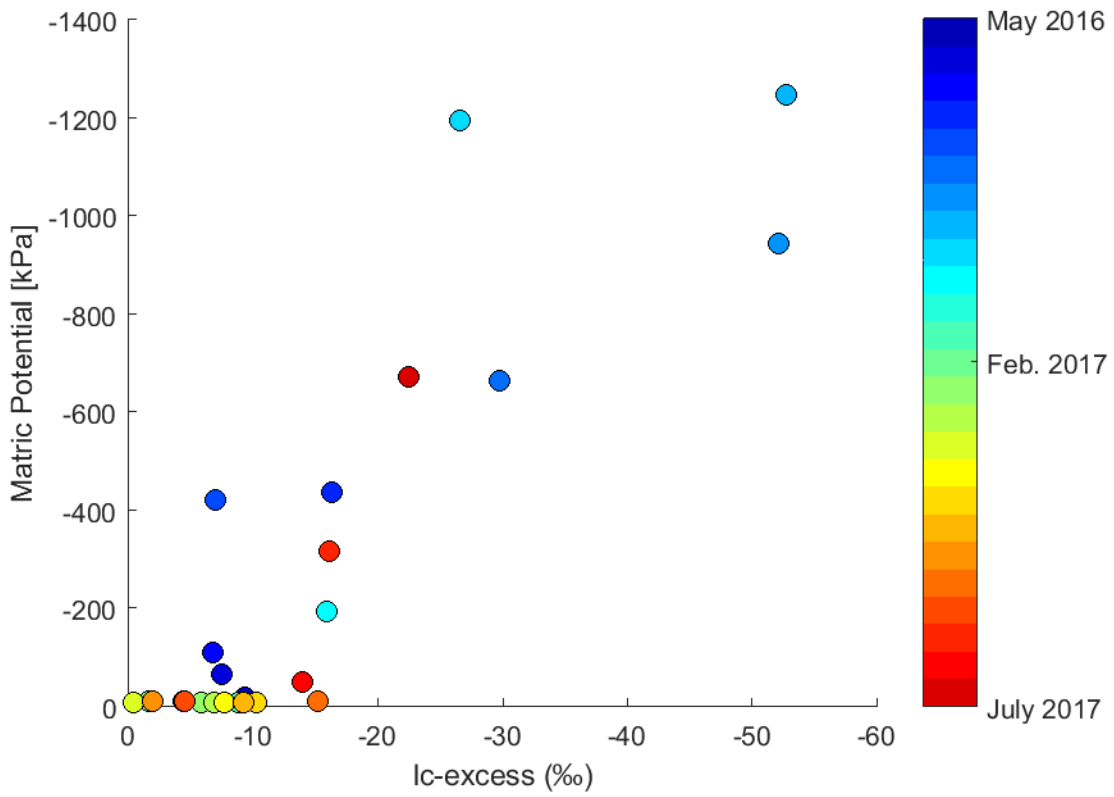

Figure 27. Temporal evolution of matric potential versus lc-excess at 20 cm at the hillslope pit. Similar to the 5 cm layer, matric potential and isotopic enrichment coevolve throughout the study. At this depth, significantly enriched water (lc-excess > -10 ‰) is frequently immobile (< -10 kPa).

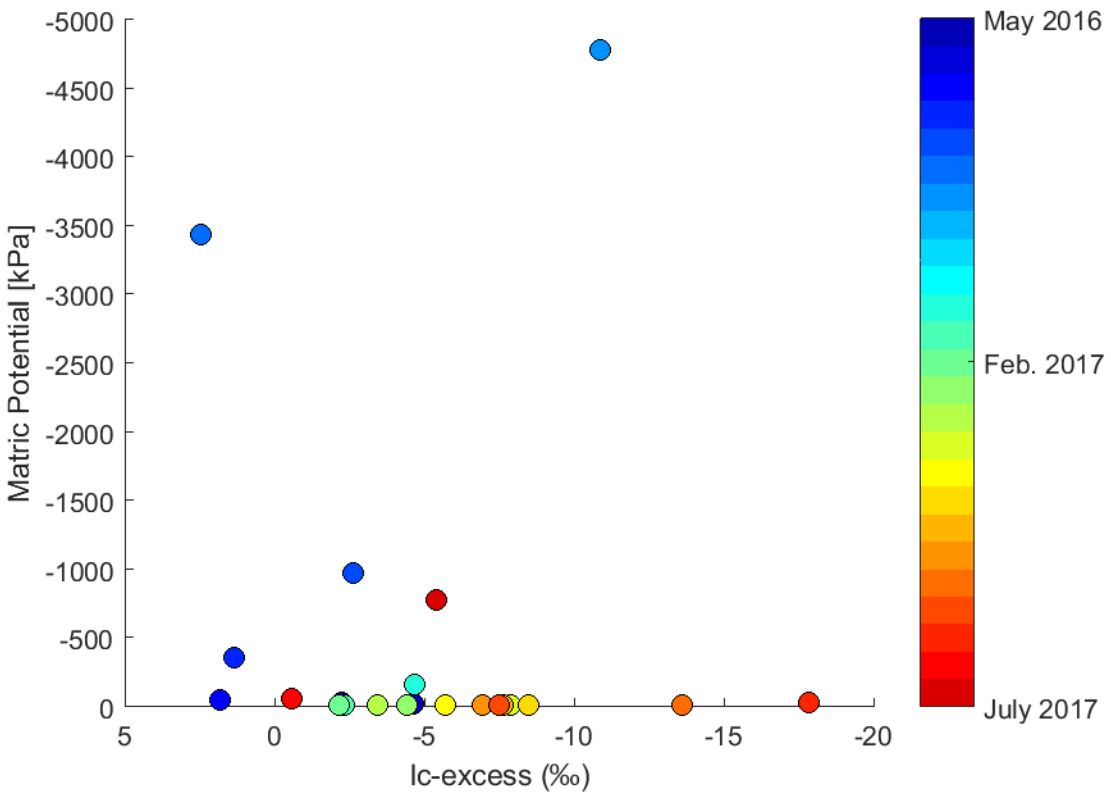

Figure 28. Temporal evolution of matric potential versus lc-excess at 45 cm at the hillslope pit. Few enriched values were found at this depth and were associated with the wet late spring and early summer period of 2017. The matric potential sensor at this depth malfunctioned around early September 2016 until mid-December, presumably due to dry conditions. Three isotope sampling dates occurred in this period and all samples had lc-excess values < -5 ‰. These observations suggest that these samples would plot in the low lc-excess/high matric potential portion of the above plot. This would strengthen the conclusion that low matric potentials at this depth are not associated with enriched isotopic composition.

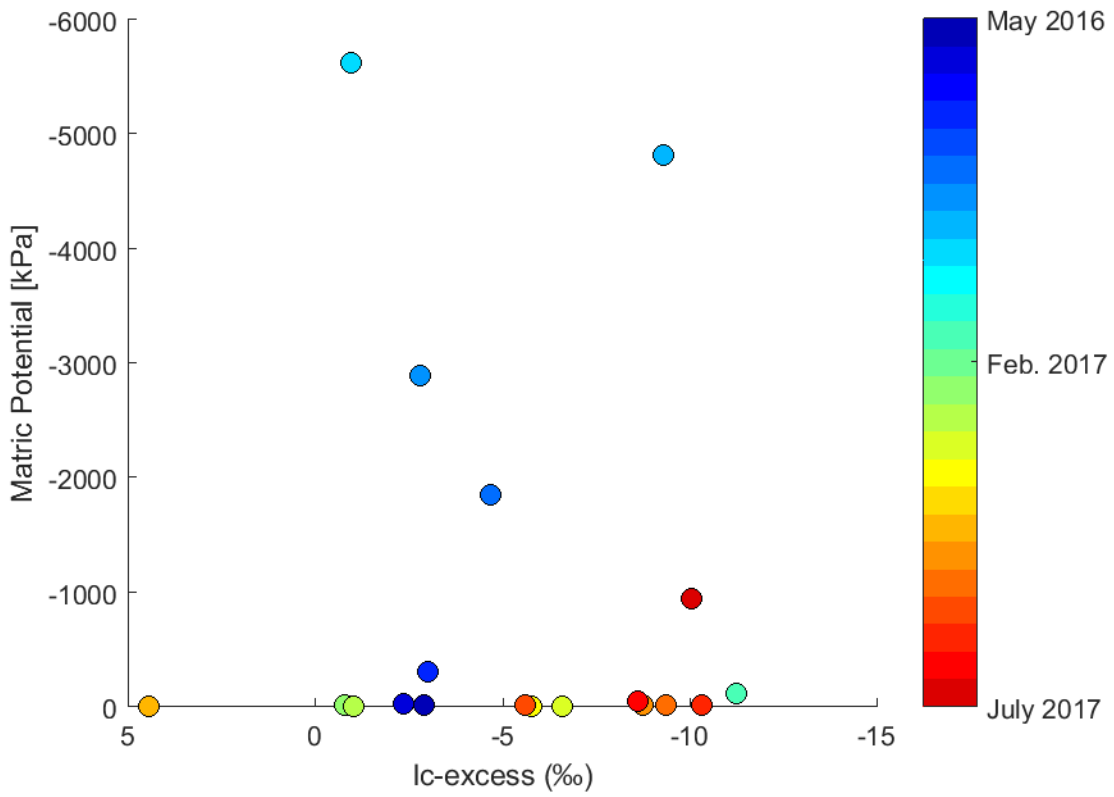

Figure 29. Temporal evolution of matric potential versus lc-excess at 70 cm at the hillslope pit. The matric potential sensor at this depth malfunctioned around early October 2016 until February 2017, presumably due to dry conditions, as corroborated by the VWC data from this period. Three isotope sampling dates occurred in this period and all samples had lc-excess values < -10 ‰. These observations suggest that these samples would plot in the low lc-excess/high matric potential portion of the above plot. This would strengthen the conclusion that low matric potentials at this depth are not associated with enriched isotopic composition and that immobile water is not necessarily isotopically enriched. Most isotopic compositions cluster between lc-excess values of 5 and -10 ‰. Similar to the 45 cm water from the same period, early summer 2017 lc-excess values approach or slightly exceed significant enrichment (>-10 ‰) but are mostly associated with matric potentials near field capacity (~ -10 kPa).

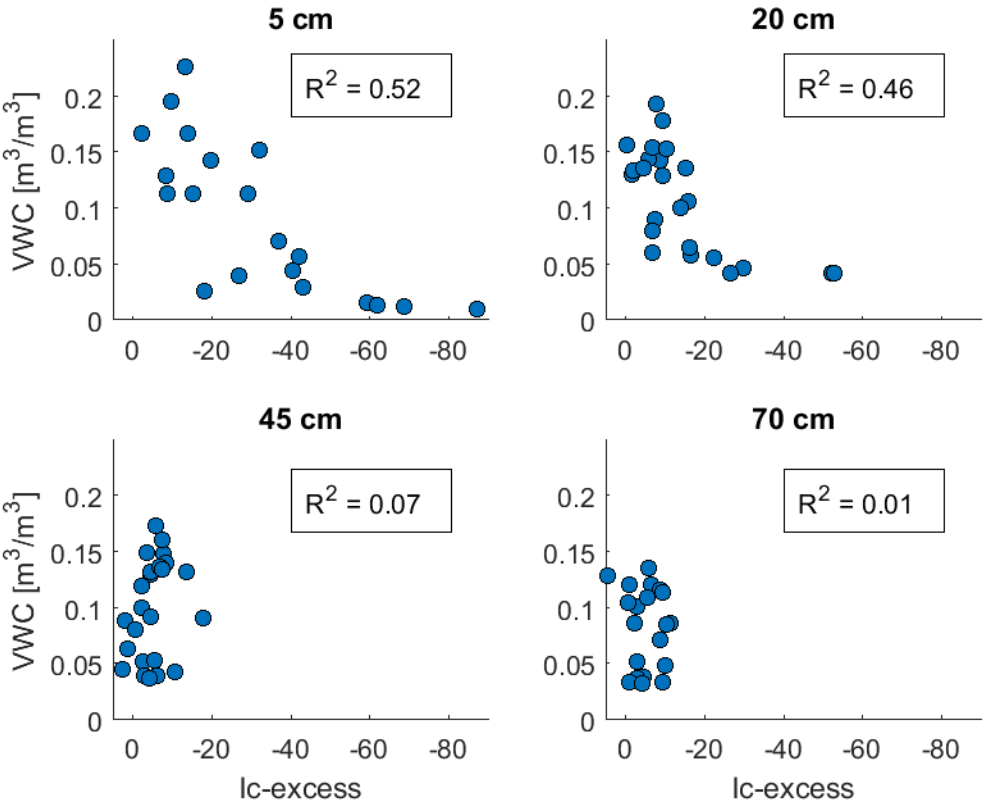

Figure 30. VWC versus lc-excess at each sensor depth. As with Figure 36, strong relationships exist at 5 and 20 cm and virtually no relationship exists at the two lower depths. Samples from 100 cm were not included due to small sample size.

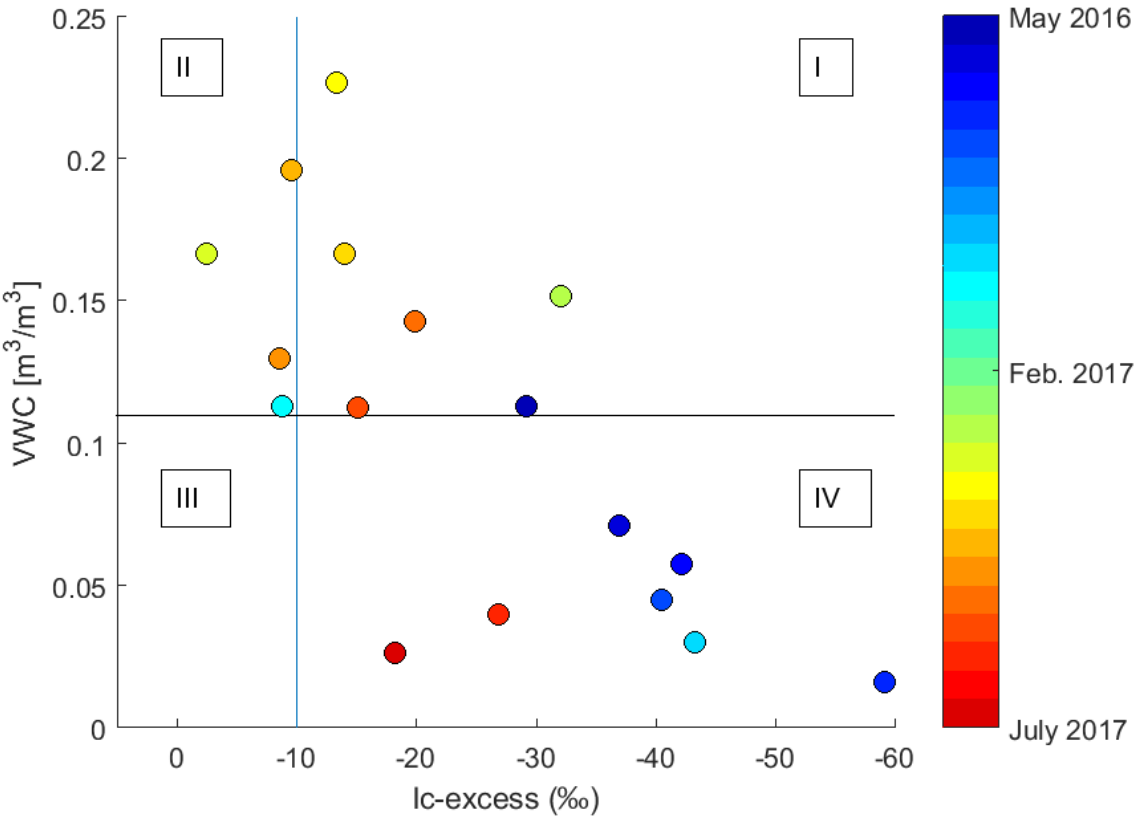

Figure 31. Temporal evolution of VWC versus lc-excess at 5 cm at the hillslope pit. The horizontal line represents field capacity as estimated by the frequency of occurrence method. The vertical line represents the threshold for significant isotopic enrichment as defined by the 95% CI for the LMWL. Labeled quadrants represent the following soil waters: I- enriched/mobile, II- unenriched/mobile, III- unenriched/immobile, IV- enriched/immobile.

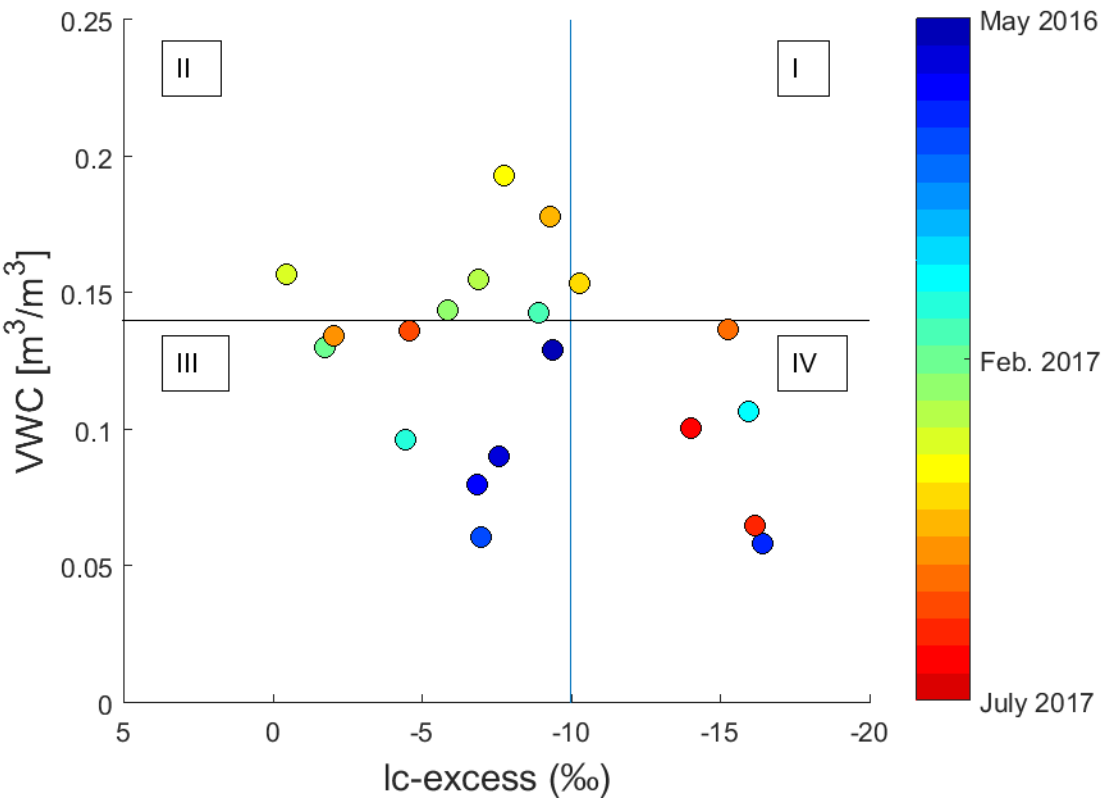

Figure 32. Temporal evolution of VWC versus lc-excess at 20 cm at the hillslope pit. Almost all enriched water plots in Quadrant IV, while no soil water plots in Quadrant I.

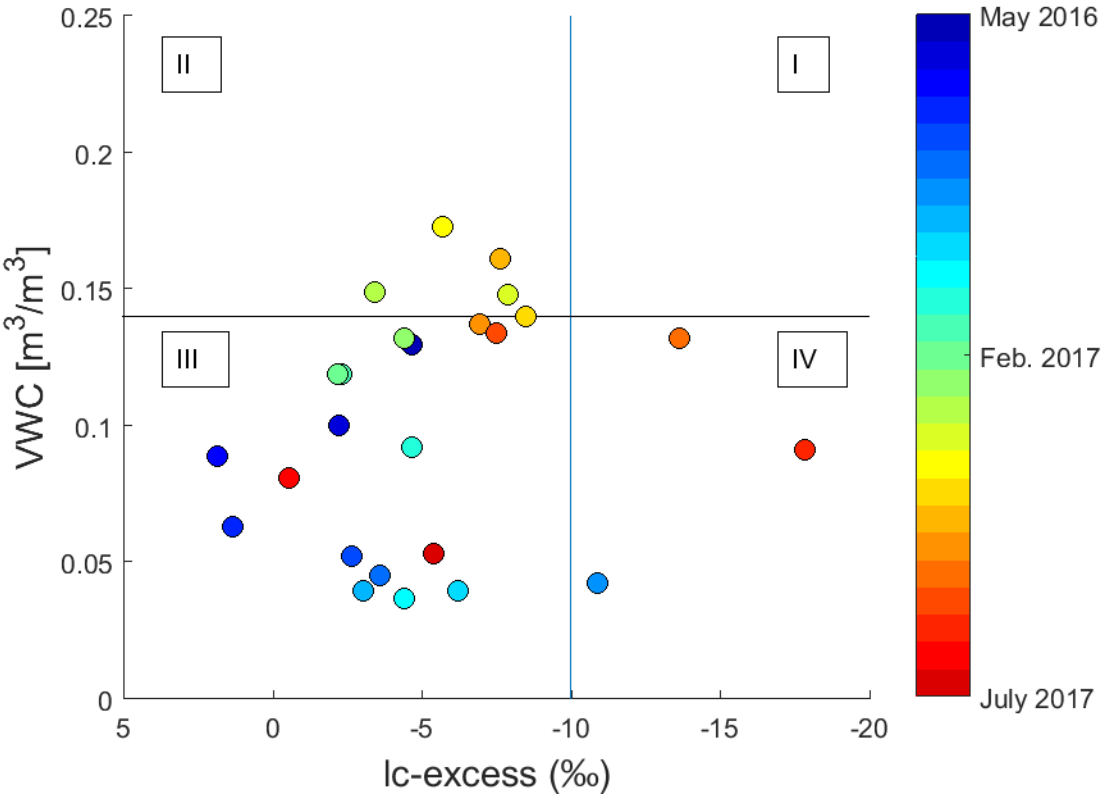

Figure 33. Temporal evolution of VWC versus lc-excess at 45 cm at the hillslope pit.

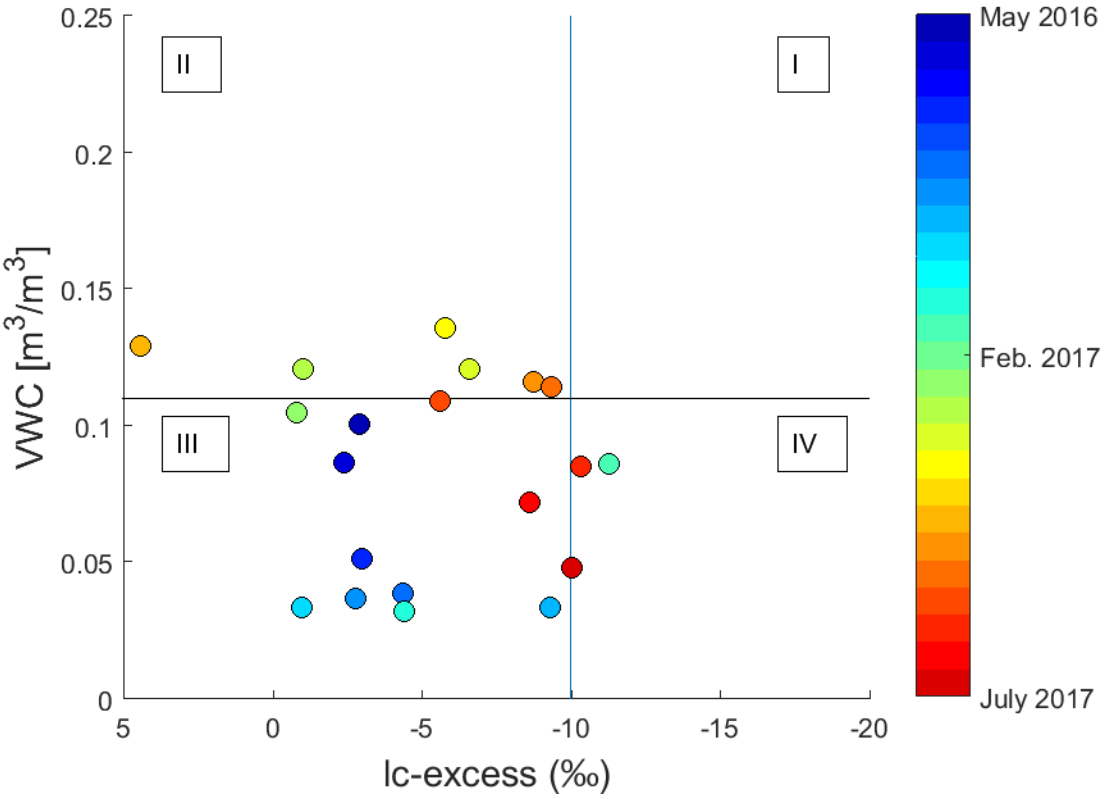

Figure 34. Temporal evolution of VWC versus lc-excess at 70 cm at the hillslope pit.

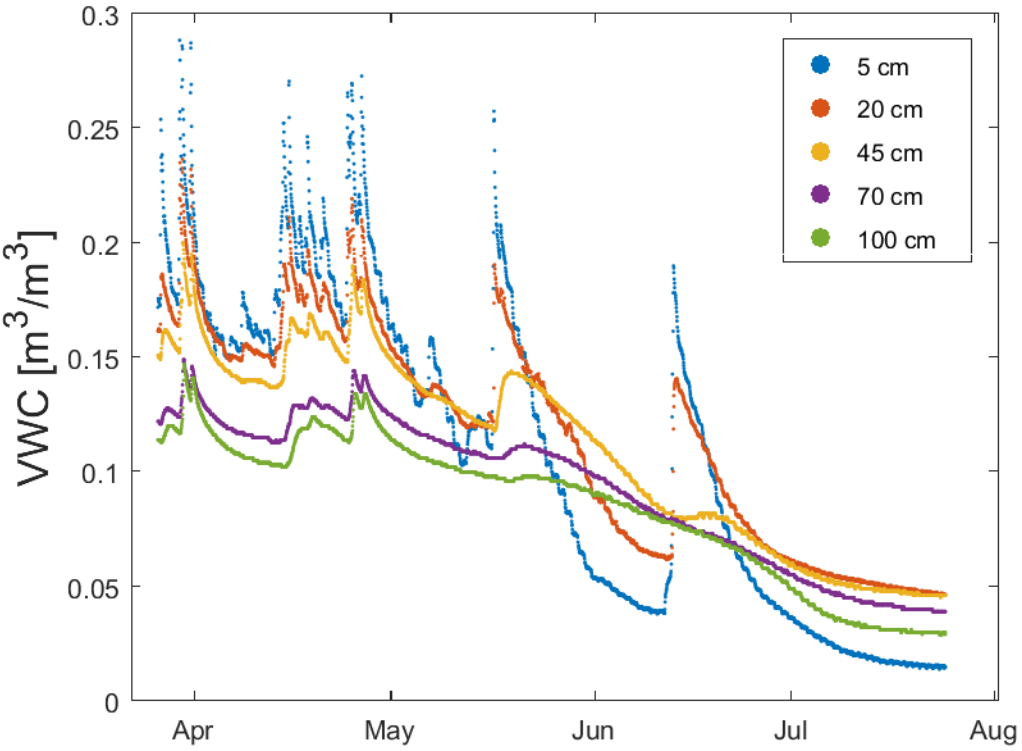

Figure 35. Time series of VWC at the hillslope pit from May 27th to July 24th, 2017. Dry down curve slope is similar in the 5, 20 and 45 cm sensors through mid-May. Two subsequent infiltration and dry down events show that curves are much steeper at 5 and 20 cm than for 45 cm.

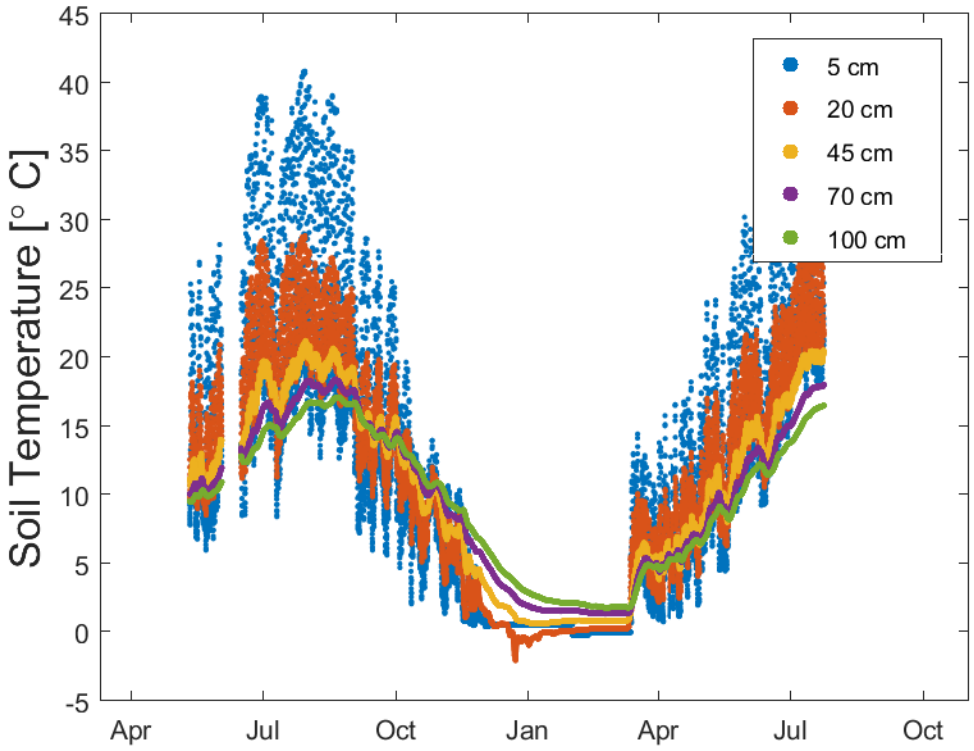

Figure 36. Time series of soil temperature at the hillslope pit from May 12th, 2016 to July 24th, 2017.

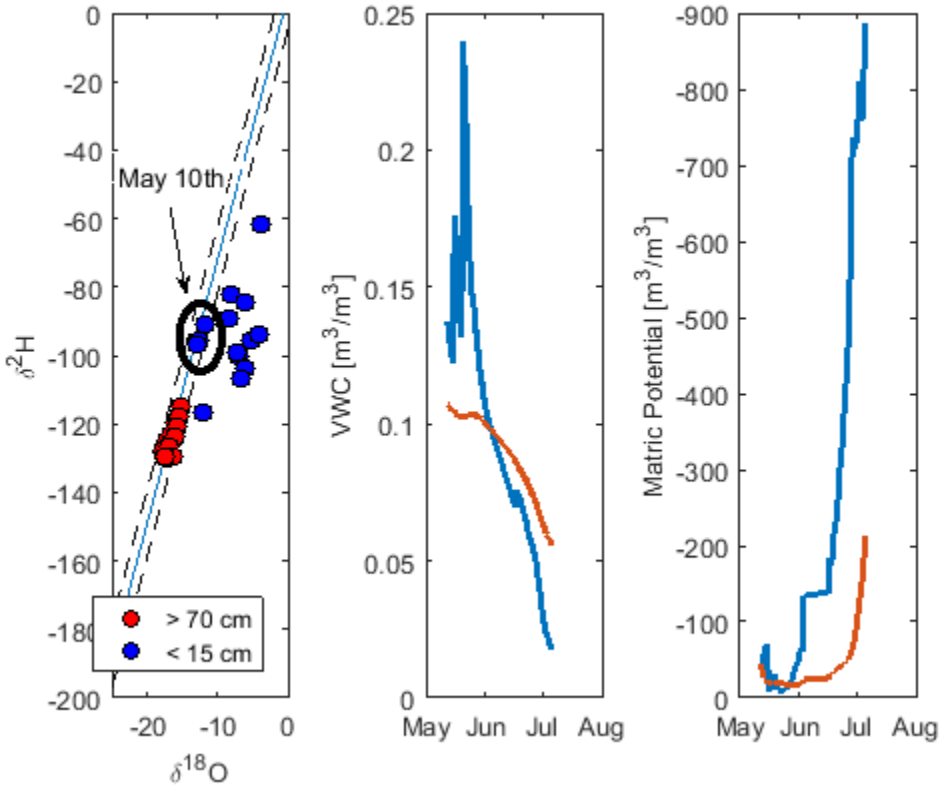

Figure 37. Soil water, VWC, and matric potential at the hillslope site from May 10th to September 9th, 2016. Deep (> 70 cm) and shallow (< 15 cm) soil water isotopes from this time period are shown in Panel 1.

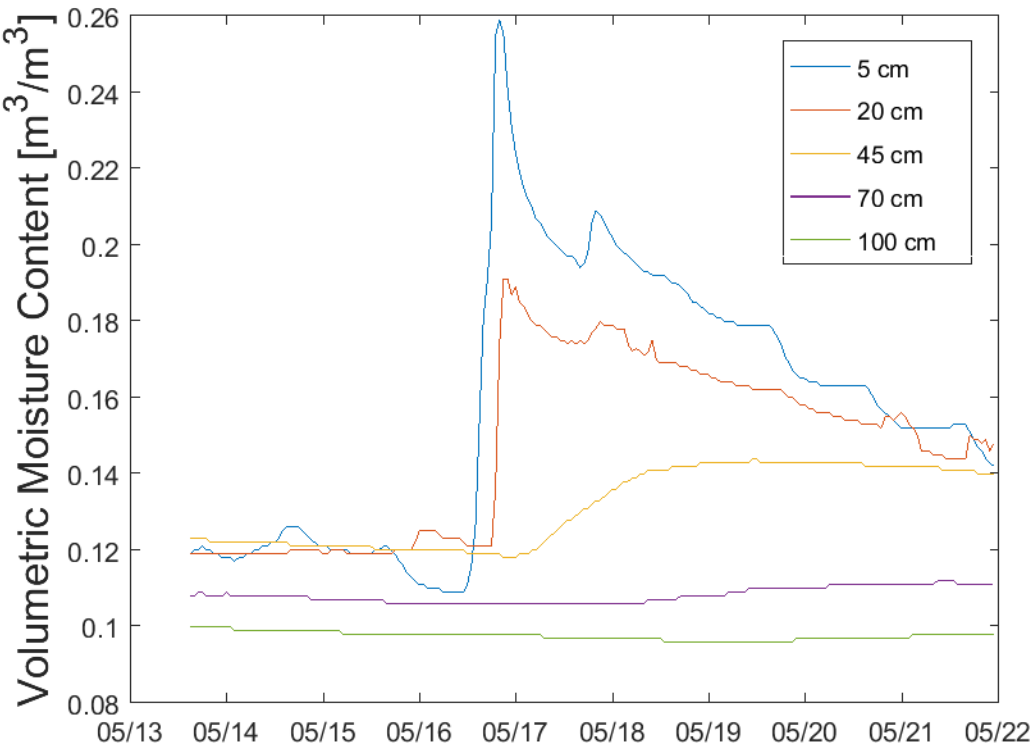

Figure 38. Time series of soil moisture at the hillslope pit from May 13th to May 22th, 2017. VWC increases progressively from 5 cm to 100 cm, with no sudden spikes at depth. This pattern was consistent for all infiltration events during the study period.

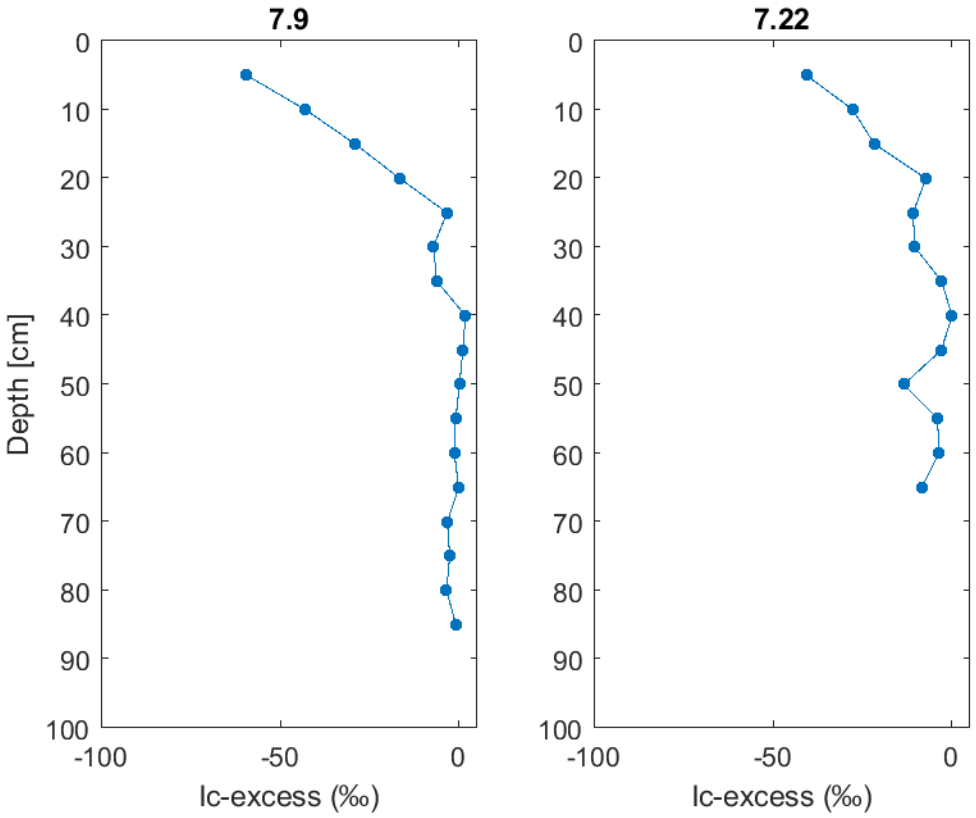

Figure 39. Soil water isotopes profiles at the hillslope site before and after July 10th, 2016 storm.

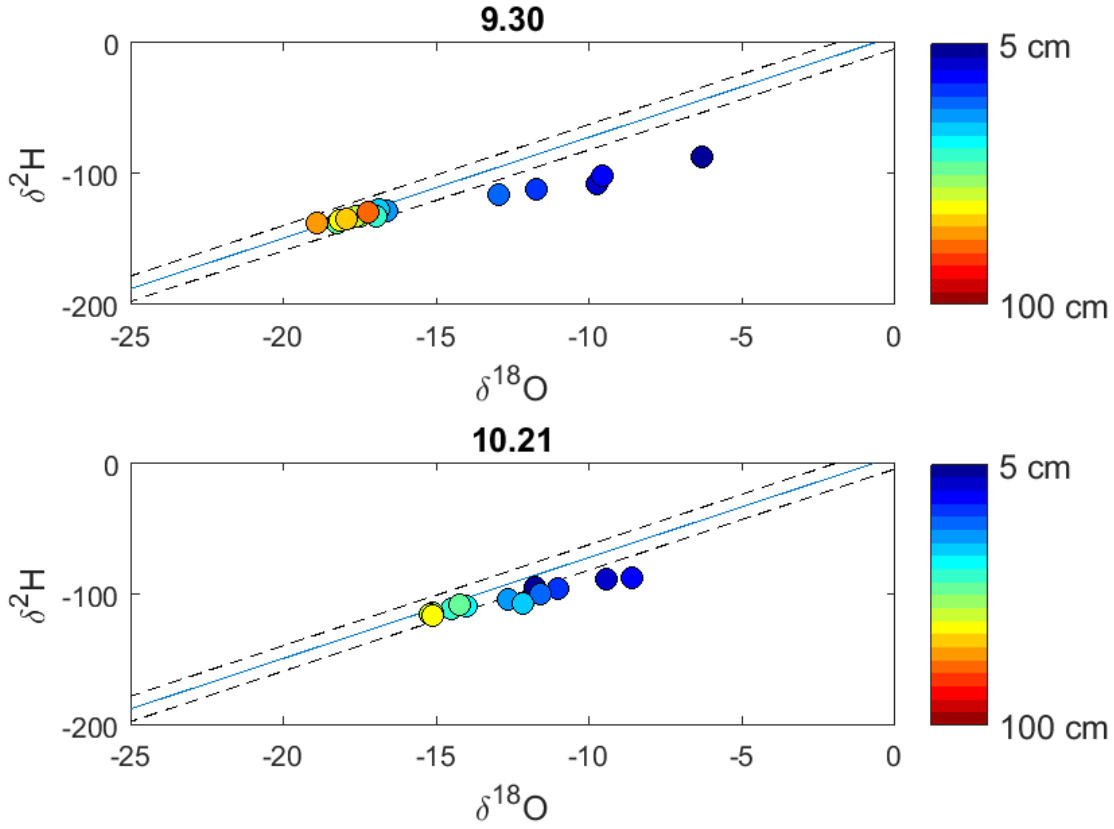

Figure 40. δ^2H and $\delta^{18}O$ for hillslope soil water on September 30th and October 21st, 2016. Shallow soil water isotopes move closer to the LMWL in response to fall rain. Deeper soil water becomes more enriched, but stays on the LMWL.

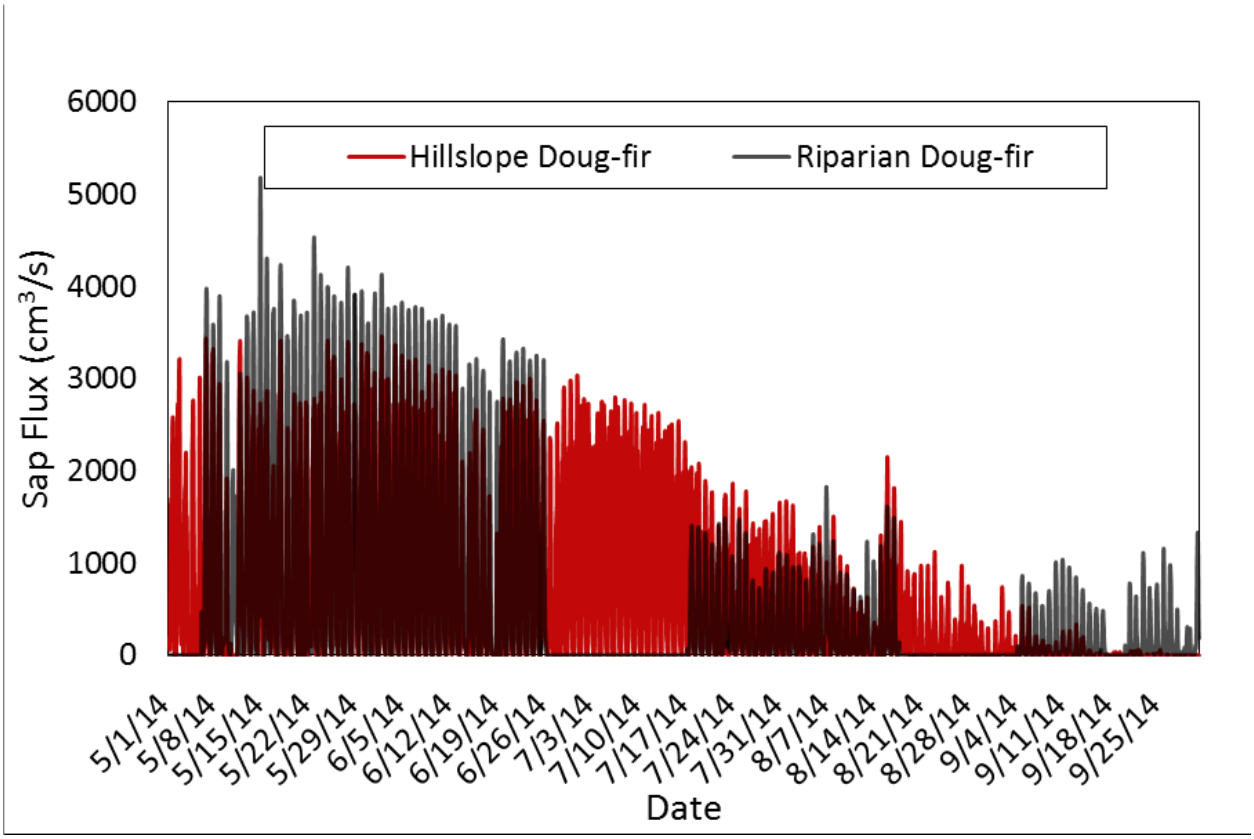

Figure 41. Sap flux data from Con 1 site. Taken from *Geisler* [2016].

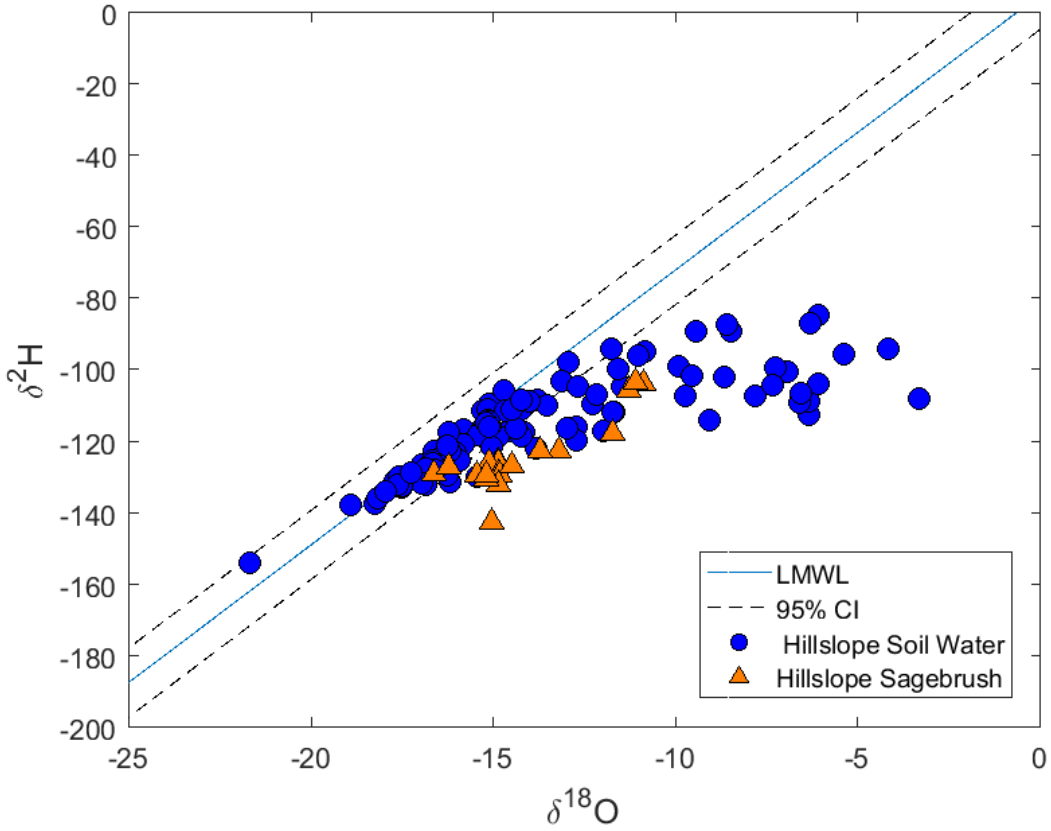

Figure 42. δ^2H and $\delta^{18}O$ for hillslope soil water and hillslope sagebrush from July 9th to October 21st, 2016.